Abstract of thesis entitled

Passivity Assessment and Model Order Reduction for Linear Time-Invariant Descriptor Systems in VLSI Circuit Simulation

Submitted by

Zheng ZHANG

for the degree of Master of Philosophy

at the University of Hong Kong

in June 2010

This thesis presents some theoretical and numerical results for linear time-invariant (LTI) descriptor systems (DSs), with emphasis on their corresponding passivity assessment and model order reduction (MOR). DSs are widely used in VLSI circuit modeling, including on-chip parasitics, RF passives, chip packagings, as well as linearized models of transistor networks.

In the first part (Chapters 2 to 4), we focus on the passivity assessments of LTI DSs. In Chapter 2, a generalized Hamiltonian method (GHM) and its half-size version (HGHM) are developed. The most significant advantage of GHM/HGHM passivity test is that they are purely algebraic routines, thereby rendering the test results highly accurate. Not only can they tell a LTI DS is passive or not, but they also accurately locate the possible nonpassive regions, thereby providing a versatile tool for subsequent DS passivity enforcements. Chapter 3 presents a projector-based passivity test for large-size LTI DS models which can not be readily tackled by GHM. It is the first time that spectral projectors are used, which are based on our proposed fast canonical projector construction, to efficiently decompose a large DS model into its proper and improper subsystems. After the fast system decomposition, the proper

part is tested by GHM, via a fast iterative numerical implementation. Chapter 4 presents the S-parameter generalized Hamiltonian method (S-GHM), and also its half-size algorithm (S-HGHM). Similar to GHM/HGHM, S-GHM and S-HGHM can locate all possible nonpassive regions with high numerical accuracy. A passivity test flow for admittance/impedance DSs is also proposed, based on S-GHM and S-HGHM after a Moebious transform of DS state-space equations.

The second part (Chapters 5 & 6) solves two issues in DS MOR: passivity and improper part preservation, as well as efficient MOR for multi-port DS models. Chapter 5 focuses on the first issue. The improper part of a DS is preserved by fast spectral projector-based additive system decomposition. After that, the proper part is reduced via DS-format positive-real balanced truncation (DS-PRBT). Since the main bottleneck of DS-PRBT is in solving the dual generalized algebraic Riccati equations (GAREs), a generalized quadratic alternating direction implicit (GQADI) algorithm is developed to efficiently compute the positive-real Gramians. To further speed up the matrix solver, a low-rank version of GQADI (LR-GQADI) is also devised, which reduces the complexity from $O(n^3)$ to $O(n^2)$. Chapter 6 constructs "good" macromodels for multi-port LTI DSs, motivated by power grid simulation in modern VLSI design. Due to the large number of ports, existing MOR techniques are not efficient for power grids. To overcome this problem, we develop a MOR routine based on input matrix splitting, called BDSM (block-diagonal structured model order reduction). The BDSM ROM (reduced-order model) is as accurate as standard moment-matching MORs; its resultant ROMs are block-diagonal structured which permits high efficiency for subsequent simulations; the BDSM ROM size can be further scaled down for clock-gated power grid models; finally and most importantly, unlike many existing power grid MORs that need to generate different ROMs for different input waveforms, the resultant ROM from BDSM is reusable under various input wave patterns.

Abstract word count: 504

Passivity Assessment and Model Order Reduction for Linear Time-Invariant Descriptor Systems in VLSI Circuit Simulation

by

Zheng ZHANG

B.Eng in 2008, Department of Electronic Science and Technology

Huazhong University of Science and Technology, P. R. China

A thesis submitted in partial fulfilment of the requirements for

the Degree of Master of Philosophy

at The University of Hong Kong.

June 2010

Declaration

I declare that this thesis represents my own work, except where due acknowledgement is made, and that it has not been previously included in a thesis, dissertation or report submitted to this University or to any other institution for a degree, diploma or other qualifications.

Signed _____

Zheng ZHANG

Acknowledgements

This thesis could not have been finished without my supervisor Dr. Ngai Wong's guidance and supervision. In the past two years, Dr. Wong helped gear up my mathematics, pushed me forward to exercise independent thinking, and more importantly, taught me to be self-motivated and enjoy research.

I would like to thank Prof. Cheng-Kuan Cheng, my supervisor for four months during my visit to UCSD. In Prof. Cheng's group, I learnt much about circuit theory and power grid simulation. This pleasant experience has largely broadened my research insights. Prof. Cheng's patience, kindness, and continuous encouragement not only impressed me, but also moved me.

Many thanks to my labmates at the University of Hong Kong. Thanks to CHEN Quan, LEI Chi-Un and LIN Yu, WANG Yuanzhe, XU Yuanzhe and WANG Xiang, for their valuable suggestions, kindly help, inspiring discussions, as well as lots of laughters. I wish them best of luck in the future postgraduate or faculty careers. My thanks also go to my friends in UCSD, especially HU Xiang, who helped me a lot in the research of power grid simulation.

I am grateful to my family. Thanks to my parents and my sister for their care since my childhood. And especially, I owe my thanks and love to my fiancee, who has provided me with endless love, understanding and support in the past five years.

Contents

List of Tables

List of Figures

List of Abbreviations

LTI	linear time-invariant
DS	descriptor system
MOR	model order reduction
ROM	reduced-order model
EROM	effective reduced-order model
IC	integrated circuit
EDA	electronic design automation
CAD	computer aided design
VLSI	very large-scale integration
MEMs	micro-electromechanical systems
EM	electromagnetic
PEEC	partial element equivalent circuit
VF	vector fitting
pMOR	parameterized model order reduction
vMOR	variational model order reduction
PRIMA	passive and reduced-order interconnect macromodeling algorithm
MNA	modified nodal analysis
RLC	resistor, inductor and capacitor
PVL	Páde via Lanczos
MPVL	matrix Páde via Lanczos

EKS	extended Krylov subspace
POD	propoer orthogonal decomposition
BDSM	block-diagonal structured model order reduction
BT	balanced truncation
PRBT	positive-real balanced truncation
BRBT	bounded-real balanced truncation
DS-BT	balanced truncation for descriptor systems
DS-PRBT	positive-real balanced truncation for descriptor systems
ETBR	extended truncated balanced realization
PSD	positive semidefinite
ImPT	improper part test
GHM	generalized Hamiltonian method
HGHM	half-size generalized Hamiltonian method
S-GHM	S-parameter generalized Hamiltonian method
S-HGHM	S-parameter half-size generalized Hamiltonian method
LMI	linear matrix inequality
SHH	skew-Hamiltonian/Hamiltonian
ARE	algebraic Riccati equation
GARE	generalized algebraic Riccati equation
GALE	generalized algebraic Lyapunov equation
ADI	alternating direction implicit
LR-ADI	low-rank alternating direction implicit
QADI	quadratic alternating direction implicit
LR-QADI	low-rank quadratic alternating direction implicit
GQADI	generalized quadratic alternating direction implicit
LR-GQADI	low-rank generalized quadratic alternating direction implicit
SVD	singular value decomposition

Chapter 1

Introduction

1.1 Research Motivation

Macromodeling is a very important step in the computer-aided design (CAD) of very large-scale integration (VLSI). Typical examples include (but are not restricted to): modeling of on-chip parasitic effects (such as interconnects and power ground networks), chip packaging, microelectronic-mechanical systems (MEMS), analog and radio-frequency (RF) circuits and components (such as on-chip inductors), chemical or biological systems. Normally, these systems, components or structures are described by detailed mathematical models such as differential equations. Based on these models, simulation, analysis, verification and optimization procedures can be performed before the final manufacturing step.

This thesis focuses on one of the important modeling frameworks: linear time-invariant descriptor system (LTI DS) [1–3], which is a generalization of the standard state-space model [4] and has found increasing applications in VLSI CAD. Typical DS applications include: description of linear circuits [5] [such as those containing only resistors (R), capacitors (C) and/or inductors (L)], discretized electromagnetic (EM) equations [6] used in accurate parasitic extractions, linearization of nonlinear

systems [7] (such as analog and RF circuits, MEMS devices etc.). Recently, DS technique has also been used in data fittings [49, 50] that attempt to build behavioral models of electronic components/systems from some available response data. These frequency-domain or time-domain data may be from practical measurements or simulation results generated by complex mathematical models.

Specifically, this thesis addresses two issues about LTI DS: model order reduction (MOR) and passivity characterization.

MOR is a popular and indispensable step to reduce circuit simulation complexity in VLSI design flow. In practical VLSI design, the linear circuits (such as those from parasitic extraction) and nonlinear blocks (e.g., those functional or logic blocks containing transistors, diodes or MEMS devices) can be extremely complex, rendering direct computer-aided simulation impractical or prohibitively time-consuming. A viable solution is to approximate the original models, which are constantly of high orders and thus difficult to solve, by reduced-order models (ROMs) that are amenable for efficient computer simulation.

System passivity [8–14] is required in the physical modeling and MOR procedures of linear passive systems (such as RLC models of interconnects and power grids, EM extraction of on-chip inductors, data fitting of electrical packagings). This is because: from the physical perspective, all RLC networks are energy-consuming or equivalently dissipative systems, and thereby can not generate energy internally. However, the system passivity may be lost during the process of MOR, which results in unsound physical behaviors. Specifically, from the control perspective, all passive sub-blocks connected together would yield a globally stable system; while stable but nonpassive models may lead to unstable global behaviors (such as blowing-up node voltage). A remedy for nonpassive models is passivity enforcement [10, 11]. Passivity enforcement consists of two steps. First, the models are checked by passivity verification algorithms [8–14], to see if they are globally passive. Second, if nonpassive, the models

are slightly perturbed (subject to some accuracy criteria), such that the new models are passive in the whole frequency band. From the numerical perspective, passivity verification is the main bottleneck, due to its expensive computational load, as well as high accuracy requirements.

Therefore, this thesis is devoted to passivity and MOR of LTI DSs. In the system passivity part, we try to solve the following problems:

1. Flexible passivity assessment algorithms for reduced DS models with impedance or admittance parameters.

2. Fast algorithms of passivity assessment to large-scale DSs, such as those from EM solvers.

3. Passivity verification technique for DSs with scattering port parameters. This case is mostly encountered in high-speed circuit modeling and EM component description.

In the DS MOR part, we address two issues:

1. Passivity-preserving MOR for DSs based on fast numerical implementation. In the MOR flow, we also aim to preserve the possible improper part of a DS, subject to some numerical accuracy requirements.

2. Efficient MOR for multi-port (or many-port) DSs. This issue is mainly encountered in the simulation of power grid networks [91], whose large port number makes traditional MOR approaches inefficient. We aim to develop more efficient power grid MOR, such that the subsequent simulation can be significantly speeded up.

Before unfolding the contributions of this thesis in later chapters, we begin with some preliminaries about state-space modeling technique, and briefly review some existing results regarding passivity assessments and DS MORs.

1.2 LTI State-Space Model

A LTI system is one that satisfies the following two conditions:

- Linearity, which means that the input-output relationship is a linear map. Specifically, if the input $u_k(t)$ generates an output $y_k(t)$, then the scaled and summed input $\sum c_k u_k(t)$ would generate a scaled and summed output $\sum c_k y_k(t)$.

- Time invariance, which means that whether we apply an input to a system at time t or after a delay t_d, the output will be identical except for a time delay of t_d. For example, if $y(t)$ is the output excited by $u(t)$, then the output corresponding to $u(t - t_d)$ is $y(t - t_d)$.

1.2.1 Standard State-Space Model

A LTI standard state-space model is described by

$$\frac{dx(t)}{dt} = Ax(t) + Bu(t), \quad y = Cx(t) + Du(t), \tag{1.1}$$

where $x \in \mathbb{R}^n$ denotes the state variables, $A \in \mathbb{R}^{n\times n}$, $B \in \mathbb{R}^{n\times m}$, $C \in \mathbb{R}^{p\times n}$ and $D \in \mathbb{R}^{p\times m}$ are system matrices. The input matrix B maps the input vector $u(t)$ to the state variables $x(t)$, while the output matrix C maps $x(t)$ to the output response $y(t)$.

Assume the above system is zero initial-conditioned. In Laplace domain, (1.1) can be written as

$$sX(s) = AX(s) + BU(s), \quad Y(s) = CX(s) + DU(s), \tag{1.2}$$

where $X(s)$, $U(s)$ and $Y(s)$ are the Laplace transforms of $x(t)$, $u(t)$ and $y(t)$, respectively. The frequency-domain input-output relationship can be characterized through

the transfer matrix $H(s)$

$$Y(s) = H(s)U(s), \text{ where } H(s) = \underbrace{C(sI - A)^{-1}B}_{H_{sp}(s)} + D \in \mathbb{C}^{p\times m}. \tag{1.3}$$

The transfer matrix $H(s)$ is a proper matrix function that approaches D as $s \to \infty$, while its strictly proper part is denoted by $H_{sp}(s)$ which is zero at $s = \infty$. Note that $H(s)$ can also be written as a rational matrix function:

$$H(s) = \underbrace{\frac{R_1}{s - p_1} + \cdots + \frac{R_n}{s - p_n}}_{H_{sp}(s)} + D \in \mathbb{C}^{p\times m} \tag{1.4}$$

where p_k $(k = 1, \cdots, n)$ are the eigenvalues of A, $R_k \in \mathbb{R}^{p\times m}$ is the corresponding residual matrix. The system is strictly stable if $spec(A) = \{p_1, \cdots, p_n\} \subset \mathbb{C}^-$, where $\mathbb{C}^-$ denotes the open left-hand side of the complex plane. This is because, in this case, the impulse response would not have exponentially increasing terms, which is readily seen by inverse Laplace transform.

1.2.2 Descriptor System

In practical circuit modeling, a descriptor system (DS), rather than a standard state-space model, is more frequently used. A DS is also called as generalized system or singular system, which is a superset of standard state-space models. We study a linear time-invariant (LTI) DS in the form

$$E\tfrac{dx}{dt} \quad = Ax + Bu, \;\; y = Cx + Du, \tag{1.5}$$

where $E, A \in \mathbb{R}^{n\times n}$, $B \in \mathbb{R}^{n\times m}$, $C \in \mathbb{R}^{p\times n}$ and $D \in \mathbb{R}^{p\times m}$. Also, $u \in \mathbb{R}^m$, $y \in \mathbb{R}^p$ and $x \in \mathbb{R}^n$ are the input, output and state vectors, respectively. The matrix E is generally

singular with $\text{rank}(E) \leq n$. We assume that the matrix pencil $\lambda E - A$ is regular, i.e., $\det(\lambda_0 E - A) \neq 0$ for some $\lambda_0 \in \mathbb{C}$. Then, there always exist nonsingular $W, T \in \mathbb{R}^{n\times n}$ that transform E and A into the so-called *Weierstrass canonical form* [15]:

$$E = W \begin{bmatrix} I_q & 0 \\ 0 & N \end{bmatrix} T, \; A = W \begin{bmatrix} J & 0 \\ 0 & I_{n-q} \end{bmatrix} T, \tag{1.6}$$

where I_q denotes an identity matrix of order q (though the dimension is omitted whenever it is clear from context). The matrix J corresponds to the finite eigenvalues of $\lambda E - A$, whereas N is nilpotent and corresponds to the infinite eigenvalues. When all eigenvalues of J have negative real parts, the pencil $\lambda E - A$ is said to be stable. The nilpotency index μ of N, viz. $N^{\mu-1} \neq 0$ and $N^{\mu} = 0$, is called the *index* of the matrix pencil $\lambda E - A$.

Referring to the Weierstrass canonical form (1.6), we define the left and right (spectral) projectors, P_l and P_r, respectively, as [16, 19, 20]

$$P_l = W \begin{bmatrix} I_q & 0 \\ 0 & 0 \end{bmatrix} W^{-1}, \; P_r = T^{-1} \begin{bmatrix} I_q & 0 \\ 0 & 0 \end{bmatrix} T. \tag{1.7}$$

Obviously, P_l and P_r are the projectors *onto* the left and right deflating subspaces, respectively, corresponding to the finite eigenvalues *along* the left and right deflating subspaces corresponding to the eigenvalue at infinity, whereas $Q_l = I - P_l$ and $Q_r = I - P_r$ are the complementary projectors.

Using (1.6) and partitioning $[C_p \;\; C_\infty] = CT^{-1}$ and $[B_p^T \;\; B_\infty^T]^T = W^{-1}B$ conformal to (1.6), the DS transfer function $H(s) = D + C(sE - A)^{-1}B$ of (1.5) can be

expressed as

$$H(s) = D + C(sE - A)^{-1}B = D + \begin{bmatrix} C_p & C_\infty \end{bmatrix} \begin{bmatrix} (sI_q - J)^{-1} & \\ & -(I_{n-q} - sN)^{-1} \end{bmatrix} \begin{bmatrix} B_p \\ B_\infty \end{bmatrix}$$

$$= \underbrace{D - C_\infty B_\infty + \overbrace{C_p(sI_q - J)^{-1}B_p}^{H_{sp}(s)}}_{H_p(s)} \underbrace{-sC_\infty NB_\infty - s^2C_\infty N^2B_\infty - s^3C_\infty N^3B_\infty - \cdots}_{H_\infty(s)}, \quad (1.8)$$

where $H_p(s)$ is the proper part of $H(s)$ (bounded as $s \to \infty$), $H_{sp}(s)$ is the strictly proper part that approaches zero as $s \to \infty$ and $H_\infty(s)$ the improper part (unbounded as $s \to \infty$).

1.3 System Passivity and Existing Assessment Methods

In this section, we introduce the concepts related to system passivity, and briefly review existing passivity assessment techniques. A system is passive if it cannot generate energy internally; it is strictly passive (or dissipative) if it consumes energy [21]. The passivity of a LTI system is normally described by the positive realness or bounded realness of its transfer function.

1.3.1 Positive Realness and Bounded Realness

Assume that $H(s)$ is the transfer matrix of a LTI system, and it is a square matrix (which means the system's input and output port numbers are identical). Depending on the physical meaning of $H(s)$, system passivity can be defined in different ways. In passivity assessments and circuit model reduction, we are interested in the case that $H(s)$ represents admittance/impedance parameters or scattering parameters.

If the square matrix function $H(s)$ represents the frequency-domain admittance

or impedance of an electrical network, the corresponding LTI system is (strictly) passive if and only if $H(s)$ is (strictly) positive real. A square transfer matrix $H(s)$ is (strictly) positive real if and only if [21, 39]:

1. $H(s)$ has no poles in $Re(s) > 0$;
2. $\overline{H(s)} = H(\overline{s})$ for all $s \in \mathbb{C}$;
3. $H(s) + H^*(s) \geq 0$ ($>$ for strict positive realness) for all $Re(s) \geq 0$.

The first condition means that the system is stable; the second condition implies that the system matrices are real; and the third condition implies that all eigenvalues of $H(s) + H^*(s)$ are positive real for any $s = j\omega$ where $\omega \in \mathbb{R}$ is the angular frequency.

If $H(s)$ represents the frequency-domain scattering matrix (normally used in EM modeling or high-frequency applications such as RF circuit design), the system is (strictly) passive if and only if $H(s)$ is (strictly) bounded real [13, 21]:

1. $H(s)$ is analytic on the open right half plane ($\mathrm{Re}(s) > 0$);
2. $\overline{H(s)} = H(\overline{s})$ for all $s \in \mathbb{C}$;
3. $I - H^*(s)H(s) \geq 0$ for all $Re(s) \geq 0$.

Also, condition 1 requires the system to be stable. Condition 2 implies that all singular values of $H(s)$ should be unit bounded (i.e., ≤ 1, where $<$ corresponds to the strict bounded realness), for any $s = j\omega$.

1.3.2 Methods for Standard State-Space Models

We consider the LTI standard state-space model (1.1), whose transfer matrix is readily given as $H(s) = C(sI - A)^{-1}B + D$. It is obvious that D should be a positive definite matrix if this LTI is strictly passive. Numerous passivity verification approaches have been developed for LTI standard state-space models, mainly including:

1. Frequency sweeping method [8,9]. The idea is to check the positive (or bounded) realness of $H(s)$ at a set of sampling points $s = j\omega_k$ $(k = 1, 2, \cdots)$, along the imaginary axis. The idea is simple, but the algorithms are not reliable: although an adaptive sampling and a reciprocal sampling methods are developed in [8] and [9] respectively, some nonpassive regions among neighboring sampling points are missed and passivity can not be accurately tested by finite sampling.

2. Linear matrix inequality (LMI) and algebraic Riccati equation (ARE) [4, 21], which were developed in control community. The LMI method tests system passivity via convex programming at the cost of $O(n^6)$ complexity. Using Schur complement [40], the LMI test can be converted to the ARE test and then solved at the cost of $O(n^3)$. The ARE test checks system passivity via solving the positive-real (or bounded-real) Gramian matrices [4] of an LTI system. Unfortunately, neither of them could tell the system's possible non-passive regions, which is necessary in the subsequent passivity enforcements.

3. Hamiltonian method [10–12]. This is the most accurate and widely used algorithm in passivity assessments and enforcements. By solving the eigenvalues of a size-$2n$ Hamiltonian matrix, every possible nonpassive region can be accurately located. Recently, the half-size variants [13, 14] of Hamiltonian methods have been developed, with better numerical accuracy and an $8\times$ speedup over traditional Hamiltonian methods.

1.3.3 Methods for Descriptor Systems

The passivity assessment of a DS is much more involved. The difficulty arises from the singularity of E in the system model, which may lead to an improper part in the transfer matrix. For example, for an admittance/impedance case, according to the definition of system passivity, $H(s)$ is (strictly) positive real if and only if [39]:

1. The only admissible form of the improper part is $H_\infty(s) = sM_1$, and M_1 must be either zero (which means the DS being impulse-free) or positive semidefinite (i.e., $M_1 \geq 0$).

2. The proper part $H_p(s)$ is (strictly) positive real.

These dual conditions imply that we need to test both the improper and proper parts of a DS. However, the two parts can not be easily separated. Although the Weierstrass canonical form can be used, it is extremely expensive (with $O(n^4)$ complexity) and numerically unstable, thus only applicable to theoretical analysis. Compared with its standard state-space counterpart, DS passivity test is much less investigated. Existing DS passivity characterization methods include:

1. Half-unit circle sweeping [41]. This method first maps the s-domain to z-domain to obtain a nonsingular system. Then the sampling points are selected along the half-unit circle on the complex plane, followed by checking the positive realness or bounded realness at these sampling points. Similar to the sweeping methods used for standard state-space models, this approach may miss nonpassive regions between the neighboring sampling points and is therefore inaccurate.

2. Passivity test by LMI or generalized algebraic Riccati equation (GARE) [39, 42–45]. For admittance/impedance DSs [39, 42–44], these methods require the DSs to be admissible, impulse-free or minimally realized, which are normally not satisfied in practice. Note that for S-parameter DSs, the model is not required to be impulse-free in passivity test, since the DS should be nonpassive if an improper part is involved in its transfer matrix. Similar to their counterparts for standard state-space models, LMI and GARE based methods generally can not tell the nonpassive regions, and therefore can not be used in passivity enforcement flows.

3. Decompose-and-test methods [20, 46, 47]. These methods first decompose the original DS to an improper part and a proper subsystem via Weierstrass decomposition [46, 47] or spectral projector technique [20]. After decomposition, the proper part can be converted to a standard state-space model, and then checked by existing approaches (e.g., Hamiltonian methods). Therefore, these methods can detect and locate the possible nonpassive regions. The drawbacks of these methods include: 1) the Weirstrass decomposition is prohibitively expensive and unstable; 2) the spectral projector technique, which is obtained via canonical projector [20], requires expensive matrix factorization (e.g., full-size SVD), thus is infeasible for medium and large-size DSs; 3) converting the proper subsystem to a standard state-space model is in general numerically expensive, unstable and error-prone.

1.4 Existing Model Order Reduction Schemes

Numerous MOR algorithms have been developed to generate macromodels for fast circuit simulation. According to their application areas, these MOR algorithms can be classified into three groups.

1. Linear MOR [22–30]. These techniques are mostly used to reduce the complexity of parasitic networks (such as RLC networks of interconnects or power grids, which are described by differential circuit equations or discretized EM models), RF passive components that require accurate description by full-wave EM equations, chip packagings. Linear MORs can be implemented by various approaches, such as Krylov-subspace projection [22–25], Gramian-based reduction originated from control community [27–30], proper orthogonal decomposition (POD) reduction [61,62]. Given a set of measured or simulated data, linear macromodels can also be constructed via data fittings [48–50].

2. Nonlinear MOR [31–33]. They are mainly used to simplify the mathematical models of nonlinear devices (e.g., transistors, MEMS devices) or systems. Nonlinear systems are very common in circuit design, including almost all analog and RF blocks, such as amplifiers, mixers, oscillators, phase-locked loops (PLL) etc. For different situations (e.g., strongly nonlinear circuits, weakly nonlinear circuits, or nonlinear circuits with periodic or quasi-periodic signals), the MOR algorithms might be slightly different such that some important properties or parameters could be captured (e.g., high-order harmonics, signal intermodulation).

3. Parametric MOR (pMOR) [34, 35]. Parametric MOR is also referred to variational MOR [36] (vMOR), which is developed to address the variation-induced issues in circuit and system modeling. Typical cases are geometric variations [34] and process uncertainty [35] that are inherent in manufacturing, as well as temperature fluctuations [37, 38] that have strong impacts on interconnect signal delay, power consumption and chip reliability. pMOR can be applied to both linear and nonlinear systems.

In this thesis, we focus on linear MORs with application to LTI DSs. In these MOR schemes, the projection technique is the most widely used method. From the black-box perspective, system models can also be constructed by data fitting methods, either in standard state-space [48] or DS form [49,50]. However, these macromodeling techniques are beyond our scope.

In projection-based linear MORs, we attempt to find two projection matrices W and V (with $W^T, V \in \mathbb{R}^{n\times q}$) for the DS (1.5), such that a much smaller size-q model can be generated:

$$E_r \frac{dz(t)}{dt} = A_r z(t) + B_r u(t), \quad y_r(t) = C_r z(t) \tag{1.9}$$

with $E_r = W^T EV$, $A_r = W^T AV$, $B_r = W^T B$ and $C_r = CV$, such that $H_r(s) = C_r(sE_r - A_r)^{-1}B_r \approx H(s)$ or $Y_r(s) = H_r(s)U(s) \approx Y(s)$, subject to some accuracy requirements. Typical methods of constructing the projection matrices include: POD [61, 62], moment-matching technique [22, 25, 52], and Gramian-based method [26, 29, 30]. The reader is referred to the survey paper [51] and the references therein for details. In circuit context, moment-matching and Gramian-based MORs are most widely applied and thereby reviewed below.

1.4.1 Moment-Matching-Based MOR

Many moment-matching MOR algorithms stem from Pillage's work on asymptotic waveform evaluation (AWE) [52]. In the frequency domain, the transfer matrix $H(s)$ of the DS in (1.5) can be written as a Taylor expansion around s_0

$$H(s) = \sum M_k (s - s_0)^k, \text{ for } k = 0, 1, \cdots . \tag{1.10}$$

The matrix $M_k(s_0) = CF^k R$ is the order-k moment at expansion point s_0, with $R = (s_0 E - A)^{-1} B$ and $F = -(s_0 E - A)^{-1} E$. The idea of moment matching is that we can approximate $H(s)$ by capturing some of its important moment matrices. In [52], the moments are computed in an explicit way, which suffers from numerical instability.

An alternative is to match the moments implicitly by Krylov subspace method. An order-l block Krylov subspace $\mathcal{K}_l(F, R)$ is defined as

$$\mathcal{K}_l(F, R) = \text{span}\left\{R, FR, \cdots, F^{l-1}R\right\}. \tag{1.11}$$

For simplicity we assume that $m = p$. The matrix Páde via Lanczos algorithm

(MPVL) [25] constructs the projection matrices by

$$V = \mathcal{K}_l\left(F, R\right),\ W = \mathcal{K}_l\left(\hat{F}, \hat{R}\right),\ \text{with } \hat{F} = F^T,\ \hat{R} = (s_0E - A)^{-T}C^T. \tag{1.12}$$

By MPVL, a size-q ROM (1.9), with $q = ml$, could be constructed to capture the first $2l$ moments of $H(s)$, i.e.,

$$\begin{aligned} &H_r(s) = \sum M_{r,k}(s - s_o)^k,\ \text{with } M_{r,k} = C_r\left(-(s_0E_r - A_r)^{-1}E_r\right)^k(s_0E_r - A_r)^{-1}B_r. \\ &\text{and } M_{r,k} = M_k,\ \text{for } k = 0, 1, \cdots, 2l-1. \end{aligned} \tag{1.13}$$

Obviously, the error between $H_r(s)$ and $H(s)$ is $O\left((s - s_0)^{2l}\right)$.

Another way to construct the projection matrices by only one Krylov subspace, resulting in $W = V$. This method is called congruence transform [53], by which the first l moments can be matched for a general DS model. For a symmetric model, such as a RC network with voltage sources as excitations and port currents as outputs, congruence transform can capture $2l$ moments.

1.4.2 Gramian-Based MOR

The Gramian-based MOR [26, 28–30, 57, 58] originated from the control community. Compared with moment-matching methods, Gramian-based MORs have two advantages: stability (or passivity) preservation for even unstructured system, plus an analytical error bound for quantifying numerical accuracy. Here we give the basic flows of classic balanced truncation (BT), as well as positive-real or bounded-real balanced truncation (PRBT or BRBT) which preserve system passivity.

Given a stable LTI state-space model (1.1) (i.e., $spec(A) \in \mathbb{C}^-$), the controllability

Gramian Q_c and observability Gramian Q_o are defined as

$$Q_c = \int_0^\infty e^{At} B B^T e^{A^T t} dt, \quad Q_o = \int_0^\infty e^{A^T t} C^T C e^{At} dt \tag{1.14}$$

which are the symmetric positive semi-definite solutions to the dual Lyapunov equations

$$AQ_c + Q_c A^T + BB^T = 0, \quad A^T Q_o + Q_o A + C^T C = 0. \tag{1.15}$$

Due to the positive semi-definiteness of the Gramians, there exist two factors L_c and L_o, such that $Q_c = L_c L_c^T$ and $Q_c = L_o L_o^T$. We compute the singular value decomposition of $L_o^T L_c$:

$$L_o^T L_c = \begin{bmatrix} U_1 & U_2 \end{bmatrix} \begin{bmatrix} \Sigma_1 & \\ & \Sigma_2 \end{bmatrix} \begin{bmatrix} V_1 & V_2 \end{bmatrix}^T, \tag{1.16}$$

where $\Sigma_1 = \text{diag}(\sigma_1, ..., \sigma_q)$, $\Sigma_2 = \text{diag}(\sigma_{q+1}, ..., \sigma_n)$ and $\sigma_1 \geq ... \geq \sigma_q \geq \sigma_{q+1} \geq ... \geq \sigma_n$ are called the Hankel singular values. To this end, the left projection matrix W and the right projection matrix V are constructed as

$$W = L_o U_1 \Sigma_1^{-\frac{1}{2}}, \quad V = L_c V_1 \Sigma_1^{-\frac{1}{2}}. \tag{1.17}$$

Finally, the ROM could be constructed as $A_r = W^T A V$, $B_r = W^T B$, $C_r = CV$. One advantage of balanced truncation is that an upper error bound is provided for the resulting transfer matrix

$$\|H(s) - H_r(s)\|_\infty \leq 2 \sum_{k=q+1}^{n} \sigma_k. \tag{1.18}$$

Compared with moment-matching methods, BT is capable of providing stable ROMs and an analytical error bound, but it is much more expensive ($O(n^3)$ complexity).

An ADI iteration and its low-rank variant (LR-ADI) are proposed in [57, 58] to solve Lyapunov equations at the cost comparable to that of Krylov-subspace projection. The details of ADI and LR-ADI algorithms are not presented here, and interested readers may refer to [57, 58] for details.

Classic BT can generate stable macromodels, but the ROMs are not guaranteed to be passive, which is normally expected in interconnect and RF passive component modeling. To preserve system passivity, PRBT (for admittance/impedance systems) or BRBT (for scattering systems) can be used. In PRBT, we need to solve the dual Lur'e equations [26] or algebraic Riccati equations (AREs) [30], which are essentially equivalent. The dual AREs are formulated as

$$\begin{aligned} AQ_c + Q_cA^T + \left(Q_cC^T - B\right) P^{-1}(CQ_c - B^T) = 0 \\ A^TQ_o + Q_oA + \left(Q_oB - C^T\right) P^{-1}(B^TQ_o - C) = 0 \end{aligned} \tag{1.19}$$

where $P = D + D^T > 0$ for strict positive real systems, Q_c and Q_o (which are positive semidefinite) denote the positive-real controllability Gramian and positive-real observability Gramian, respectively. After computing Q_c and Q_o, the projection matrices W and V can be computed in the same way as in classic BT. PRBT is the same with BRBT, except for that the bounded real controllability and observability Gramians Q_c and Q_o are the solutions to (1.19) after replacing P with $I - DD^T$. An ARE equation could be solved via Newton iteration, and inside each iteration a Lyapunov equation needs to be solved. Recently, a quadratic ADI (QADI) is proposed in [30] to solve the ARE at the cost of approximately only that of one Lyapunov equation.

For the DS in (1.5), stability-preserving balanced truncation has also been developed based on solving the dual generalized Lyapunov equations. The ADI and LR-ADI algorithms have also been extended to efficiently solve the dual generalized

Lyapunov equations. Details about DS BT and related fast matrix solvers could be found in [54–56].

1.4.3 Passivity-Preserving DS MOR

In practice, almost all LTI models encountered in circuit simulation are in the DS form, including linear circuit equations formulated by modified nodal analysis (MNA), RF passive component models extracted by EM field solvers, as well as many linearized models from nonlinear equations. For DS cases, the passivity-preserving MOR becomes much more involved.

There indeed exists a special case: positive semidefinite (PSD) structured DS, where passivity-preserving MOR could be easily performed. For example, in the MNA formulation of linear RLC circuits, if we are interested in the port admittance or impedance parameters, the DS matrices are PSD structured:

$$E \geq 0, \quad A + A^T \leq 0, \quad C = B^T. \tag{1.20}$$

Subsequently, using congruence transform would generate a positive-real ROM, as detailed in the famous PRIMA paper [22]. But there are many cases where their system matrices are not PSD structured, thus system passivity cannot be preserved by simply using Krylov-subspace based moment matching. Even for a PSD structured DS, system passivity could not be preserved by congruence transform when its transfer matrix represents the scattering parameters.

To preserve system passivity during the MOR of general DSs, we need to use passivity-preserving DS BT [16–18]. Assuming the DS (1.5) is impulse-free, the DS-PRBT algorithm is based on solving the dual generalized algebraic Riccati equations

(GAREs):

$$\begin{aligned} AQ_cE^T + EQ_cA^T + \left(EQ_cC^T - B\right) P^{-1}(CQ_cE^T - B^T) = 0 \\ A^TQ_oE + E^TQ_oA + \left(E^TQ_oB - C^T\right) P^{-1}(B^TQ_oE - C) = 0 \end{aligned} \tag{1.21}$$

with $D + D^T > 0$. Similar to the classic BT and PRBT, we can get the Cholesky factor (or square-root factor) of the Gramian matrices, such that $Q_c = L_cL_c^T$ and $Q_o = L_oL_o^T$. Then we continue to compute the skinny SVD:

$$L_o^TEL_c = \begin{bmatrix} U_1 & U_2 \end{bmatrix} \begin{bmatrix} \Sigma_1 & \\ & \Sigma_2 \end{bmatrix} \begin{bmatrix} V_1 & V_2 \end{bmatrix}^T, \tag{1.22}$$

where Σ_1 and Σ_2 contain the descending Hankel singular values. Finally, the projection matrices could be constructed as in (1.17), and the reduced-order model is obtained by

$$E_r = W^TEV, \quad A_r = W^TAV, \quad B_r = W^TB, \quad C_r = CV, \quad D_r = D. \tag{1.23}$$

In the above MOR, the dual GARE (1.21) may be solved by state-of-the-art matrix solvers in [59, 60]. These GARE solvers use Newton iteration that converts the quadratic matrix equations (generalized algebraic Riccati equations) to linear matrix equations (generalized Lyapunov functions), and then solve each generalized Lyapunov equation by (LR)-ADI. Consequently, the overall cost approximates that of solving tens of generalized Lyapunov functions. Note that some DSs may not be impulse-free, and the improper part may be extracted by spectral projectors. If the circuit topology is given, the spectral projector could be constructed by a closed form [17, 18]. Nevertheless, the spectral projector construction is not trivial for most DSs (such as DS models from EM solvers). A fast numerical implementation will be

presented in Chapter 5.

1.5 Thesis Contributions

The work included in this thesis consists of two parts. Chapters 2 to 4 propose a set of new methods for DS passivity assessments, including both admittance/impedance DSs and S-parameter DSs; Chapter 5 and Chapter 6 address some issues involved in DS MOR: passivity preservation and the multi-port problem.

1.5.1 Generalized Hamiltonian Methods (GHMs)

In Chapter 2, we present the generalized Hamiltonian method (GHM) for DSs with admittance or impedance transfer matrices.

First, a pre-processing step called improper part test (IMPT), is proposed to characterize the improper part without system decomposition. If the improper part is passive, GHM could be used to test the proper part.

Then, GHM is proposed. GHM is a generalization (and superset) of the widely used Hamiltonian method. But different from traditional Hamiltonian methods, GHM can be used to test the passivity of both standard state-space models and DS models, without system decomposition. Similar to the Hamiltonian method, the proposed GHM is capable of detecting and locating every possible nonpassive region, thus it could be used as a reliable test in DS passivity enforcements.

Then, we further develop a half-size variant of GHM, called HGHM. HGHM can be used to test the passivity of symmetric DSs. On top of all the advantages of GHM, HGHM is more efficient (8$\times$ faster over GHM). From the numerical perspective, HGHM is also more reliable.

1.5.2 Spectral Projector Technique and Fast GHM

Chapter 3 presents a DS passivity test for large-scale systems, such as those from EM solvers. We aim to efficiently test the proper part of a DS model even when its improper part is nonpassive.

First, we present the theories regarding canonical projectors, and then show how to construct a right (or left) spectral projector via a canonical projector technique. Based on the spectral projector technique, the proper and improper parts of a DS model can be separated in an elegant way.

However, the conventional canonical projector-based spectral projector construction is inefficient. To solve this problem, we present a fast numerical implementation, based on sparse LU-based fast null space construction, as well as low-rank matrix multiplication. To this end, the spectral projector could be efficiently computed for large-scale DSs.

After decomposing the original DS into its proper and improper subsystems, the improper part can be tested easily. To efficiently test the proper subsystem, we use the GHM approach presented in Chapter 2, based on fast numerical implementation. In our implementation, the multi-shift Arnoldi iteration [78] is extended to compute those generalized eigenvalues close to the imaginary axis. Since only a small part of the eigenvalues are needed for passivity test, the GHM-based verification can be applied to large systems with size up to 10^4.

1.5.3 S-Parameter GHMs (S-GHMs)

Chapter 4 addresses the passivity test of a scattering DS, based on the bounded realness of its transfer matrix.

We first extend the GHM theory to a scattering DS, to characterize the singular values of its transfer matrix; then, for symmetric S-parameter DSs, a half-size variant

of S-GHM, called S-HGHM, with better numerical accuracy and efficiency, is also developed.

With the S-GHM and S-HGHM theories, we can test general DS models very efficiently. We also present an interesting method for admittance/impedance DS passivity test: using Moebious transform, the original admittance/impedance DS is converted to a new S-parameter model, which is then tested by S-GHM/S-HGHM.

1.5.4 Fast DS PRBT

Chapter 5 is concerned with Gramian-based passivity-preserving MOR of DSs. We aim to solve two problems in DS MOR: 1) preservation of the possible improper part, if any; 2) preservation of system passivity. To achieve these objectives, we first use a spectral projector to extract the proper and improper subsystems efficiently; after that, we use PRBT to get a ROM of the proper subsystem.

For the reduction of the proper subsystem, we develop a fast algorithm to solve the dual generalized algebraic Riccati equations (GAREs). Unlike existing state-of-the-art GARE solver that uses Newton's iteration, we propose a generalized AQDI (GQADI) to solve the dual GAREs with much shorter CPU times. We then give the theoretical proofs of the convergence and well posedness of the proposed algorithm. Finally, noting the positive semidefiniteness of the Gramians, a low-rank algorithm called LR-GQADI is proposed, which solves the GARE with further speedup.

1.5.5 Block-Diaognal Structured MOR for Multi-Port DSs

Chapter 6 addresses the issue in the MOR of multi-port LTI descriptor systems. Multi-port systems are normally used in power grid simulation. Due to the huge port size, Krylov-subspace projections cannot generate good macromodels that allow fast subsequent simulation.

Our proposed block-diagonal structured model reduction (BDSM) can generate sparse and structured ROMs that can be efficiently simulated. First, using input matrix splitting and parallel connection of LTIs, a block-diagonal structured (but much larger) DS model is constructed, which has the same transfer matrix of the original one. Then we use Krylov subspace to generate the projection matrices. In the projection matrix construction, the columns corresponding to different ports are sorted to different groups, which finally results in block-diagonal structured projection matrices and ROMs. The BDSM has several advantages: 1) it is based on exact moment matching, thus it is very accurate; 2) it has the same size as traditional Krylov-subspace MORs, but the resulting ROMs are sparse and block-diagonal structured; 3) its special structure allows fast computation and very flexible parallel implementation; 4) in power grid simulation, the problem size of the BDSM ROM can be further scaled down, if the power gating technique is considered.

Chapter 2

Generalized Hamiltonian Methods (GHMs)

A generalized Hamiltonian method (GHM) and its half-size variant (HGHM) are proposed to characterize the spectral behaviors of descriptor systems (DSs). With the preprocess ImPT (Improper Part Test), GHM and HGHM can be applied to test the passivity of immittance (impedance or admittance) DSs without system decomposition, system index assumption or minimal realization requirement, which are the major bottlenecks of existing algebraic DS passivity tests. The proposed method allows exact detection of nonpassive frequency intervals which is not possible with frequency sweeping techniques. Numerical results confirm the effectiveness of the proposed method.

2.1 Introduction

This work is motivated by the demand of passive modeling of admittance or impedance on-chip components and electrical circuits in VLSI simulations [11,22,25]. In this case,

system passivity can be interpreted as the positive realness of system transfer matrix, which is of great importance for stable global simulations. However, nonpassive models may be generated from some stability-preserving algorithms (e.g., vector fitting (VF) [48] and balanced truncations (PVL) [57, 58]) or even some theoretically passivity-preserving techniques (e.g., [22]) on finite-precision machines. As a remedy, passivity enforcement techniques [11] can eliminate or mitigate passivity violations. These enforcements need to locate the possible nonpasive regions via passivity test in advance. For regular (or nonsingular) systems, numerous passivity assessments have been proposed. Readers are referred to [11, 14] and the references therein.

Nevertheless, DS passivity tests are much less developed compared with their regular system counterparts. The $O(n^6)$ computation renders the extended LMI (linear matrix inequality) tests [39, 42] impractical for general DSs. Reference [42] presents a cheaper method based on generalized Schur decomposition, but it poses strict restrictions on system observability and controllability. Some literatures assess positive realness via generalized algebraic Riccati equations (GAREs) [43, 44], but the admissible requirement is also a very strong condition for practical physical models. Furthermore, none of these methods can locate the possible nonpassive frequency regions, which is normally required in testing the validity of circuit and component models. Some decompose-and-test flows [46, 47] require the DSs to be minimal, and the system decomposition and transformation may induce large numerical errors (caused by possibly ill-conditioned matrix inversions). The eigenvalue-based DS passivity test in [64] is only applicable to scalar function. Frequency sweeping methods [20, 41] detect nonpassive regions at a set of frequency points, but they may miss nonpassive frequency intervals. Therefore, it is desirable to develop a passivity assessment that can identify the nonpassive regions of general DSs efficiently and accurately.

We propose, for the first time, a flexible passivity test flow for general DSs based on generalized Hamiltonian methods. The main contribution of this chapter includes:

1) GHM and HGHM to characterize the eigenvalues of DS spectral functions; 2) A complete DS passivity test based on ImPT, GHM and HGHM to test the improper and proper parts easily without system decomposition; 3) The observation that the GHM- and HGHM-based passivity tests are the supersets of traditional Hamiltonian method and its half-size [14] counterpart, respectively, as well as the connection of GHM with GAREs [43, 44]. Part of this work is presented in [65], which mainly discusses GHM and ImPT.

2.2 Review of DS Positive Realness

We first recall the positive realness of LTI models. For an immittance linear time-invariant (LTI) system, the (strict) passivity is equivalent to its square transfer matrix $H(s)$ being (strictly) positive real [39]:

1. $H(s)$ has no poles in $\mathrm{Re}(s) > 0$;
2. $\overline{H(s)} = H(\bar{s})$ where $\bar{o}$ stands for the conjugate of o;
3. The spectral function $G(j\omega) = \left(H(j\omega) + H^*(j\omega)\right)/2 \geq 0$ for all $\omega \in \mathbb{R}$ ($>$ for strict positive realness), where * means the conjugate transpose operation.

For a regular state-space system $H(s) = C(sI - A)^{-1}B + D$, its positive realness can be tested by the Hamiltonian matrix [14]:

$$M = \begin{bmatrix} \hat{A} & -\hat{R} \\ \hat{P} & -\hat{A}^T \end{bmatrix} \tag{2.1}$$

of which any purely imaginary eigenvalue defines a boundary frequency of passivity violations. In (2.1), $\hat{A} = A - B(D + D^T)^{-1}C$, $\hat{R} = B(D + D^T)^{-1}B^T$ and $\hat{P} = C^T(D + D^T)^{-1}C$.

In circuit modeling and reduction, we usually use the LTI DS:

$$E\dot{x} = Ax + Bu, \quad y = Cx + Du, \tag{2.2}$$

where $x \in \mathbb{R}^n$ denotes the state variables, $E, A \in \mathbb{R}^{n\times n}$, $B, C^T \in \mathbb{R}^{n\times m}$, $D \in \mathbb{R}^{m\times m}$, and $rank(E) \leq n$ ("=" corresponds to regular cases). The transfer matrix of (2.2) is

$$H(s) = C(sE - A)^{-1}B + D. \tag{2.3}$$

Here (A, E) is assumed to be regular, i.e., $det(sE - A)$ is not identically zero. There exists a Weierstrass form [39]:

$$(A, E) = W(\begin{bmatrix} F & 0 \\ 0 & I_{n-q} \end{bmatrix}, \begin{bmatrix} I_q & 0 \\ 0 & N \end{bmatrix})T, \tag{2.4}$$

where W and T are nonsingular, I_q denotes an identity matrix of dimension q, F and N (an index-μ nilpotent matrix, i.e., $N^\mu = 0$ and $N^{\mu-1} \neq 0$) correspond to the finite and infinite generalized eigenvalues of (A, E), respectively. The Weierstrass form implies

$$H(s) = \underbrace{C_p(sI_q - F)^{-1}B_p + M_0}_{H_p(s)} + \underbrace{\sum_{k=1}^{\mu-1} s^k M_k}_{H_{imp}(s)}, \tag{2.5}$$

where $\begin{bmatrix} C_p & C_\infty \end{bmatrix} = CT^{-1}$ and $\begin{bmatrix} B_p \\ B_\infty \end{bmatrix} = W^{-1}B$, $M_0 = D - C_\infty B_\infty$, $M_k = -C_\infty N^k B_\infty$ $(k = 1, ..., \mu - 1)$. $H_p(s)$ and $H_{imp}(s)$ are the proper and improper parts, respectively. The immittance DS in (2.5) is passive if and only if [39]: 1) $H_p(s)$ is passive; 2) $M_1 \geq 0$ and $M_k = 0$ for any $k \geq 2$. An LMI test [at the cost of $O(n^6)$] is developed in [39] for the characterization of DS positive realness.

1. **Sufficient Condition:** If there exists a solution X to the following LMIs:

$$\begin{bmatrix} A^TX + X^TA & X^TB - C \\ B^TX - C^T & -D - D^T \end{bmatrix} \leq 0, \;\; E^TX = X^TE \geq 0, \tag{2.6}$$

   then $H(s)$ defined by (2.3) is positive real.

2. **Necessary Condition:** Assume that (E, A, B, C, D) is a minimal realization of $H(s)$ and $D + D^T \geq M_0 + M_0^T$, then the LMIs in (2.6) have a solution X if $H(s)$ is positive real.

Obviously, besides the extremely expensive computation, the minimal realization requirement is also highly restrictive.

2.3 GHM and HGHM Theories for DSs

2.3.1 GHM for General DSs

Theorem 2.1: *Assume that λ is not an eigenvalue of $(D + D^T)/2$ for the stable DS (E, A, B, C, D) (i.e., any finite s satisfying $det(A - sE) = 0$ is located on the left half plane), then λ is an eigenvalue of $G(j\omega)$ if and only if $j\omega$ is a generalized eigenvalue of the matrix pencil $(J,\ K)$, defined as*

$$(J, K) = \left(\begin{bmatrix} A + BQ^{-1}C & BQ^{-1}B^T \\ -C^TQ^{-1}C & -A^T - C^TQ^{-1}B^T \end{bmatrix}, \begin{bmatrix} E & 0 \\ 0 & E^T \end{bmatrix} \right), \tag{2.7}$$

where $Q = (2\lambda I - D - D^T)$. Note that the matrix J is a Hamiltonian matrix.

Proof: Assume that λ is an eigenvalue of the spectral function defined as $G(j\omega) = (H(j\omega) + H^*(j\omega))/2$. Since the system matrices are real, we have $H^*(j\omega) = H^T(-j\omega)$,

then there exists $x \neq 0$, such that

$$2G(j\omega)x = \left(\begin{bmatrix} C & B^T \end{bmatrix} \Omega_\omega^{-1} \begin{bmatrix} B \\ -C^T \end{bmatrix} + D + D^T \right) x = 2\lambda x. \tag{2.8}$$

Here we have used Ω_ω to denote $\begin{bmatrix} j\omega E - A & \\ & j\omega E^T + A^T \end{bmatrix}$ for simplicity. We could rewrite (2.8) in a compact matrix form as

$$Q^{-1} \begin{bmatrix} C & B^T \end{bmatrix} z = x \tag{2.9}$$

with $z = \Omega_\omega^{-1} \begin{bmatrix} B \\ -C^T \end{bmatrix} x \neq 0$. By pre-multiplying both sides of (2.9) by $\Omega_\omega^{-1} \begin{bmatrix} B \\ -C^T \end{bmatrix}$, we further get

$$\Omega_\omega^{-1} \begin{bmatrix} B \\ -C^T \end{bmatrix} Q^{-1} \begin{bmatrix} C & B^T \end{bmatrix} z = z \tag{2.10}$$

which is essentially equivalent to

$$Jz = j\omega Kz. \tag{2.11}$$

To this end, we have shown that the imaginary scalar $j\omega$ is a generalized eigenvalue of matrix pencil (J, K) if λ is an eigenvalue of $G(j\omega)$.

To prove the converse, we denote $w := Q^{-1} \begin{bmatrix} C & B^T \end{bmatrix} z$ [which should be a nonzero vector, since $z \neq 0$ in (2.10)]. Pre-multiplying both sides of (2.10) by $Q^{-1} \begin{bmatrix} C & B^T \end{bmatrix}$, we would reach

$$Q^{-1} \begin{bmatrix} C & B^T \end{bmatrix} \Omega_\omega^{-1} \begin{bmatrix} B \\ -C^T \end{bmatrix} w = w, \tag{2.12}$$

which is equivalent to (2.8), implying λ is an eigenvalue of $G(j\omega)$ if $j\omega$ is a generalized eigenvalue of (J, K).

□

2.3.2 HGHM for Symmetric DSs

Next, we consider a special case: symmetric DSs. For symmetric DSs, the matrix pencil in GHM theory could be reduced to a half-size one, and the imaginary eigenvalue computation would be replaced by positive real eigenvalue calculation.

Theorem 2.2: *For symmetric DSs [i.e., $H(s) = H^T(s)$], if λ is not an eigenvalue of D, the matrix pencil (J, K) defined in (2.7) could be reduced to a half-size matrix pencil*

$$(J_h, K_h) = (A + B(\lambda I - D)^{-1}C,\ EA^{-1}E), \tag{2.13}$$

and accordingly, the generalized eigenvalue $j\omega$ could be replaced by $\beta = \omega^2$.

Proof: Given a symmetric DS, we have$H^*(j\omega) = H(-j\omega) = -C(j\omega E + A)^{-1}B + D$. In such case, the matrix pencil (J, K) could be written as

$$(J, K) = \left(\begin{bmatrix} S & T \\ -T & -S \end{bmatrix}, \begin{bmatrix} E & 0 \\ 0 & E \end{bmatrix} \right) \tag{2.14}$$

where $S = A + B(2\lambda I - 2D)^{-1}C$, $T = B(2\lambda I - 2D)^{-1}C$. Noting that $(J', K') = Z(J, K)Z^T$ has the same generalized eigenvalues as (J, K) if Z is invertible, if we set $Z = \begin{bmatrix} I & I \\ I & -I \end{bmatrix}$, then we could get a structured matrix pencil

$$(J', K') = \left(\begin{bmatrix} 0 & 2(S-T) \\ 2(S+T) & 0 \end{bmatrix}, \begin{bmatrix} 2E & \\ & 2E \end{bmatrix} \right). \tag{2.15}$$

Assume that λ is an eigenvalue of $G(j\omega)$, then $j\omega$ is a generalized eigenvalue of (J, K) (which is a trivial result from the proposed GHM theory). Because (J, K) and (J', K') have the same spectrum, $j\omega$ should also be a generalized eigenvalue of (J', K'). Based on this, we know that there exist x_1 and x_2, such that

$$\begin{bmatrix} -j\omega E & S-T \\ S+T & -j\omega E \end{bmatrix} \begin{bmatrix} x_1 \\ x_2 \end{bmatrix} = 0, \quad \begin{bmatrix} x_1 \\ x_2 \end{bmatrix} \neq 0. \tag{2.16}$$

This is a size-$2n$ matrix equation, which can be further reduced to

$$(J_h - \omega^2 K_h)x_1 = 0, \;\; x_1 \neq 0. \tag{2.17}$$

Therefore, $\beta = \omega^2$ is a generalized eigenvalue of (J_h, K_h).

Conversely, by setting $x_2 = j\omega(S-T)^{-1}x_1$, we can arrive at (2.16) from (2.17) and then go back to Theorem 2.1.

□

2.4 Admittance/Impedance DS Passivity Assessment

DS passivity test is more involved than its standard state-space model because it requires testing both the proper and improper part. In this section, we introduce a passivity verification flow for DSs with admittance or impedance transfer matrix, based on the proposed GHM and HGHM theory. In the first step, a preprocessing step is needed to check the improper part.

2.4.1 Testing the Improper Part by ImPT

We begin the passivity verification with **ImPT** (**Im**proper **P**art **T**est), which is developed to characterize the improper part of a DS. Denoting the highest order of $H_{imp}(s)$ by the integer $\zeta - 1$ ($1 \leq \zeta \leq \mu$), then the improper part could be written as $H_{imp}(s) = \sum_{k=1}^{\zeta-1} s^k M_k$ with $M_{\zeta-1} \neq 0$. Given a set of positive real scalars s_i ($i = 1, 2, ...$) with $s_{i+1} = \eta s_i$ ($\eta > 1$), the matrix norm of $H(s_i)$ could be written as

$$\|H(s_i)\| = s_i^{\zeta-1} \left\| M_{\zeta-1} + \frac{M_{\zeta-2}}{s_i} + \cdots + \frac{H_p(s_i)}{s_i^{\zeta-1}} \right\|. \tag{2.18}$$

Clearly, if s_i is large enough, the highest-order term $s_i^{\zeta-1} M_{\zeta-1}$ would dominate $H(s_i)$. As a result, we have $M_{\zeta-1} + \frac{M_{\zeta-2}}{s_i} + \cdots + \frac{H_p(s_i)}{s_i^{\zeta-1}} \approx M_{\zeta-1}$, which further implies

$$\frac{\|H(s_{i+1})\|}{\|H(s_i)\|} \approx \eta^{\zeta-1}. \tag{2.19}$$

Consequently, the system index can be evaluated by

$$\zeta = \left[\log_\eta \left(\frac{\|H(s_{i+1})\|}{\|H(s_i)\|} \right) \right] + 1, \tag{2.20}$$

where $[o]$ represents rounding operation. We select positive real scalar s_i in the computation based on two reasons: 1) for a stable DS, its poles are located on the left-half plane, thus the peaks from the proper part could be avoided; 2) numerical calculation on real numbers is faster and more reliable than on complex numbers. In practical implementations, η can be set around $10 - 100$, and we may start with a randomly selected number (e.g., $s_1 = 10^5$) and then replace s_i with s_{i+1} until $\left| \left[\log_\eta \left(\frac{\|H(s_{i+1})\|}{\|H(s_i)\|} \right) \right] - \log_\eta \left(\frac{\|H(s_{i+1})\|}{\|H(s_i)\|} \right) \right| < \delta$. Here δ is a small positive constant used to control numerical errors. Since s_i is exponentially increased, the iteration would converge very fast. If $\zeta \geq 3$, we have $M_2 \neq 0$ and thus the DS is nonpassive, since

repeated infinite poles exist in the transfer matrix. If $\zeta = 2$, we have $H(s_i) = H_p(s_i) + H_{imp}(s_i) \approx s_i M_1 + M_0$, then the coefficient of the improper part could be computed by

$$M_1 \approx \frac{H(s_{i+1}) - H(s_i)}{s_{i+1} - s_i}. \tag{2.21}$$

With a numerical error control, (2.21) can be used to compute M_1 with a high accuracy. In impulse-free DSs, the denominator in (2.20) might approach zero in case $M_0 = 0$, and directly using (2.20) may give erroneous results. In this case, we replace $H(s_i)$ with $H(s_i) + I_m$ to compute ζ.

Hereafter, we assume that $H_{imp}(s)$ has been checked by ImPT, $\zeta \leq 2$, and $M_1 \geq 0$ (or else the passivity test terminates since we have already known the improper part is nonpassive). In this case $H_p(j\omega) + H_p^*(j\omega) = H(j\omega) + H^*(j\omega)$, then the proper part can be tested by GHM or HGHM.

2.4.2 Testing the Proper Part by GHM and HGHM

In admittance/impedance passivity assessment, we are most interested in the situations where the positive realness is violated. Clearly, $\lambda = 0$ is the boundary case where a system becomes nonpassive from being passive (or vice versa). By setting $\lambda = 0$, we could have $(J, K) = (J_0, K_0)$ with

$$J_0 = M = \begin{bmatrix} \hat{A} & -\hat{R} \\ \hat{P} & -\hat{A} \end{bmatrix}, \quad K_0 = K. \tag{2.22}$$

Here M is the Hamiltonian matrix [66] defined in (2.1). For HGHM, setting $\lambda = 0$ gives a half-size matrix pencil

$$(J_{h0}, K_{h0}) = (A - BD^{-1}C, \quad EA^{-1}E). \tag{2.23}$$

The resulting matrix pencils (J_0, K_0) and (J_{h0}, K_{h0}) could be used to test the positive realness of a DS, i.e., the passivity of an admittance or impedance DS model: any purely imaginary (or positive real) generalized eigenvalue $j\omega$ (or $\beta = \omega^2$) of (J_0, K_0) (or (J_{h0}, K_{h0}) for symmetric DSs) defines a crossover angular frequency ω where the eigenvalue of $G(j\omega)$ crosses the imaginary axis on the complex plane. These crossover points can be used to locate the possible nonpassive frequency intervals. Denote $\Theta := \{\omega_1, ..., \omega_p\}$ where ω_i $(i = 1, ..., p)$ represents the p crossover points obtained from GHM or HGHM, then the passive and nonpassive regions of $H(j\omega)$ can be identified as follows.

1. If Θ is empty, test $G(j\omega_0)$ at a randomly selected sampling point ω_0. The system is strictly passive if $G(j\omega_0) > 0$, otherwise nonpassive at any frequency point.

2. If Θ is not empty, test $G(j\omega'_k)$ at $\omega'_k \in \ell_k$ $(k = 1, 2, ..., p+1)$ where $\ell_1 = (0, \omega_1)$, $\ell_i = (\omega_{i-1}, \omega_i)$ for $i = 2, ..., p$ and $\ell_{p+1} = (\omega_p, \infty)$. If $G(j\omega'_k) > 0$, then the DS is passive in the interval ℓ_k, otherwise nonpassive in ℓ_k.

An illustrative example is shown in Fig. 2.1. For this DS, GHM and HGHM produce 3 crossover points. We randomly select one sampling point in each interval. Since $G(j\omega'_3) < 0$ and $G(j\omega'_k) > 0$ for $k = 1, 2, 4$, the DS is nonpassive in (ω_2, ω_3) but passive in other frequency bands.

2.4.3 Equivalent Model Conversion

At the first glance, GHM/HGHM test requires $D + D^T$ to be nonsingular, which is not always satisfied in practical DSs. In this case, we need to perform an equivalent model conversion in advance. Assume that $\alpha \in \mathbb{R}$ is not an eigenvalue of D, then $D_\alpha = \alpha I - D$ is nonsingular. A new DS $H'(s)$ realized by (E', A', B', C', D') can be

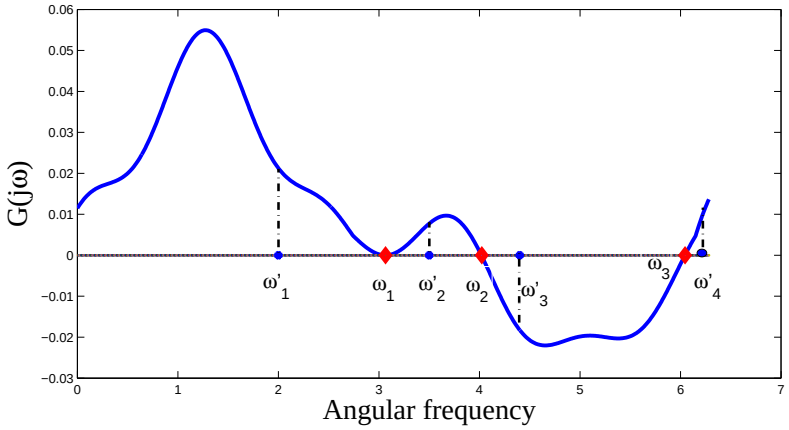

Figure 2.1: An illustrative example for nonpassive region identification.

constructed as

$$E' = \begin{bmatrix} E & \\ & 0 \end{bmatrix}, \quad A' = \begin{bmatrix} A & \\ & D_\alpha^{-1} \end{bmatrix}, \quad B' = \begin{bmatrix} B \\ I \end{bmatrix}, \tag{2.24}$$
$$C' = \begin{bmatrix} C & I \end{bmatrix}, \quad D' = \alpha I.$$

We note that the resulting DS model has the same transfer matrix as the original one [i.e, $H'(s) = H(s)$], but $D' + D'^T$ and D' are nonsingular. Therefore, the proper part of $H(s)$ can be assessed by testing the passivity of $H'(s)$ via GHM or HGHM. We remark that, given a standard state-space model (with $E = I$), the equivalent model conversion would generate a DS model, which can be tackled by GHM, or HGHM if its transfer matrix is symmetric. The main computation in GHM and HGHM tests is the $O(n^3)$ generalized eigenvalue solution. HGHM-based test should be 8 times faster than GHM-based method due to its half-size nature. With equivalent model conversion, GHM (HGHM) can also be applied to (symmetric) regular systems with singular $D + D^T$ (D) where traditional Hamiltonian method and half-size singularity test [14] fail to work.

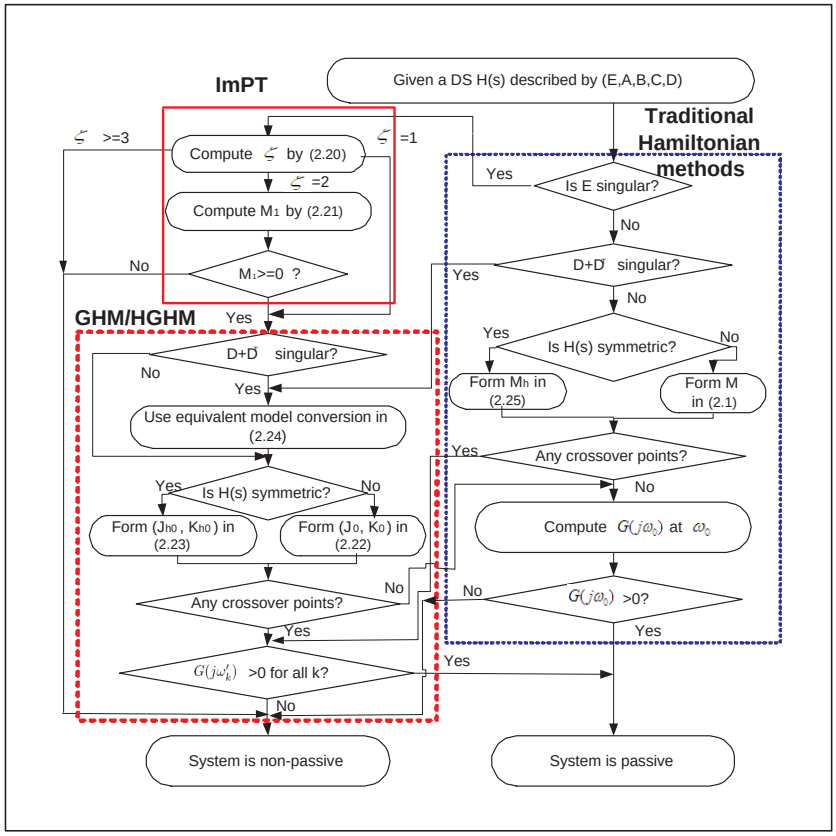

Figure 2.2: The complete passivity test flow for DSs, including regular systems.

2.4.4 Connection to Traditional Hamiltonian Methods

An interesting observation is that the proposed GHM and HGHM methods are in fact a superset of the widely used Hamiltonian method [11] and its half-size variant [14]. Given a standard state-space models ($E = I$), the generalized eigenvalue solution of (J, K) reduces to the eigenvalue solution of J defined in (2.7), which has been widely used in passivity enforcements [11] for nonpassive regular state-space models. To check system passivity, we could set $\lambda = 0$ and get $J_0 = M$ [defined in (2.1)]. For symmetric standard state-space models, the generalized eigenvalue solution of

(J_{h0}, K_{h0}) in (2.23) can be replaced by the eigenvalue solution of

$$M_h = A(A - BD^{-1}C) \tag{2.25}$$

which is the half-size singularity test recently proposed in [14].

Therefore, Hamiltonian method and its half-size variant are special cases of GHM and HGHM, respectively. All of them detect passivity violation regions by finding boundary frequencies, but GHM and HGHM can deal with DSs as well as regular systems, without restrictions on D, which implies much wider applications. The complete test flow is illustrated in Fig. 2.2, where ImPT and traditional Hamiltonian methods are also included.

2.4.5 Strict Positive Realness of Impulse-free DSs

GARE [43,44] is widely used to characterize the positive realness of impulse-free DSs. This part shows its connection with GHM.

Lemma 2.1: *Suppose (A, E) is regular, impulse-free and $D+D^T > 0$ (otherwise, the proposed equivalent model conversion can be performed to meet this requirement), then the following statements are equivalent.*

1) $H(s)$ is strictly positive real.

2) The generalized algebraic Riccati equation (GARE)

$$\hat{A}^T X + X^T \hat{A} + X^T \hat{R} X + \hat{P} = 0,\ E^T X = X^T E \geq 0 \tag{2.26}$$

has a solution X such that $(\hat{A} + \hat{R}X, E)$ is stable.

3) The matrix pencil (J_0, K_0) has no purely imaginary generalized eigenvalues and $M_0 > 0$ [M_0 is defined in (2.5)].

Proof: The equivalence of 1) and 2) has been proved in [43]. The proof of 3)⇒1)

is trivial based on the GHM theory. From Statement 2), we get

$$\begin{aligned}
\det(J_0 - sK_0) &= \det\left(\begin{bmatrix} I & \\ -X^T & I \end{bmatrix}(J_0 - sK_0)\begin{bmatrix} I & \\ X & I \end{bmatrix}\right) \\
&= \det\left(\begin{bmatrix} sE - (\hat{A} + \hat{R}X) & 0 \\ 0 & sE^T + (\hat{A}^T + X^T\hat{R}^T) \end{bmatrix}\right) \\
&= \det\Big(sE - (\hat{A} + \hat{R}X)\Big)\det\Big(sE + (\hat{A} + \hat{R}X)\Big).
\end{aligned} \tag{2.27}$$

Since $(\hat{A} + \hat{R}X, E)$ is stable, $\hat{A} + \hat{R}X \pm j\omega E$ is nonsingular. Therefore, the matrix pencil (J_0, K_0) has no purely imaginary generalized eigenvalues. The equivalence of 1) and 2) also implies $M_0 > 0$, therefore, 3) can be derived from 2) and the above statements are equivalent.

□

We remark that GARE requires (E, A) to be admissible, but GHM only requires $M_1 = M_1^T$. GHM can locate the passive/nonpassive regions whereas GARE cannot.

2.5 Numerical Examples

This section presents some numerical examples to verify the proposed passivity test flow. All experiments are performed in MATLAB R2006a on a 2.66-GHz 2G-RAM PC.

2.5.1 MNA Example for ImPT

This 9-port order-10913 MNA model describes a large RLC network. Since the RLC circuit is passive, ζ should be 1 or 2 and $M_1 \geq 0$. To show the convergence of ImPT, we set $s_1 = 10^3$ and $\eta = 10$, and plot the numerical error ε_i for $i = 1, 2, .., 6$ in

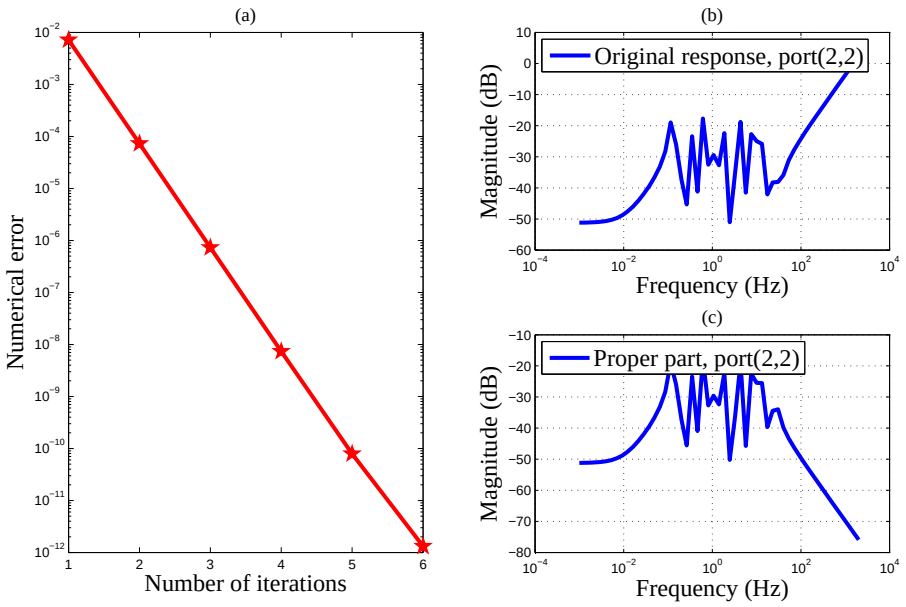

Figure 2.3: ImPT test for the MNA model [the iteration number means i in (2.20)].

Fig. 2.3(a), which shows ε_i decreases by about 2 orders in each iteration. Setting $s_i = 10^4$ and $s_{i+1} = 10^5$ in (2.20) yields $\zeta = 2$ after 2.1 seconds. The frequency response of port-2 to port-2 in Fig. 2.3(b) shows its magnitude increases linearly in the high-frequency band, which also implies $\zeta = 2$. Via (2.21), we get a 9×9 diagonal matrix with positive diagonal elements, so $M_1 > 0$.

To verify the numerical accuracy of M_1, we compute ζ of the "proper part" $H_1(s) = H(s) - sM_1$ by (2.20). We get $\zeta = 1$ for $H_1(s)$, implying $H_1(s)$ is impulse-free as expected. Meanwhile, the port-2 to port-2 response of $H_1(s)$ in Fig. 2.3(c) also shows $H_1(s)$ has no impulsive part. This example shows that ImPT is efficient and accurate in practical implementations.

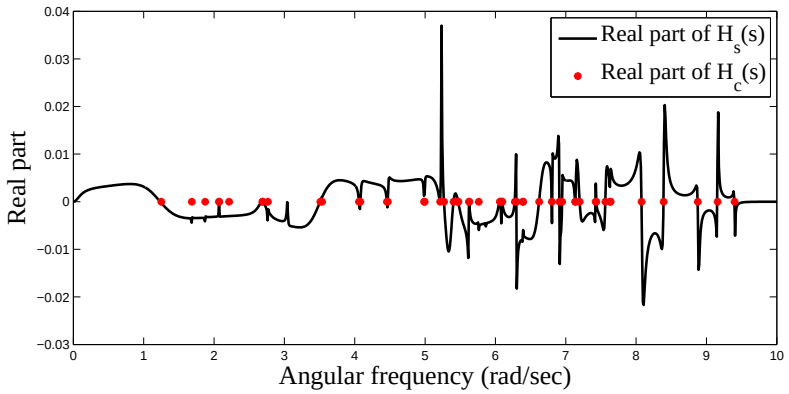

Figure 2.4: GHM and frequency sweeping results for the PEEC model.

2.5.2 PEEC Example for GHM

The SISO order-51 reduced model is obtained by performing PRIMA [22] on a PEEC DS model of dimension 480 with $D = 0$. Both of them are nonpassive in the low-frequency band. ImPT shows they are impulse-free. After equivalent model conversion, GHM test on the original model produces 59 crossover points. We compute the transfer functions at these 59 points (denoted by $H_c(s)$). Fig. 2.4 shows that the real part of $H_c(s)$ is zero. By frequency sweeping, we get 29 boundary frequency points. The frequency sweeping result $H_s(s)$ is plotted in Fig. 2.4. We note that all these 29 points are also detected by GHM. However, the other 30 crossover points are missed in frequency sweeping test. Therefore, GHM is more reliable than frequency sweeping.

For the reduced model, GHM produces 4 purely imaginary results listed in Table 2.1, which represent 2 crossover frequency points. We also plot the real part of the transfer function of the reduced model ($H_r(s)$) in Fig. 2.5. The GHM results are accurately located at the crossover points of $real\,(H_r(s))$ with the x-axis. We note that GHM test results in Table 2.1 contain some numerical noise in the real parts, which is also observed in traditional Hamiltonian method [14].

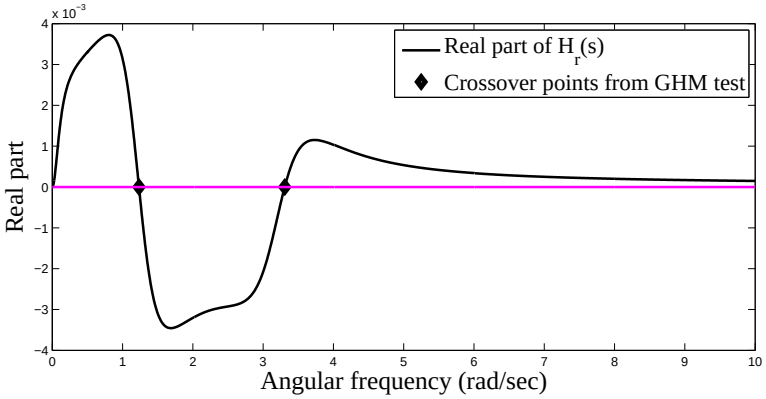

Figure 2.5: Real part of $H_r(s)$.

Table 2.1: GHM test results for the reduced model.

Imaginary generalized eigenvalues of (J_0, K_0)	$H_r(j\omega)$
3.65e-13 $\pm$ $j3.3078$	0.0000 $+j0.0031$
5.00e-14 $\pm$ $j1.2345$	0.0000 $-j0.0060$

2.5.3 A SAW Filter for HGHM

This order-126 admittance symmetric DS is from a 3-terminal SAW filter. ImPT shows this DS is impulse-free. HGHM test produces 3 positive real generalized eigenvalues, and GHM test produces 6 imaginary generalized eigenvalues. Table 2.2 shows that the results from GHM test have numerical noise in the real parts, but HGHM does not suffer from this problem. The 3 crossover frequency points from HGHM are plotted in Fig. 2.6, which shows the HGHM test is very accurate.

2.5.4 CPU Time Comparison

We compare the CPU timing of GHM and HGHM with two decompose-and-test methods: SHH [46] and Weierstrass passivity test [47]. For fairness, in decompose-and-test routines the proper parts are tested by Hamiltonian method. Experiments are performed on some symmetric DSs with order from 50 to 800. The CPU times

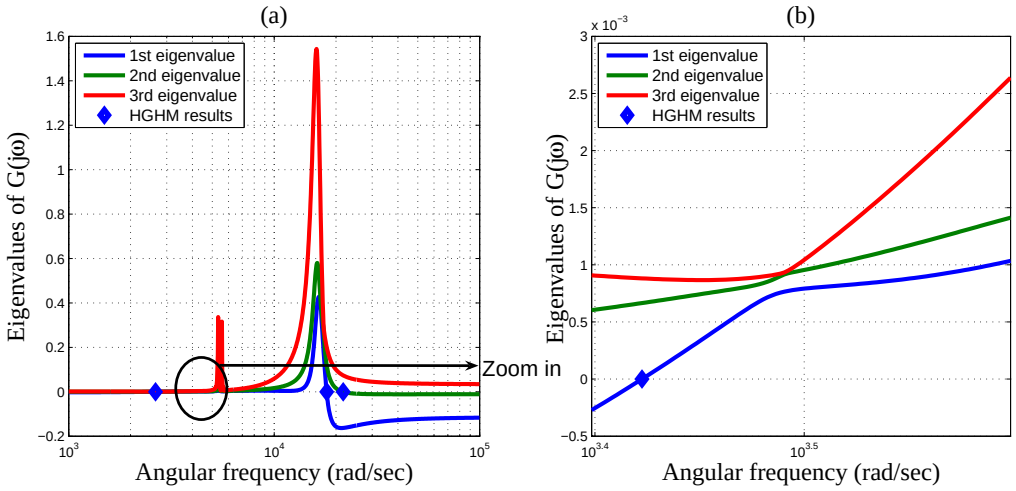

Figure 2.6: HGHM test for the SAW model.

Table 2.2: GHM and HGHM test results for the SAW model.

Imaginary results of GHM	Positive results of HGHM (β)	$\sqrt{\beta}$
$-1.4\text{e-}8 \pm j21671.377$	469648579	21671.377
$-1.9\text{e-}8 \pm j18029.84$	325075192.6	18209.84
$3.38\text{e-}8 \pm j2645.316$	6997698.35	2645.316

of GHM, HGHM, SHH and Weierstrass passivity tests are listed in Table 2.3. It is shown that HGHM is about 8 times faster than GHM, which is expected due to its half-size property. GHM is (> 2 times) faster than SHH. The additional cost of SHH is mainly from system decompositions. GHM, HGHM and SHH are all faster than Weierstrass test, which coincides with the observations in [46].

2.6 Summary

A new DS passivity test flow based on GHM and HGHM has been proposed for the first time. The most significant advantage of the proposed method is its ability of accurately detecting the possible nonpassive regions, some of them may be missed with frequency sweeping techniques. With ImPT and equivalent model conversion, GHM

Table 2.3: CPU times (sec) of different DS passivity tests.

Model order	Weierstrass	SHH	GHM	HGHM
50	0.2270	0.0781	0.0156	0.0013
100	0.4470	0.2969	0.1406	0.0156
150	1.1093	0.9375	0.3906	0.0625
200	2.6872	2.3281	0.8706	0.1250
300	10.725	8.2500	3.3750	0.3906
400	32.781	20.125	7.7938	0.8906
500	51.676	39.719	17.328	1.7788
600	124.83	69.208	25.813	2.9688
700	161.21	108.40	38.906	4.9219
800	289.37	166.64	65.670	7.6406

and HGHM can be used to deal with general and symmetric DSs, respectively, without system decompositions. Experiments have demonstrated the much higher accuracy of GHM than frequency sweeping, and faster computation than SHH and Weierstrass test. In symmetric DSs, HGHM enjoys a $8\times$ speedup and a higher numerical accuracy over GHM.

Chapter 3

Projector-Based Passivity Test for Large Descriptor Systems

This chapter presents an efficient passivity test based on canonical projector techniques for admittance/impedance DSs with large sizes. The test features a natural flow that first evaluates the index of a DS by matrix chain, followed by possible decoupling into its proper and improper subsystems by spectral projectors. Explicit state-space formulations for respective subsystems are derived to facilitate further processing such as MOR and/or passivity enforcement. Efficient projector construction and a fast generalized Hamiltonian test for the proper-part passivity are also elaborated. Numerical examples then confirm the superiority of the proposed method over existing passivity tests for DSs based on linear matrix inequalities (LMIs) or skew-Hamiltonian/Hamiltonian (SHH) matrix pencils.

3.1 Introduction

The GHM methods in Chapter 2 has provided a reliable solution to admittance/impedance DS models. Two issues still need to be addressed. First, in GHM test, the proper

part is tested based on the assumption that the improper part is passive, otherwise, the passivity test flow terminates. Second, the complexity of GHM is $O(n^3)$, which is prohibitively expensive for large-scale DS models (such as those extracted from EM field solvers). In practice, we expect to verify the validity of the proper part even when the improper part is nonpassive, such that passivity enforcement could be used to modify the model. In such a case, we need to extract the proper and improper parts from a given DS. Also, we expect to reduce the complexity of passivity verification scheme to extend its application to larger systems. Therefore, faster numerical implementation is highly desired.

To overcome the computational hurdle of system decomposition, the emerging canonical projector technique [19, 73, 74] is revised and utilized to formulate a highly efficient DS passivity test. In short, the canonical projectors give rise to a spectral projector that provides a natural and conceptually simple way to decouple a DS into its proper (impulse-free) subsystem and improper (impulsive) subsystem, if any. Such decoupling is considered the major difficulty in the passivity tests for DSs [46] (this is different from the early work of Cauer [75] on passive systems based on matrix polynomial transfer functions where subsystem decomposition is trivial compared to the otherwise DS formulation here). A major difference that marks the efficiency of the proposed method over existing ones is the early knowledge of the matrix pencil index, which quickly manifests as a direct consequence of constructing the matrix projector chain. Given that an (infinite) minimal passive system is of index at most two, the test quickly screens out nonpassive systems after two initial matrix chain iterations. Then, depending on the need, the proper and improper parts can be completely decoupled via spectral projectors and respectively tested for passivity.

In this chapter, we present a novel LU-based construction of projectors and an efficient implementation of the generalized Hamiltonian method proposed in Chapter 2, for testing the passivity of the proper part. Such combination has made the

proposed test truly applicable to large-scale practical DSs, as demonstrated in the numerical section wherein the model sizes are up to 10^4. We also present a concise complexity analysis of existing DS passivity tests.

3.2 DS Passivity and System Decomposition

We study a linear time-invariant (LTI) DS in the form

$$E\dot{x} \ = Ax + Bu, \ \ y = Cx + Du, \tag{3.1}$$

where $E, A \in \mathbb{R}^{n\times n}$ and $B, C^T \in \mathbb{R}^{n\times m}$. Also, $u, y \in \mathbb{R}^m$ and $x \in \mathbb{R}^n$ are the input, output and state vectors, respectively. The matrix E is generally singular with $\text{rank}(E) \leq n$. We assume that the matrix pencil $\lambda E - A$ is regular, i.e., $\det(\lambda_0 E - A) \neq 0$ for some $\lambda_0 \in \mathbb{C}$. Recalling from Chapters 1 & 2, we have the *Weierstrass canonical form* [73]:

$$E = W \begin{bmatrix} I_q & 0 \\ 0 & N \end{bmatrix} T, \ \ A = W \begin{bmatrix} J & 0 \\ 0 & I_{n-q} \end{bmatrix} T, \tag{3.2}$$

as well as the left and right (spectral) projectors, P_l and P_r, respectively, as

$$P_l = W \begin{bmatrix} I_q & 0 \\ 0 & 0 \end{bmatrix} W^{-1}, \ \ P_r = T^{-1} \begin{bmatrix} I_q & 0 \\ 0 & 0 \end{bmatrix} T. \tag{3.3}$$

Given either of them, the DS transfer matrix can be decomposed as follows

$$\begin{aligned} G(s) =& D + C(sE - A)^{-1}B \\ =& \underbrace{D - C_\infty B_\infty + C_p(sI_q - J)^{-1}B_p}_{G_p(s)} \\ & \underbrace{-sC_\infty N B_\infty - s^2 C_\infty N^2 B_\infty - s^3 C_\infty N^3 B_\infty - \cdots}_{G_\infty(s)}, \end{aligned} \tag{3.4}$$

where $G_p(s)$ is the proper part (bounded as $s \to \infty$) and $G_\infty(s)$ the improper part (unbounded as $s \to \infty$) of $G(s)$.

If $G(s)$ in (3.4) is viewed as

$$G(s) = \overbrace{\underbrace{G_{sp}(s)}_{\text{strictly proper}} + M_0}^{G_p(s)} + \underbrace{sM_1 + \sum_{k=2}^{\infty} s^k M_k}_{G_\infty(s)}, \tag{3.5}$$

then $G(s)$ is positive real if and only if $G_p(s)$ is positive real, $M_1 \geq 0$ and $M_k = 0$ for $k \geq 2$. Comparing (3.5) and (3.4), it is obvious that (3.1) is passive if and only if $G_p(s)$ in (3.4) is passive and $M_1 = -C_\infty N B_\infty \geq 0$, whereas $C_\infty N^i B_\infty = 0$, $i = 2, 3, \cdots$. Consequently, a key to testing the passivity of a DS is to first decouple it into its proper and improper parts.

3.3 Matrix Projector Chain

Setting $E_0 := E$ and $A_0 := A$, we consider a matrix chain

$$E_{j+1} := E_j + A_j Q_j, \quad A_{j+1} := A_j P_j, \tag{3.6}$$

where Q_j is a projector *onto* $\ker E_j$, i.e., $Q_j^2 = Q_j$ and $\operatorname{im} Q_j = \ker E_j$, and $P_j = I - Q_j$ is a projector *along* $\ker E_j$ for $j = 0, 1, \ldots$. Obviously, $P_j Q_j = Q_j P_j = 0$. The

following theorem establishes the properties of the matrices E_j's.

Theorem 3.1 *[73] For a regular index-μ pencil $\lambda E - A$, the matrices $E_0, \cdots, E_{\mu-1}$ are singular, while E_μ is nonsingular.*

Consequently, for the matrix chain $\{E_j, A_j\}$ we have:

- If E_1 is nonsingular, i.e., $\mu = 1$ or $N = 0$, then system (3.1) is impulse-free [46]. In this case, a standard state space system can be extracted and tested for passivity, see Section 3.4.1.

- If E_1 is singular but E_2 is nonsingular, we then proceed to form the spectral projector P_r (or P_l) through constructing canonical projectors, which allows the decoupling of $G(s)$ into the proper and improper parts $G_p(s)$ and $G_\infty(s)$, respectively.

- If E_2 is singular, then (infinite) minimality of the DS dictates $M_k \neq 0$ for $k \geq 2$ [39] (see also discussion #3 in Section 3.7), so the system is nonpassive and the passivity test is complete.

Next, we present some important properties of the matrix chain.

1. Post-multiplying the left equation in (3.6) by Q_j and P_j, respectively, yields

$$E_{j+1}Q_j = A_jQ_j, \tag{3.7a}$$

$$E_{j+1}P_j = E_j, \tag{3.7b}$$

   for $j = 0, 1, \cdots, \mu - 1$.

2. The projectors $Q_0, \cdots, Q_{\mu-1}$ are called *admissible* if they satisfy $Q_jQ_i = 0$ for $j > i$. Many new properties arise from using admissible projectors. For

example, for $j = 0, \cdots, \mu - 1$, we have

$$E_\mu Q_j = A_j Q_j, \tag{3.8a}$$

$$A_{j+1} = A - E_\mu (Q_0 + \cdots + Q_j). \tag{3.8b}$$

3. *Canonical projectors* are admissible projectors that further satisfy

$$\begin{aligned} Q_j &= Q_j P_{j+1} \cdots P_{\mu-1} E_\mu^{-1} A_j \\ &= Q_j P_{j+1} \cdots P_{\mu-1} E_\mu^{-1} A, \end{aligned} \tag{3.9}$$

for $j = 0, \cdots, \mu - 2$, and

$$Q_{\mu-1} = Q_{\mu-1} E_\mu^{-1} A_{\mu-1} = Q_{\mu-1} E_\mu^{-1} A. \tag{3.10}$$

The second equality signs in (3.9) and (3.10) can be established from (3.8b).

4. In the matrix chain (3.6), the projector Q_j is, generally, not unique as only its range is constrained. Suppose that $\bar{Q}_j = \bar{Q}_j^2$ is another projector onto $\ker E_j$. Then $\bar{Q}_j Q_j = Q_j$, $Q_j \bar{Q}_j = \bar{Q}_j$ and $-\bar{Q}_j P_j = Q_j \bar{P}_j$. This permits a relationship between the E_{j+1}'s generated by different projectors. We have

$$\begin{aligned} \bar{E}_{j+1} &= E_j + A_j Q_j \bar{Q}_j = E_j + A_j Q_j (I - \bar{P}_j) \\ &= (E_j + A_j Q_j)(I + \bar{Q}_j P_j) \\ &= E_{j+1}(I + \bar{Q}_j P_j). \end{aligned} \tag{3.11}$$

Provided E_{j+1} is invertible, the inverse of $\bar{E}_{j+1}$ is easily shown to be $\bar{E}_{j+1}^{-1} = (I - \bar{Q}_j P_j) E_{j+1}^{-1}$.

The following depicts the formation of canonical and spectral projectors for the

non-trivial case $\mu = 2$. Compared to [19], our presentation is highly straightforward and the proofs in the appendices are either new or much more elegant.

3.3.1 Constructing Canonical projectors

Setting $E_0 := E$ and $A_0 := A$, the matrix chain in the case of $\mu = 2$ takes the form

$$E_1 := E_0 + A_0 Q_0 \quad \text{and} \quad A_1 := A_0 P_0, \tag{3.12a}$$

$$E_2 := E_1 + A_1 Q_1, \tag{3.12b}$$

where E_2 is nonsingular. The projectors Q_0 and Q_1 in (3.12) are, generally, neither canonical nor admissible, but a new matrix chain with canonical (and, therefore, admissible) projectors can be derived from (3.12) with careful reformulation, as illustrated in Appendix 3.9.1. In short, the canonical projectors Q_1' and Q_0' can be computed as

$$Q_1' = Q_1 E_2^{-1} A_1, \tag{3.13a}$$

$$\begin{aligned} Q_0' &= Q_0 P_1' E_2'^{-1} A_0 = Q_0 P_1' (I - Q_1' P_1) E_2^{-1} A_0 \\ &= Q_0 P_1' E_2^{-1} A_0 = Q_0 (I - Q_1 E_2^{-1} A_1) E_2^{-1} A_0. \end{aligned} \tag{3.13b}$$

3.3.2 Constructing Spectral Projectors

Following from above, an important result of canonical projectors is that the right spectral projector P_r is readily given by

$$P_r = P_0' P_1' = (I - Q_0')(I - Q_1'). \tag{3.14}$$

The proof is shown in Appendix 3.9.2. Via the expressions in (3.13) and (3.14) [or (3.47)], it can be shown that simple analytical spectral projectors are readily derived for some structured DSs [56, 77], thereby allowing fast spectral decomposition. Nonetheless, analytical projectors generally do not exist and specific numerical considerations are needed for practical spectral projector construction, as will be discussed in Section 3.5.1.

3.4 Passivity Test

The canonical projector technique provides a natural way to decouple the proper (impulse-free) and improper (impulsive) parts of the DS in (3.1), which translates into a highly effective way for checking passivity based on the conditions listed after (3.5). Moreover, all that is needed is one, either the left or right, spectral projector. Without loss of generality, we assume the availability of P_r in (3.3). The case when P_l is available follows analogously. In the following, we see how P_r permits a simple and explicit construction of the proper and improper subsystems by the additive decomposition procedure.

3.4.1 Additive Decomposition by Spectral Projectors

Assume that the proper part is realized by $G_p(s) = \tilde{C}(s\tilde{E} - \tilde{A})^{-1}\tilde{B} + \tilde{D}$. With spectral projectors, the proper subsystem can be formed in various ways. By additive decomposition, a regular system can be constructed explicitly as

$$\begin{aligned} &\tilde{E} = EP_r - A(I - P_r), \tilde{A} = A, \\ &\tilde{C} = CP_r, \tilde{B} = B, \tilde{D} = M_0, \end{aligned} \tag{3.15}$$

where M_0 is readily obtained from (3.16) below. It is straightforward to prove that $\tilde{E}$ is nonsingular by this formulation, thus no further efforts (such as SVD) are needed to convert this DS to a regular one. To extract $G_\infty(s)$ in (3.4), we first construct an improper DS using the right spectral projector

$$\begin{aligned} G_1(s) &= D + C(I - Pr)(sE - A)^{-1}B \\ &= D + CT^{-1}\begin{bmatrix} 0 & \\ & I \end{bmatrix}\begin{bmatrix} sI - J & \\ & sN - I \end{bmatrix}^{-1} W^{-1}B \\ &= \underbrace{D - C_\infty B_\infty}_{M_0} - sC_\infty N B_\infty - s^2 C_\infty N^2 B_\infty - \cdots . \end{aligned} \tag{3.16}$$

Contrasting (3.4) and (3.5), it follows that $M_1 = -C_\infty N B_\infty$ which can be shown to be

$$M_1 = -CA^{-1}E_\infty A^{-1}B, \tag{3.17a}$$

$$= -C(E_f + A_\infty)^{-1}E_\infty(E_f + A_\infty)^{-1}B, \tag{3.17b}$$

where $E_f := EP_r$ and $A_\infty := A(I - P_r)$. Subsequently, M_0 and $G_p(s)$ can be decided by (3.15) and (3.16). The merit of the alternative expression in (3.17b) is that the inverse of $(E_f + A_\infty)$ always exists despite the invertibility of A [or equivalently that of J in (3.2)]. The positive semidefiniteness of M_1 and M_0, necessary for a passive DS, can then be easily tested. In fact, M_1 and M_0 are normally small-size $m \times m$ square matrices since the number of input/output ports is usually much fewer than the state space dimension, i.e., $m \ll n$.

At the first glance, the passivity test for $G_p(s)$ can make use of the Hamiltonian matrix eigenvalue test for standard state space systems [11], since $\tilde{E}$ is nonsingular such that its inverse can be absorbed into $\tilde{A}$ and $\tilde{B}$ (though this is sometimes not preferable as $\tilde{E}$ may be ill-conditioned). For large systems, a fast numerical approach

is developed [78] to compute the eigenvalues along the imaginary axis. However, Hamiltonian-based approach becomes computationally infeasible due to the expensive matrix inversion of $\tilde{E}$. Further, the matrix inversion also destroys the sparsity of system matrices, which further slows down the calculations. An alternative approach is to combine the fast eigenvalue solver of [78] with the generalized Hamiltonian method (GHM) proposed in Chapter 2, which is further elaborated in Section 3.5.2. This method directly tests passivity on the DS-form proper subsystem without loss of sparsity, thus it is more efficient than using Hamiltonian method on the converted standard state-space model.

The flow of the proposed projector-based decoupled-DS passivity test is summarized in Fig. 3.1. A note about the infinite minimality assumption of the initial DS can be found in Section 3.7 discussion #3.

3.4.2 Reconstruction into a DS

Finally, if $G_p(s) = \tilde{D} + \tilde{C}(s\tilde{E} - \tilde{A})^{-1}\tilde{B}$ is passive (possibly after passivity enforcement [11]) and $M_1 \geq 0$, a passive DS corresponding to the transfer function $G_p(s) + sM_1$ can be reconstructed for export to a simulator. Indeed, let $M_1 = ZZ^T$ be a Cholesky factorization, where $Z \in \mathbb{R}^{m\times m}$. Then the DS can be formulated as

$$\begin{bmatrix} \tilde{E} & & \\ & 0 & I_m \\ & 0 & 0 \end{bmatrix} \dot{x} = \begin{bmatrix} \tilde{A} & & \\ & I_m & 0 \\ & 0 & I_m \end{bmatrix} x + \begin{bmatrix} \tilde{B} \\ 0 \\ Z^T \end{bmatrix} u,$$
$$y = \begin{bmatrix} \tilde{C} & -Z & 0 \end{bmatrix} x + \tilde{D}u, \tag{3.18}$$

whose transfer function is easily checked to be $G_p(s) + sM_1$.

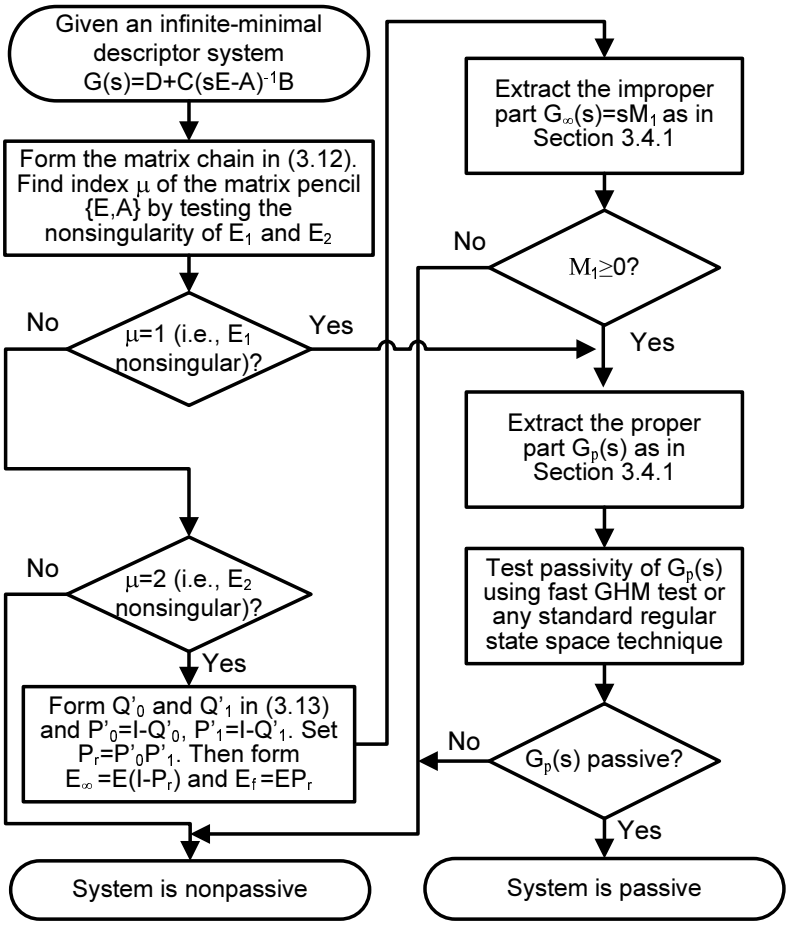

Figure 3.1: Flowchart for the proposed DS passivity test in a pseudocodes style.

3.5 Implementation and Complexity

3.5.1 Fast Spectral Projector Construction

Although there exist closed-form spectral projectors in terms of the initial (not necessarily canonical) projectors as in (3.13) and (3.14), or for some special cases further simplified forms as in [56, 77], the computation can still be expensive and constitute a bottleneck due to large-size nullspace identification, matrix multiplication and inverse. Here we elaborate an efficient numerical construction of spectral projectors,

mainly by exploiting sparsity and low-rank matrix operations inherent to many physical problems. The illustration below is based on index-2 ($\mu = 2$) systems, and that for index-1 ($\mu = 1$) systems follows similarly.

First, a key step to forming the canonical projectors in (3.13) is to find the initial projectors Q_0 and Q_1 spanning the nullspaces of the usually sparse or structured E_0 and E_1. Standard ways of identifying the nullspace include SVD or alike, which do not utilize matrix patterns and can be expensive for large-size matrices. To this end, we employ the sparse LU decomposition-based routine from [79], called LUQ, which decomposes E_j, $j = 0, 1$, into

$$E_j^T = L_j \begin{bmatrix} U_j & 0 \\ 0 & 0 \end{bmatrix} R_j, \tag{3.19}$$

where $L_j, R_j \in \mathbb{R}^{n\times n}$ are nonsingular matrices, $U_j \in \mathbb{R}^{r\times r}$ is a nonsingular upper triangular matrix, r is the rank of E_j and often $n - r \ll n$. Therefore, (3.19) is also used in our implementation for checking the nonsingularity of E_j. If E_j is singular, its nullspace is then computed via the left nullspace of E_j^T (solely due to the reason that L_j is produced with higher numerical accuracy than R_j by the LUQ routine [79]). For completeness, the LUQ routine is outlined in Appendix 3.9.3. Obviously, using $I_{(r+1:n,:)}$ to denote the last $n - r$ rows of an $n \times n$ identity matrix, the columns of $(I_{(r+1:n,:)}L_j^{-1})^T$ span $\ker E_j$. In practice, direct computation of this column matrix is not preferred as the condition number of L_j can be large rendering ill-conditioned inverse. Instead, we perform a LU factorization of L_j with permutation,

$$\tilde{P}_j L_j = \tilde{L}_j \tilde{U}_j, \tag{3.20}$$

where $\tilde{L}_j, \tilde{U}_j, \tilde{P}_j \in \mathbb{R}^{n\times n}$ such that $\tilde{P}_j$ is the permutation matrix with $\tilde{P}_j^T \tilde{P}_j = I$, $\tilde{U}_j$ is upper triangular and $\tilde{L}_j$ is lower triangular with unit diagonal entries and a condition

number around unity. Then, it is easily checked that, due to the upper triangular structure of $\tilde{U}_j$, $(I_{(r+1:n,:)}\tilde{L}_j^{-1}\tilde{P}_j)^T$ spans the same range as that by $(I_{(r+1:n,:)}L_j^{-1})^T$ and has intrinsically better accuracy due to the low condition number of $\tilde{L}_j$. It is noted that computing $\tilde{L}_j$ does not really add to the computational load since the inverse of L_j would generally proceed with an LU decomposition, of which $\tilde{L}_j$ is a by-product, followed by backward/forward substitutions. Next, a (modified) Gram-Schmidt process, denoted by gs($\circ$) below, leads to an orthonormal and usually thin column matrix, namely

$$\Psi_j = \mathrm{gs}((I_{(r+1:n,:)}\tilde{L}_j^{-1}\tilde{P}_j)^T), \tag{3.21}$$

such that $Q_j = \Psi_j\Psi_j^T$ forms an orthogonal projector onto $\ker E_j$. Subsequently, $Q_0 = \Psi_0\Psi_0^T$ and $Q_1 = \Psi_1\Psi_1^T$ are in low-rank factored forms that facilitate fast computation of canonical projectors in (3.13) by

$$Q_1' := \Psi_1\left((\Psi_1^T E_2^{-1})A_1\right), \tag{3.22a}$$

$$Q_0' := \Psi_0\left((\Psi_0^T P_1' E_2^{-1})A_0\right), \tag{3.22b}$$

which are again low-rank. Further computational savings can be achieved in (3.14) by recognizing that

$$\begin{aligned} Q_0'Q_1' &= Q_0'(Q_0 + P_0)Q_1' \\ &= Q_0Q_1' + Q_0P_1'E_2'^{-1}A_1Q_1' \\ &= Q_0Q_1' + Q_0P_1'E_2'^{-1}E_2'Q_1' = Q_0Q_1', \end{aligned}$$

so that $P_r = I - Q_0' - Q_1' + Q_0Q_1'$ where Q_0', Q_1' and Q_0Q_1' all involve low-rank factors only.

3.5.2 Fast GHM Test for Proper-Part Passivity

The spectral projector, with efficient implementation as above, allows fast decoupling of the proper and improper parts of a DS. However, the computational bottleneck for the DS passivity test still lies in testing the passivity of the proper part. To speed up the overall DS passivity test, having an efficient test for the proper part is important. For the DS-form proper subsystem constructed by (3.15), its passivity can be assessed by the matrix pencil $(\mathcal{J}, \mathcal{K})$ according to GHM in Chapter 2

$$\mathcal{J} = \begin{bmatrix} \tilde{A} - \tilde{B}(\tilde{D} + \tilde{D}^T)^{-1}C & -\tilde{B}(\tilde{D} + \tilde{D}^T)^{-1}\tilde{B}^T \\ \tilde{C}^T(\tilde{D} + \tilde{D}^T)^{-1}\tilde{C} & -\tilde{A}^T + \tilde{C}^T(\tilde{D} + \tilde{D}^T)^{-1}\tilde{B}^T \end{bmatrix}, \quad \mathcal{K} = \begin{bmatrix} \tilde{E} & 0 \\ 0 & \tilde{E}^T \end{bmatrix}, \tag{3.23}$$

any purely imaginary generalized eigenvalue of which pinpoints a crossover point of passivity violations. The proper part is strictly passive if and only if $\tilde{D} + \tilde{D}^T > 0$ and $(\mathcal{J}, \mathcal{K})$ has no eigenvalues on the imaginary axis. This eigenvalue problem consumes an $O((2n)^3)$ complexity, which is infeasible for large sparse system. In practice, the system matrices of $G_p(s)$ are normally sparse, and only results close to the imaginary axis are wanted for passivity verification. Based on this observation, the fast passivity characterization of [78] exclusive to large sparse state-space models can be extended to the DS case in (3.15).

To outline the fast Hamiltonian passivity test [78], we first assume the proper subsystem is a standard state-space model. In this case $eig(\mathcal{J}, \mathcal{K}) = eig(\mathcal{J})$ where $\mathcal{K}$ reduces to an identity matrix. In [78], the imaginary eigenvalues of $\mathcal{J}$ is computed via multi-shift Arnoldi iterations. This algorithm first builds a p-dimensional orthogonal basis

$$V_p = [v_1, v_2, \cdots, v_p], \tag{3.24}$$

of the Krylov subspace

$$\{v_1, (\mathcal{J} - \theta I)^{-1} v_1, \cdots, (\mathcal{J} - \theta I)^{-(p-1)} v_1\}, \tag{3.25}$$

($\theta \in j\mathbb{R}$) with a randomly generated initial vector $v_1 \neq 0$. After that, a $p \times p$ Hessenberg matrix $\mathcal{H}_p$ is constructed by

$$\mathcal{H}_p = V_p^H (\mathcal{J} - \theta I)^{-1} V_p. \tag{3.26}$$

Subsequently a few largest eigenvalues $\hat{\lambda}_j$ of the low-dimension Hessenberg matrix can be used to approximate the true eigenvalues λ_j of $\mathcal{J}$ close to θ by

$$\lambda_j \approx \theta + \hat{\lambda}_j^{-1}. \tag{3.27}$$

With an error control all λ's close to θ can be accurately computed. To compute all possible purely imaginary eigenvalues of $\mathcal{J}$, θ should be shifted along the imaginary axis on the upper half plane. In [78], a bisection scheme is adopted in the interval $(0, \theta_{max})$ to fix the shifted parameters, such that all imaginary eigenvalues close to θ's are accurately found (cf. [78] for the details about error control and bisection scheme). Here θ_{max} is an estimated largest-magnitude imaginary eigenvalue, which can be easily approximated by sparse power iteration. In this section, we focus on how to extend this approach to the matrix pencil $(\mathcal{J}, \mathcal{K})$. Note that $\tilde{A}$ is assumed to be diagonal in [78], which is waived here.

Assume $\lambda \in eig(\mathcal{J}, \mathcal{K})$, the nonsingularity of $\mathcal{K}$ implies $eig(\mathcal{J}, \mathcal{K}) = eig(\mathcal{K}^{-1}\mathcal{J})$. To apply the above fast eigenvalue solver, the main bottleneck lies in computing $(\mathcal{K}^{-1}\mathcal{J} - \theta I)^{-1} v_i$. First, $(\mathcal{K}^{-1}\mathcal{J} - \theta I)$ and its inverse are not sparse, which renders the matrix-vector production inefficient. Second, the matrix inversions involved are prohibitively expensive, time-consuming and unstable for large-scale systems. Therefore,

fast, sparse and stable matrix operations are needed. Since $\mathcal{K}^{-1}\mathcal{J}-\theta I = \mathcal{K}^{-1}(\mathcal{J}-\theta\mathcal{K})$, the matrix-vector production in each iteration can be expressed as

$$(\mathcal{K}^{-1}\mathcal{J} - \theta I)^{-1} v_i = (\mathcal{J} - \theta\mathcal{K})^{-1}\mathcal{K}v_i. \tag{3.28}$$

By the matrix inverse lemma [40], we have

$$\begin{aligned}
&(\mathcal{J} - \theta\mathcal{K})^{-1}\mathcal{K}v_i \\
&= \left(\begin{bmatrix} M_\theta & \\ & -M_\theta^H \end{bmatrix} - \begin{bmatrix} \tilde{B} \\ -\tilde{C}^T \end{bmatrix} (\tilde{D} + \tilde{D}^T)^{-1} \begin{bmatrix} \tilde{C} & \tilde{B}^T \end{bmatrix} \right)^{-1} w_i \\
&= \begin{bmatrix} M_\theta^{-1} & \\ & -M_\theta^{-H} \end{bmatrix} w_i + \begin{bmatrix} M_\theta^{-1}\tilde{B} \\ M_\theta^{-H}\tilde{C}^T \end{bmatrix} \times \\
&\quad \left(\tilde{D} + \tilde{D}^T - \tilde{C}M_\theta^{-1}\tilde{B} - \tilde{B}^T M_\theta^{-H}\tilde{C}^T\right)^{-1} \begin{bmatrix} \tilde{C}M_\theta^{-1} & -\tilde{B}^T M_\theta^{-H} \end{bmatrix} w_i
\end{aligned} \tag{3.29}$$

where $M_\theta = \tilde{A} - \theta\tilde{E}$, $w_i = \mathcal{K}v_i$. We first denote $w_{i1} = w_{(1:n)}$ and $w_{i2} = w_{(n+1:2n)}$. Making use of the sparsity of M_θ, (3.29) can be implemented as follows:

1. Perform a sparse LU decomposition on the $n \times n$ matrix

$$M_\theta = L_\theta U_\theta, \tag{3.30}$$

   then the sparse LU of M_θ^H is readily obtained as $M_\theta^H = U_\theta^H L_\theta^H$.

2. Compute the following vectors (or vector-like narrow matrices)

$$x_1 = U_\theta^{-1} L_\theta^{-1} w_{i1}, \tag{3.31a}$$

$$x_2 = -L_\theta^{-H} U_\theta^{-H} w_{i2}, \tag{3.31b}$$

$$x_3 = U_\theta^{-1} L_\theta^{-1} \tilde{B}, \tag{3.31c}$$

$$x_4 = L_\theta^{-H} U_\theta^{-H} \tilde{C}^T, \tag{3.31d}$$

by forward/backward iteration. Since L_θ and U_θ obtained by sparse LU are normally sparse, the above linear system solution can be as cheap as $O(n)$.

3. Finally, the inverse iteration can be computed by

$$(\mathcal{K}^{-1}\mathcal{J} - \theta I)^{-1} v_i = \begin{bmatrix} x_1 \\ x_2 \end{bmatrix} + \begin{bmatrix} x_3 \\ x_4 \end{bmatrix} \times \left(\tilde{D} + \tilde{D}^T - \tilde{C}x_3 - \tilde{B}^T x_4\right)^{-1} \left(\tilde{C}x_1 + \tilde{B}^T x_2\right). \tag{3.32}$$

Due to the low dimension, the matrix inversion in this step is trivial.

In the above procedures, the total computation and storage are low since only one $n \times n$ sparse LU factorization is needed, and only sparse upper/lower triangular matrices and vectors are stored.

To this end, the multi-shift Arnoldi algorithm can be used to compute all generalized eigenvalues of $(\mathcal{J}, \mathcal{K})$ close to (or located on) the imaginary axis. The error control and bisection methods are the same as those of the original algorithm [78], which is omitted here. It is clear that compared with standard Hamiltonian method, the GHM-based method avoids large-scale matrix inversion and preserves system sparsity.

3.5.3 Complexity Analysis

DS passivity test by the extended positive real lemma in [39] via solution of LMIs is impractical for large systems due to its $O(n^6)$ complexity [46] where n is the dimension of the state vector in (3.1). Also, direct transformation to the Weierstrass canonical form (3.2) can be numerically unstable and expensive. For example, the GUPTRI algorithm requires essentially $\geq$3$\times$SVD, $\geq$2$\times$QR and 1$\times$QZ decompositions to produce a generalized Schur form, followed by solving an additional generalized Sylvester

equation to reach the Weierstrass form, all costing expensive $O(n^3)$ work [80, 81]. Consequently, the more efficient SHH transformation technique is proposed [46] to decouple the original DS into its proper and improper subsystems. A careful inspection reveals that the major SHH steps call for 3×SVD and 2×QR factorizations, plus the optional solution of an algebraic Riccati equation (ARE) and a Lyapunov equation if the proper part is to be explicitly extracted. We are also aware of an $O(n^3)$ DS decoupling procedure in [42, 47], which costs at least 3×URV (similar to SVD), 1×QR and one generalized Schur decomposition, and therefore has comparable complexity to the SHH test (but the lack of implementation details in [42, 47] allow no further conclusion about its actual speed). A similar procedure in [72], based on the Van Dooren technique [82], also suffers from multiple SVDs, numerically sensitive sub-matrix annihilations and the costly solution of an ARE. Finally, the recent DS decoupling approach, though not exactly related to passivity test, utilizes the iterative disk function method [83]. But again it requires $10 \sim 20$ iterations of QR factorizations (on $2n \times n$ matrices) for convergence, followed by special subspace extraction procedures. Another demanding requirement in all the above mentioned procedures, where SVD/QR of dense matrices are necessary, is the $O(n^2)$ memory requirement.

After DS decoupling, either by the disk function, Weierstrass-form or SHH decoupling, the improper subsystem (specifically the residual M_1) is then checked for positive semidefinite which is fast and trivial. On the other hand, the proper-part passivity can be checked with standard regular-system passivity tests such as the Hamiltonian matrix eigenvalue test of $O\left((2n)^3\right)$ work [11], or the faster but less reliable frequency sweeping test of $O(m^3)$ to $O(n^3)$ work [9] depending on the availability of closed-form rational transfer function (e.g., a possible case where analytical transfer matrix exists is when the state-space matrices are obtained from vector fitting as in [9], but this is not always the case if the initial model is not built from rational fitting). In this chapter, we directly perform GHM passivity test on the DS-form proper

subsystem, which is implemented by the fast multi-shift Arnoldi iteration based algorithm. Assume t shift parameters in the interval $(0, \theta_{max})$ are used to compute all eigenvalues close to the imaginary axis, then t sparse LUs are needed. For each shift, several to tens of Krylov subspace iterations are needed to approximate the neighborhood eigenvalues, which depends on how dense these eigenvalues are distributed. In practice, only a small number of eigenvalues are distributed around the imaginary axis, so usually t is in the tens. Since the expensive matrix inversion is avoided and sparsity is preserved, this method is much more efficient than standard Hamiltonian test on the standard state-space model converted from (3.15).

It is seen that all the above DS decomposition/decoupling approaches require at least SVD or iterative QR operations which can of course be employed for the matrix chain formation and projector construction in Section 3.3 (e.g., [20]). Nonetheless, a key advantage of the projector-based DS passivity test is that the singularity test and spectral projector formulation can all be accomplished with the much cheaper LU-type decomposition, with $\approx O(2n^3/3)$ work versus $\approx O(20n^3)$ in SVD or $\approx O(2n^3)$ in QR for general dense matrices [40], as described in Section 3.5.1. If sparsity and low-rank operations are further exploited, the projector can be realized with $O(n^2) \sim O(n^3)$ work and $O(n)$ storage, depending on the sparsity extent. In fact, for index-2 problems, the main load in the projector construction involves only 5×sparse LU factorizations (viz. 3 rank tests and 2 nullspace computations). Subsequently, sparsity-aware LU factorization has much reduced memory storage requirement than the SHH or transformations to the Weierstrass form, where dense SVD, QR or matrix equation solves are generally unavoidable. Together with the fast GHM passivity test in Section 3.5.2, the proposed DS passivity test features remarkable computational savings and is applicable to large systems, as will be seen in the following numerical examples.

3.6 Numerical Examples

In this section, some practical DS benchmarks are tested for passivity to demonstrate the effectiveness of the proposed projector framework. These examples are mostly taken from [84] except the order-1232 and order-10082 ones which are RC networks. The order-480 system is a patch antenna model from partial element equivalent circuit (PEEC) modeling, while other higher order examples are MNA benchmarks. All MNA benchmarks are passive, while the PEEC model is nonpassive. Nonpassive PEEC models may be caused by poor meshing generation, inadequate numerical integration, matrix sparsification or inappropriate geometrical discretization, which is discussed in detail by J. Ekman, *et al* [85]. All codings are done in MATLAB and executed on a 2.66GHz PC with 2GB memory.

3.6.1 Projector-Based Decomposition

We begin by timing the index tests based on checking the nullities of E_1 and E_2 [via (3.19)] of these benchmarks, which forms the initial step in the proposed DS passivity test. Two approaches are contrasted, namely, the standard SVD and the (sparse) LU singularity test discussed in Section 3.5.1. Expectedly, Table 3.1 shows that the LU way is much more efficient than the SVD approach even though in some cases the sparsity of E_2 may not be significant due to the "fill-ins" by matrix chain formation.

Table 3.1: Total CPU times in DS index check

system order	system index	number of nonzero elements in				time (sec)	
		A_0	E_0	E_1	E_2	SVD	LU
480	2	1346 (0.584%)	18290 (7.94%)	19001 (8.25%)	71521 (31.04%)	2.411	0.8125
578	2	1694 (0.507%)	25432 (7.61%)	26601 (7.96%)	224130 (67.09%)	4.506	2.8231
980	2	2872 (0.299%)	83568 (8.70%)	85339 (8.89%)	666669 (69.42%)	20.359	12.80
1232	2	3634 (0.239%)	3608 (0.238%)	3610 (0.238%)	5504 (0.363%)	29.250	0.0469
10082	2	30184 (0.030%)	29568 (0.029%)	29570 (0.029%)	31464 (0.031%)	fail	0.0938
10913	2	54159 (0.045%)	35904 (0.030%)	36087 (0.030%)	5385968 (4.522%)	fail	93.28

Table 3.2: CPU times excluding proper-part passivity check

system order	CPU time (sec)		
	proposed	SHH	Weierstrass
480	1.73	9.53	10.92
578	3.26	15.90	18.50
980	14.84	75.83	95.41
1232	0.0625	132.2	801
10082	0.1563	fail	fail
10913	159.68	fail	fail

Next, the proposed DS passivity test is compared to the SHH [46] and the Weierstrass tests in terms of proper and improper part decoupling, where in the Weierstrass approach the public routine GUPTRI [80] and the SLICOT [86] generalized Sylvester equation solver `slgesg` (both calling compiled Fortran routines) are employed. The extended LMI test in [39] has been shown by [46] to be computationally impractical and is therefore not included here.

Table 3.2 again demonstrates the superiority of the projector approach, owing to the techniques presented in Section 3.5.1 and the reasonings in Section 3.5.3. It is noted that the much longer time in the Weierstrass column in the order-1232 case is due to the generation of complex entries by GUPTRI which has also been observed in [46]. In the same example, the speed gain from the projector approach is especially impressive (namely, four orders faster) due to the strong sparsity of the RC network. This further highlights the efficiency of the projector approach and in particular its suitability for electrical networks commonly used in VLSI interconnect/package modeling. To confirm the accuracy of the spectral projector decoupling, we decompose the 10913×10913 example which is a 9-input-9-output system. The proper and improper parts are extracted by additive decomposition (cf. Section 3.4). Fig. 3.2 shows the port-2 to port-2 decoupled responses, wherein the error is in the order of 10^{-10} (and similarly for other port-to-port responses).

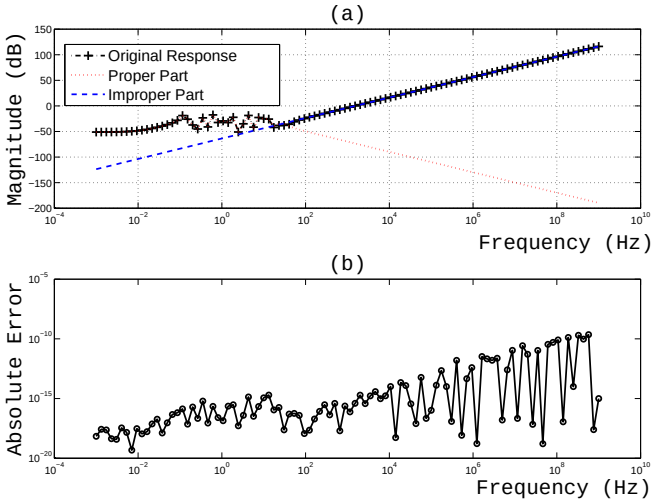

Figure 3.2: (a) Bode plots of the original, proper- and improper-subsystem responses. (b) Error between the original system and the sum of decomposed subsystems.

3.6.2 Proper Part Testing

After the decoupling, the proper part can be tested by SHH, Weierstrass and the proposed fast GHM method.

We continue to show the applicability of the projector-based DS passivity test at higher system orders than those considered in [20, 46], where the highest order is 800 and the SHH and Weierstrass tests consume about 350 $\sim$ 600s on a standard PC. The multi-shift Arnoldi iteration based GHM test in Section 3.5.2 is adopted.

We begin with the order-480 PEEC example which is a single-input-single-output DS. The projector-based decomposition shows that it is impulse-free. Its proper-part is then tested by the proposed fast GHM test. Fig. 3.3 shows that some eigenvalues of $(\mathcal{J}, \mathcal{K})$ locate on the imaginary axis, implying that this DS is nonpassive.

The next example is the order-980 case originating from a 4-input-4-output RLC network, which does not contain an improper part either. The proper-part admittance transfer function is also checked by the proposed fast GHM test. Fig. 3.4 shows the corresponding passivity test matrix pencil does not contain any purely imaginary

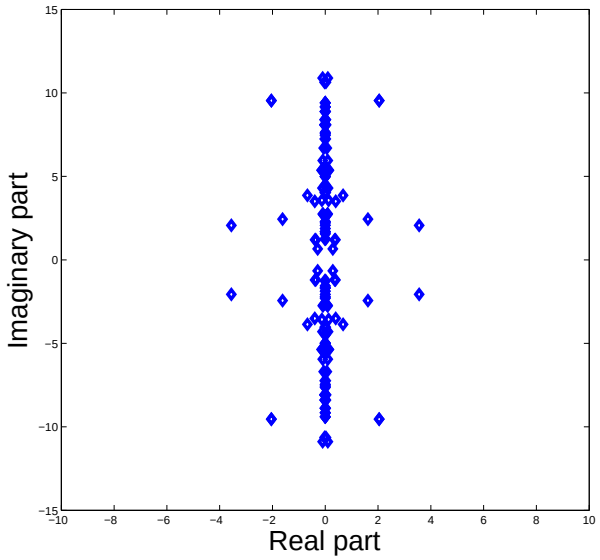

Figure 3.3: Eigenspectrum of the generalized Hamiltonian matrix pencil $(\mathcal{J}, \mathcal{K})$ for the PEEC model. Only the results close to the imaginary axis are plotted.

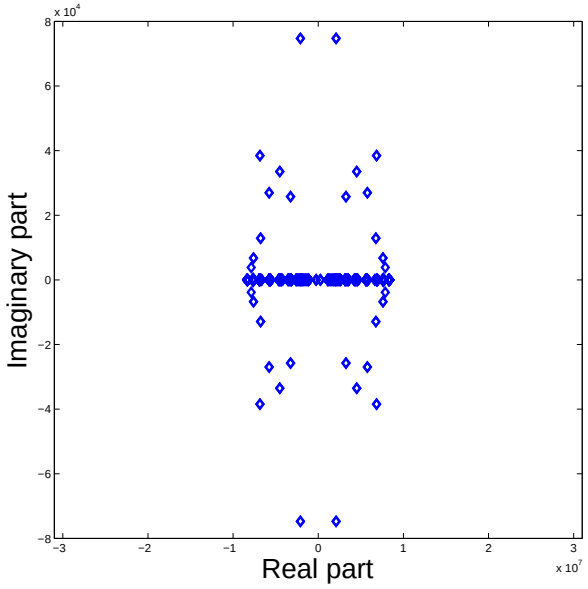

Figure 3.4: Eigenspectrum of the generalized Hamiltonian matrix pencil $(\mathcal{J}, \mathcal{K})$ for the order-980 RLC model. Only the results close to the imaginary axis are plotted.

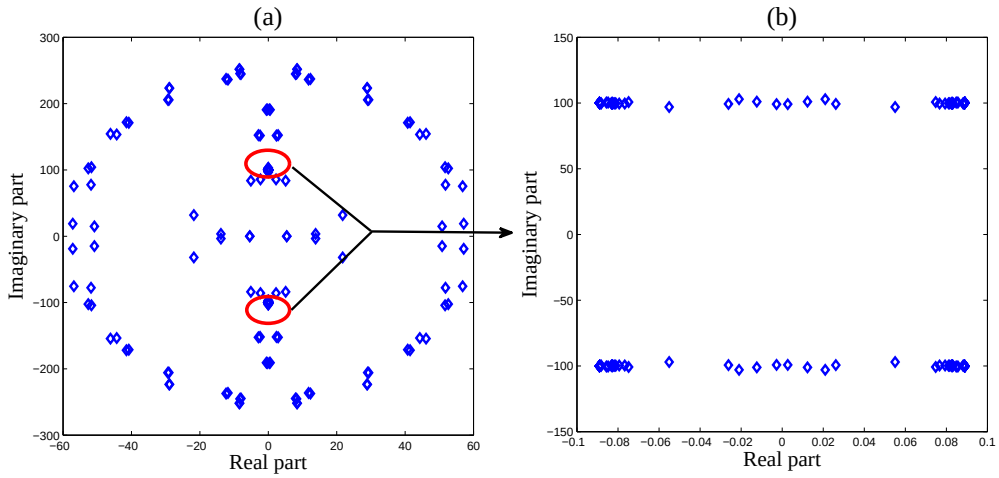

Figure 3.5: Passivity test results for the order-10913 DS model. (a) Eigenspectrum of the generalized Hamiltonian matrix pencil $(\mathcal{J}, \mathcal{K})$. Only the results close to the imaginary axis are plotted. (b) Zoom-in of the eigenvalues with small real parts (circled in the left plot).

generalized eigenvalues. This confirms the model is passive which is expected due to the RLC nature of the example. The third example is the 9-input-9-output order-10913 MNA example. The improper part contains only sM_1 where M_1 is a diagonal 9×9 positive definite matrix. As for its proper part, Fig. 3.5 plots the GHM test results which confirm its passivity, whereas the SHH, Weierstrass transformations and full-size GHM test simply fail at such high orders. In Chapter 2, the superiority of GHM over SHH and Weierstrass tests has been illustrated. We further show the speedup of the proposed fast GHM over the full-size GHM in Table 3.3. The CPU timing shows the speedup of the proposed Arnoldi iteration based GHM (fast GHM) is faster than full-size GHM, and the speedup is more significant as problem size grows. Due to the expensive storage requirement, full-size GHM is not applicable to large sparse systems, but the proposed fast GHM algorithm can still be used to characterize passivity.

Table 3.3: CPU times of full-size GHM and fast GHM tests on the proper subsystem.

system order	full-size GHM	fast GHM	speedup
480	21.3s	7.3s	2.9
980	83.7s	15.2s	5.6
10913	fail	11hrs 37min	N/A

3.7 Discussions

1. Compared to the Weierstrass-form or SHH-transformation DS passivity tests, the proposed algorithm is conceptually simple and straightforward. As described in Section 3.5.3, former DS passivity tests all involve expensive SVD or QR operations for subsystem decoupling, while the projector approach only calls for the much cheaper LU factorizations and much reduced memory requirement when sparsity is exploited. To the knowledge of the authors, this projector-based passivity test flow for DSs is by far the fastest one reported in the literature.

2. Along the same line, the speed of the proposed projector construction (either explicitly or implicitly as in [56]) is dependent on the sparsity degree and pattern. In many real-world problems, E_0 and E_1 are highly sparse and therefore the LUQ decomposition [79] is fast. If E_2 is also sparse enough, the speedup can be drastic as observed in the order-1232 & 10082 examples in Table 3.1. Moreover, the nullities of practical E_0 or E_1 are usually low which lead to efficient low-rank formulation of canonical projectors and therefore the spectral projector [cf. (3.21) and (3.22)]. This also reinforces the advantageous use of projector techniques in analyzing real-world DSs.

3. Existing DS passivity tests [16, 39, 42, 46, 47] all assume a a minimal (i.e., completely controllable and observable) initial DS, otherwise a pre-processing is done to remove the uncontrollable/unobservable states for minimal realization

(e.g., by the $O(n^3)$ algorithm in [3] or [46] which essentially reduces a DS into its Kalman canonical form using orthogonal transformations). However, such preprocessing is expensive and destroys sparsity of the system. In fact, Theorem 3.3 holds under the only assumption of regularity, and what we really require in the DS is the infinite minimality equivalent to $\operatorname{rank}\begin{bmatrix} E & B \end{bmatrix} = \operatorname{rank}[\ E^T \quad C^T\ ] = n$ [39] which determines the highest power of s in (3.5). Such infinite minimality can be obtained by running the reduction algorithms in [3, 46, 72] only partially and is therefore much cheaper to achieve than full minimality. Consequently, the minimality assumption in the proposed test is the least restrictive one among existing tests.

4. By virtue of the explicit formulation of regular state spaces for the proper and improper subsystems in Section 3.4, further processing can be readily exercised. In particular, standard state-space MOR and/or passivity enforcement procedures, e.g., [9, 11, 26], are all reusable on the extracted proper part $G_p(s)$. Perturbation of the improper part $G_\infty(s)$ into a positive semidefinite first-order residue matrix M_1, due to its small size (viz. $m \times m$), is also trivial.

5. In Chapter 2, GHM is directly performed on DS models for passivity check. However, it terminates if the improper part is nonpassive, and then the passivity of the proper subsystem cannot be verified. With the spectral projector technique, the proper part can still be checked regardless of the passivity of the improper part.

3.8 Summary

This chapter has presented a canonical projector-based passivity test for DS models commonly found in circuit modeling. Compared to the existing LMI and SHH

transformation approaches for testing DS passivity, the proposed test is theoretically straightforward and exhibits simple codings and superior computational speed. The index of a DS comes at an early stage which immediately reveals the possible passivity of a DS. Fast sparse LU-based construction of the spectral projector then permits efficient decomposition of the DS into its proper and improper subsystems, whose individual passivity can be efficiently evaluated with existing passivity check techniques. State spaces for these subsystems have also been explicitly formulated for utilization in subsequent MOR and/or passivity enforcement. A sparse LU factorization approach to projector construction, together with a fast GHM algorithm based on multi-shift Arnoldi iteration, have made possible the efficient passivity test of high-order DSs unamendable before.

3.9 Appendices

3.9.1 Matrix Chain with Canonical Projectors

We begin by making the projector in (3.12b) canonical. This is done by replacing Q_1 with

$$Q_1' := Q_1 E_2^{-1} A_1. \tag{3.33}$$

To see that Q_1' is a valid projector onto $\ker E_1$, we note that $Q_1' Q_1 = Q_1 E_2^{-1} A_1 Q_1 = Q_1 E_2^{-1} E_2 Q_1 = Q_1$ and $Q_1 Q_1' = Q_1'$, which implies $Q_1' (= Q_1'^2)$ is a projector onto the same range as Q_1. To show Q_1' and Q_0 are admissible, we have $Q_1' Q_0 = Q_1 E_2^{-1} A_1 Q_0 =$

$Q_1 E_2^{-1} A_0 P_0 Q_0 = 0$. Using Q_1' in place of Q_1, (3.12) is updated to

$$E_1 := E_0 + A_0 Q_0 \quad \text{and} \quad A_1 := A_0 P_0, \tag{3.34a}$$

$$E_2' := E_1 + A_1 Q_1'. \tag{3.34b}$$

Note that again E_2' is guaranteed to be nonsingular. Now to verify the canonicity of Q_1' in (3.34b), we make use of the property in (3.11) to get $E_2' = E_2(I + Q_1' P_1)$ and have

$$\begin{aligned} Q_1' E_2'^{-1} A_1 &= Q_1'(I - Q_1' P_1) E_2^{-1} A_1 \\ &= Q_1' Q_1 E_2^{-1} A_1 = Q_1 E_2^{-1} A_1 = Q_1', \end{aligned} \tag{3.35}$$

thus completing the proof. Next, we set

$$Q_0' := Q_0 P_1' E_2'^{-1} A_0. \tag{3.36}$$

Noting $A_0 Q_0 = E_2' Q_0$, it follows that $Q_0'^2 = Q_0'$ is a projector onto $\ker E_0$. Recompute (3.34a) with this new projector to give

$$E_1' := E_0 + A_0 Q_0' \quad \text{and} \quad A_1' := A_0 P_0'. \tag{3.37}$$

Again, from (3.11), $E_1' = E_1(I + Q_0' P_0)$ and it turns out Q_1' is also a projector onto $\ker E_1'$, namely,

$$\begin{aligned} E_1' Q_1' &= E_1(I + Q_0' P_0) Q_1' = E_1(I + Q_0 P_1' E_2'^{-1} A_0 P_0) Q_1' \\ &= E_1 Q_1' + E_1 Q_0 P_1' E_2'^{-1} A_1 Q_1' = 0, \end{aligned}$$

since $A_1Q_1' = E_2'Q_1'$. With Q_0', (3.34) is further updated as

$$E_1' := E_0 + A_0Q_0' \quad \text{and} \quad A_1' := A_0P_0', \tag{3.38a}$$

$$E_2'' := E_1' + A_1'Q_1'. \tag{3.38b}$$

Because $Q_1'Q_0 = 0$, so is $Q_1'Q_0' = 0$ (i.e., admissible) and

$$\begin{aligned} Q_0'Q_1' &= Q_0P_1'E_2'^{-1}A_0Q_1' = Q_0P_1'E_2'^{-1}A_0(Q_0 + P_0)Q_1' \\ &= Q_0P_1'E_2'^{-1}E_2'Q_0Q_1' + Q_0P_1'E_2'^{-1}A_1Q_1' \\ &= Q_0Q_1' + Q_0P_1'E_2'^{-1}E_2'Q_1' = Q_0Q_1'. \end{aligned} \tag{3.39}$$

This also implies $P_0'Q_1' = P_0Q_1'$ and $A_1'Q_1' = A_1Q_1'$, from which a link can be found between E_2'' and E_2' as

$$\begin{aligned} E_2'' &= E_1(I + Q_0'P_0) + A_1Q_1' \\ &= E_2'P_1'(I + Q_0'P_0) + E_2'Q_1' = E_2'(I + Q_0'P_0). \end{aligned} \tag{3.40}$$

Still, we need to show both Q_0' and Q_1' in (3.38) are indeed canonical. Utilizing properties (3.39), (3.40) and noting that $A_1 = A_0P_0 = A_0P_0P_0' = A_1' - E_2'Q_0P_0'$, we get

$$\begin{aligned} Q_0'P_1'E_2''^{-1}A_0 &= Q_0'(I - Q_1')(I - Q_0'P_0)E_2'^{-1}A_0 \\ &= (Q_0' - Q_0'Q_1' - Q_0'P_0)E_2'^{-1}A_0 \\ &= (Q_0'Q_0 - Q_0'Q_1')E_2'^{-1}A_0 \quad \text{[cf. (3.39)]} \\ &= Q_0P_1'E_2'^{-1}A_0 = Q_0' \quad \text{[cf. (3.36)]} \end{aligned}$$

$$\begin{aligned} Q_1' E_2''^{-1} A_1' &= Q_1'(I - Q_0' P_0) E_2'^{-1} A_1' \\ &= Q_1' E_2'^{-1}(A_1 + E_2' Q_0 P_0') \\ &= Q_1' E_2'^{-1} A_1 = Q_1' \quad \text{[cf. (3.35)]}. \end{aligned}$$

Of course, in practice, only the canonical projectors Q_0' and Q_1' are required for computing the spectral projectors, and the matrix chain updates from (3.12) to (3.34) and then to (3.38) never need to be computed explicitly.

3.9.2 Spectral Projectors from Canonical Projectors

We give a constructive proof for $P_r = P_0' P_1'$ for the case $\mu = 2$. This complements, and is also in contrast to, the indirect argument towards spectral projector presented in [19]. Taking the Weierstrass viewpoint for E_0 and A_0 (wherein $N^2 = 0$) and assuming canonical Q_0' and Q_1', we can easily show

$$Q_0' = T^{-1} \begin{bmatrix} 0 & 0 \\ 0 & \widehat{Q}_0' \end{bmatrix} T \quad \text{and} \quad Q_1' = T^{-1} \begin{bmatrix} 0 & 0 \\ 0 & \widehat{Q}_1' \end{bmatrix} T, \tag{3.41}$$

where $\widehat{Q}_0', \widehat{Q}_1' \in \mathbb{R}^{(n-q)\times(n-q)}$ project onto $\ker N$ and $\ker(N + \widehat{Q}_0')$, respectively. Moreover,

$$N_2 := N + \widehat{Q}_0' + \widehat{P}_0' \widehat{Q}_1' = N + I - \widehat{P}_0' \widehat{P}_1' \tag{3.42}$$

is nonsingular due to Theorem 3.3. By canonicity,

$$\widehat{Q}_0' = \widehat{Q}_0' \widehat{P}_1' N_2^{-1} \quad , \quad \widehat{Q}_1' = \widehat{Q}_1' N_2^{-1} \quad \text{and} \quad \widehat{Q}_1' \widehat{Q}_0' = 0. \tag{3.43}$$

Next, we prove $\widehat{P}_0'\widehat{P}_1' = 0$. First,

$$NN_2 = N^2 + N\widehat{Q}_0' + N\widehat{P}_0'\widehat{Q}_1' = N\widehat{Q}_1'. \tag{3.44}$$

Post-multiplying N_2^{-1} to (3.44) and using (3.43) we have $N = N\widehat{Q}_1'$ or equivalently $N\widehat{P}_1' = 0$. Next, recognizing $\widehat{P}_0'\widehat{P}_1'$ is a projector by itself, i.e., $(\widehat{P}_0'\widehat{P}_1')^2 = \widehat{P}_0'\widehat{P}_1'$, and post-multiplying it to (3.42), we obtain

$$N_2\widehat{P}_0'\widehat{P}_1' = N\widehat{P}_0'\widehat{P}_1' = N\widehat{P}_1' = 0. \tag{3.45}$$

Nonsingularity of N_2 then implies $\widehat{P}_0'\widehat{P}_1' = 0$. Consequently, the right (spectral) projector P_r in (3.3) is given by

$$P_r = P_0'P_1' = T^{-1}\begin{bmatrix} I_q & 0 \\ 0 & \widehat{P}_0'\widehat{P}_1' \end{bmatrix} T = T^{-1}\begin{bmatrix} I_q & 0 \\ 0 & 0 \end{bmatrix} T. \tag{3.46}$$

To obtain the left projector, canonical projectors are constructed from the matrix chain starting instead with $E_0 := E^T$ and $A_0 := A^T$. It is then easily verified that

$$P_l = (P_0'P_1')^T = W\begin{bmatrix} I_q & 0 \\ 0 & 0 \end{bmatrix} W^{-1}. \tag{3.47}$$

3.9.3 Outline of the LUQ Factorization

Given a sparse $n \times n$ matrix Z, the LUQ routine gives

$$Z = L_Z\begin{bmatrix} U_Z & 0 \\ 0 & 0 \end{bmatrix} Q_Z, \tag{3.48}$$

with L_Z, U_Z, Q_Z being nonsingular and U_Z being upper triangular. In the first step of LUQ, Z is factorized by sparse LU with permutation

$$Z = PL \begin{bmatrix} U_1 & U_2 \\ 0 & U_3 \end{bmatrix} Q. \tag{3.49}$$

Here P and Q are permutation matrices, L is lower triangular, U_1 is an upper triangular matrix with nonzero diagonal elements, $U_3 \in \mathbb{R}^{s\times s}$ is a very sparse upper triangular matrix with zero diagonals, and U_2 is a nonzero matrix. The zero/nonzero diagonal elements can be distinguished by setting a small numerical threshold as adopted in economic SVD in Matlab. Denoting $L := \begin{bmatrix} L_1 & L_2 \end{bmatrix}$ and $Q := \begin{bmatrix} Q_1 \\ Q_2 \end{bmatrix}$, (3.49) can be rewritten as

$$Z = P \begin{bmatrix} L_1 & L_2 \end{bmatrix} \begin{bmatrix} U_1 & 0 \\ 0 & U_3 \end{bmatrix} \begin{bmatrix} Q_1 + U_1^{-1} U_2 Q_2 \\ Q_2 \end{bmatrix}. \tag{3.50}$$

If U_3 (which is normally of low dimension if Z has a low nullity) has nonzero elements, we can recursively perform LUQ on this block such that

$$U_3 = L_{U3} \begin{bmatrix} U_{U3} & 0 \\ 0 & 0 \end{bmatrix} Q_{U_3}, \tag{3.51}$$

with U_{U3} being a nonsingular upper triangular matrix. Then L_Z, U_Z and Q_Z in (3.48) can be decided by

$$L_Z = \begin{bmatrix} PL_1 & PL_2 L_{U3} \end{bmatrix}, \tag{3.52a}$$

$$U_Z = \begin{bmatrix} U_1 & 0 \\ 0 & U_{U3} \end{bmatrix}, \tag{3.52b}$$

$$Q_Z = \begin{bmatrix} Q_1 + U_1^{-1} U_2 Q_2 \\ Q_{U3} Q_2 \end{bmatrix}. \tag{3.52c}$$

The cost of LUQ mainly comes from the sparse LU of Z, since U_3 is highly sparse and of low dimension. From (3.52) it is clear that L_Z is a product of a permutation matrix and a sparse lower triangular matrix. Nevertheless, Q_Z might be full and inaccurate since U_1^{-1} is involved. That is why we perform LUQ on E_j^T (see (3.19)) to construct the null space of E_j.

Chapter 4

S-Parameter Generalized Hamiltonian Methods (S-GHMs)

This chapter extends the generalized Hamiltonian method (GHM) and its half-size variant (HGHM) to their S-parameter counterparts (called S-GHM and S-HGHM, respectively), for testing the passivity of S-parameter descriptor-form models widely used in high-speed circuit and electromagnetic (EM) simulations. The proposed methods are capable of accurately detecting the possible nonpassive regions of descriptor-form models with either scattering or hybrid (impedance or admittance) transfer matrices. Their effectiveness and accuracy are verified with several practical examples. The S-GHM and S-HGHM methods presented here provide a foundation for the passivity enforcement of S-parameter descriptor systems (DSs).

4.1 Introduction

The transfer matrix of a LTI system may represent the admittance, impedance or scattering parameters in the frequency domain. The admittance/impedance case has been discussed in Chapters 2 & 3. In high-frequency applications where the electrical

variables behave like waves, scattering parameters are more commonly used, due to their relative ease of measurement. Besides its wide application in EM simulation, measured or simulated scattering parameters may also be used to build compact macromodels by data fitting techniques, such as vector fitting [48] that constructs standard state-space macromodels. Recently, the Loewner matrix interpolation technique [49, 50] has been advocated to fit measured/simulated data of electronic circuits/systems to produce the corresponding DS. Such framework is superior to the traditional vector fitting approach in the sense that no manual pole initialization is needed and that the optimal model order can be automatically extracted. For these S-parameter models, passivity is crucial for stable simulation, thus passivity verification and enforcement are needed to preserve model validity [8–12].

For DS models, several algebraic passivity tests have been proposed for hybrid (admittance or impedance) cases [39, 42–44, 46, 47]. However, their expensive computation [39] and requirements of minimal or admissible [42–44, 46, 47] realizations render them impractical for general DS models. Moreover, due to their inability to locate DS nonpassive regions, they are not good choices for passivity enforcement flows. To address this problem, the frequency sweeping technique has been extended to DS cases [20, 41]. However, due to the sampling nature of frequency sweeping, no guarantee can be made for the complete identification of all nonpassive regions. In Chapters 2 & 3, the proposed GHM/HGHM test delivers as high a numerical accuracy (of locating *all* nonpassive frequency intervals) for DSs as that of Hamiltonian methods [10–14] for regular state spaces.

In the context of S-parameter DSs, passivity verification is still not well addressed. Although the extended bounded-real lemma [45] and GARE-based method [77] have been proposed for passivity check, no reliable technique exists for the nonpassive region identification. Due to the lack of reliable S-parameter DS passivity verification algorithms, passivity enforcement can not be performed for nonpassive models at

present. Motivated by this demand, this chapter extends the GHM and HGHM theories to their S-parameter counterparts called the S-GHM and S-HGHM, respectively, to verify the passivity of the S-parameter models in circuit or EM simulation.

4.2 Review of Passivity Check for S-Parameter Models

We consider the continuous linear time-invariant (LTI) S-parameter DS model [denoted by $\Sigma : (E, A, B, C, D)$], with the state-space equations

$$E\dot{x} = Ax + Bu, \quad y = Cx + Du. \tag{4.1}$$

Here $E, A \in \mathbb{R}^{n\times n}, B \in \mathbb{R}^{n\times m}, C \in \mathbb{R}^{m\times n}, D \in \mathbb{R}^{m\times m}$, and $x \in \mathbb{R}^n$ represents the state variables. In this DS, $rank(E) \leq n$ and the matrix pencil (A, E) is assumed to be regular, i.e., $\det(A - sE) \neq 0$ for some $s \in \mathbb{C}$. If E is full-rank (or invertible), the DS reduces to a regular system which can be converted to a standard state-space equation by absorbing E^{-1} into A and B. To distinguish from the admittance/impedance cases, we use $S(s)$ to denote the S-parameter transfer matrix

$$S(s) = C(sE - A)^{-1}B + D. \tag{4.2}$$

Recalling from Chapter 1.3.1, the (strict) passivity of the S-parameter DS (4.1) is equivalent to the (strict) bounded realness of $S(s)$ ($s = \delta + j\omega,$ where $\delta, \omega \in \mathbb{R}$), i.e.,

1. $S(s)$ is analytic on the open right half plane $\mathrm{Re}(s) > 0$);

2. $I - S^*(j\omega)S(j\omega) \geq 0$ ($>$ for strict bounded realness) for all ω.

The second condition implies $\sigma_1(S(j\omega)) \leq 1$ (or < 1 for strict bounded realness), which can be checked by sampling some points (frequencies) along the imaginary axis $s = j\omega$ [8, 9, 41]. However, erroneous results may be obtained if nonpassive regions between sampling points are missed. For standard state-space models (A, B, C, D) [with $E = I$ in (4.1)], the more reliable Hamiltonian method is preferred. The corresponding $2n \times 2n$ Hamiltonian matrix for S-parameter standard state-space model is defined as

$$\mathcal{M} = \begin{bmatrix} A - BD^T\hat{S}^{-1}C & -B\hat{R}^{-1}B^T \\ C^T\hat{S}^{-1}C & C^TD\hat{R}^{-1}B^T - A^T \end{bmatrix} \tag{4.3}$$

where $\hat{S} = (DD^T - I)$ and $\hat{R} = (D^TD - I)$. Since any purely imaginary scalar $j\omega \in \lambda(\mathcal{M})$ pinpoints a crossover point ω (in rad/sec) of passivity violations, the (possible) nonpassive regions can be accurately located by the imaginary eigenvalue calculation of $\mathcal{M}$. To speed up calculation, [13] has further developed a half-size singularity matrix for symmetric standard state-space models:

$$\mathcal{P} = \left(A - B(D - I)^{-1}C\right)\left(B(D + I)^{-1}C - A\right). \tag{4.4}$$

It has been proved that ω is a crossover point of passivity violation if and only if $\hat{\beta}$ is an eigenvalue of $\mathcal{P}$, where $\hat{\beta}(\in \mathbb{R}) = \omega^2 > 0$. Since $\mathcal{P} \in \mathbb{R}^{n\times n}$ and the eigenvalue computation has $O(n^3)$ complexity, the half-size singularity test is about $8\times$ faster than the full-size Hamiltonian method. Both of them are reliable but only applicable to standard state-space models. Besides that, another limitation of Hamiltonian-based passivity test is that (4.3) [or (4.4)] requires $I - D^TD$ (or $I - D^2$ for symmetric cases) to be nonsingular, which is not guaranteed in all cases.

4.3 S-GHM and S-HGHM

In this section we present the S-parameter GHM theories, which characterize the norm of $S(j\omega)$ and thus could be utilized for reliable passivity assessment of S-parameter DSs. For symmetric DSs, a half-size matrix pencil can be derived to characterize the bounded realness of an S-parameter model.

4.3.1 S-Parameter GHM (S-GHM) Theory

Theorem 4.1: *Given the DS (4.1), assume that $j\omega$ is not a system pole [i.e., $j\omega \notin \lambda(A, E)$] and γ is not a singular value of D [i.e., $\gamma \notin \sigma(D)$], then γ is a singular value of $S(j\omega)$ if and only if $j\omega$ is a generalized eigenvalue of the matrix pencil (M, N). The size-$2n$ matrix pencil is defined as*

$$M = \begin{bmatrix} A - BD^T S^{-1} C & -\gamma B R^{-1} B^T \\ \gamma C^T S^{-1} C & -A^T + C^T D R^{-1} B^T \end{bmatrix}, \quad N = \begin{bmatrix} E & \\ & E^T \end{bmatrix} \tag{4.5}$$

where $S = DD^T - \gamma^2 I$ and $R = D^T D - \gamma^2 I$. It is trivial to prove that M is a Hamiltonian matrix.

Proof: Since the system matrices are real, we have $S^*(j\omega) = B^T(-j\omega E^T - A^T)^{-1} C^T + D^T$. Assuming $\gamma \in \sigma(S(j\omega))$ and $\gamma \notin \sigma(D)$, singular value decomposition (SVD) implies that there exist non-zero vectors v and u such that $S(j\omega)u = \gamma v$ and $S^*(j\omega)v = \gamma u$, i.e.,

$$\left[C(j\omega E - A)^{-1} B + D\right] u = \gamma v, \quad \left[B^T (j\omega E^T + A^T)^{-1} (-C^T) + D^T\right] v = \gamma u.$$

The above relationship can be reformulated as the compact matrix form

$$\begin{bmatrix} C & \\ & B^T \end{bmatrix} \underbrace{\Omega_\omega^{-1} \begin{bmatrix} B & \\ & -C^T \end{bmatrix} \begin{bmatrix} u \\ v \end{bmatrix}}_{z} = \begin{bmatrix} -D & \gamma I \\ \gamma I & -D^T \end{bmatrix} \begin{bmatrix} u \\ v \end{bmatrix}. \tag{4.6}$$

Here $\begin{bmatrix} j\omega E - A & \\ & j\omega E^T + A^T \end{bmatrix}$ has been denoted by Ω_ω. Because γ is not a singular value of D, it is straightforward to prove that $\begin{bmatrix} -D & \gamma I \\ \gamma I & -D^T \end{bmatrix}$ is a nonsingular matrix, thus no non-zero vectors are contained in its null space. Since neither u nor v is zero, the right-hand side of (4.6) is non-zero, which further implies z is a non-zero vector [since it is a factor of the left-hand side of (4.6)]. Pre-multiplying both sides of (4.6) by $\begin{bmatrix} B & \\ & -C^T \end{bmatrix} \begin{bmatrix} -D & \gamma I \\ \gamma I & -D^T \end{bmatrix}^{-1}$ would lead to

$$\begin{bmatrix} B & \\ & -C^T \end{bmatrix} \begin{bmatrix} -D & \gamma I \\ \gamma I & -D^T \end{bmatrix}^{-1} \begin{bmatrix} C & \\ & B^T \end{bmatrix} z = \Omega_\omega z. \tag{4.7}$$

Because

$$M - j\omega N = \begin{bmatrix} B & \\ & -C^T \end{bmatrix} \begin{bmatrix} -D & \gamma I \\ \gamma I & -D^T \end{bmatrix}^{-1} \begin{bmatrix} C & \\ & B^T \end{bmatrix} - \Omega_\omega$$

(4.7) can be rewritten as

$$Mz = j\omega N z. \tag{4.8}$$

Therefore, $j\omega$ is a purely imaginary generalized eigenvalue of the matrix pencil (M, N). To prove the converse, we define

$$z' = \begin{bmatrix} -D & \gamma I \\ \gamma I & -D^T \end{bmatrix}^{-1} \begin{bmatrix} C & \\ & B^T \end{bmatrix} z = \begin{bmatrix} u' \\ v' \end{bmatrix} \tag{4.9}$$

which is a factor for the left-hand side of (4.7). Here $u', v' \in \mathbb{C}^n$. Because Ω_ω is nonsingular and $z \neq 0$, the right-hand side of (4.7) and thus z' should be non-zero vectors. Pre-multiplying (4.7) by $\begin{bmatrix} C & \\ & B^T \end{bmatrix} \Omega_\omega^{-1}$would lead to

$$\begin{bmatrix} C & \\ & B^T \end{bmatrix} \Omega_\omega^{-1} \begin{bmatrix} B & \\ & -C^T \end{bmatrix} z' = \begin{bmatrix} -D & \gamma I \\ \gamma I & -D^T \end{bmatrix} z'. \tag{4.10}$$

From (4.10), one can easily get $S(j\omega)u' = \gamma v'$ and $S^*(j\omega)v' = \gamma u'$. Because neither u' nor v' is zero (otherwise z' should be a zero vector), γ is a singular value of $S(j\omega)$.

□

4.3.2 S-Parameter HGHM (S-HGHM) for Symmetric DSs

Theorem 4.2*: Assume the S-parameter DS (4.1) is symmetric [i.e., $S^T(j\omega) = S(j\omega)$], $j\omega$ is not a generalized eigenvalue of (A, E) and γ is not a singular value of D, then γ is a singular value of $S(j\omega)$ if and only if $\beta = \omega^2 > 0$ is a generalized eigenvalue of the half-size matrix pencil*

$$(M_h, N_h) = \left(X + Y, E(Y - X)^{-1}E\right) \tag{4.11}$$

with X and Y defined as

$$X = A - BDS^{-1}C, \;\; Y = -\gamma BR^{-1}C. \tag{4.12}$$

Proof: If the S-parameter transfer matrix of DS (4.1) is symmetric, we have

$$S^*(j\omega) = S(-j\omega) = C(j\omega E + A)^{-1}(-B) + D. \tag{4.13}$$

Consequently, E^T, A^T, B^T, C^T and D^T in (4.5) can be replaced by E, A, C, B and D, respectively. The following congruence transform on (M, N) gives a new matrix pencil

$$\begin{aligned}(M', N') &= \begin{bmatrix} I & I \\ I & -I \end{bmatrix} (M, N) \begin{bmatrix} I & I \\ I & -I \end{bmatrix} \\ &= \left(\begin{bmatrix} & 2X - 2Y \\ 2X + 2Y & \end{bmatrix}, \begin{bmatrix} 2E & \\ & 2E \end{bmatrix} \right).\end{aligned} \tag{4.14}$$

An important property of the above nonsingular congruence transform is that: $j\omega$ is a generalized eigenvalue of (M', N') if and only if it is a generalized eigenvalue of (M, N). As we have proved the equivalence of $j\omega \in \lambda(M, N)$ with $\gamma \in \sigma\left(S(j\omega)\right)$ in Section 4.3.1, $j\omega$ should also be a generalized eigenvalue of(M', N') if $\gamma \in \sigma(S(j\omega))$. In this case, $\det(M' - j\omega N') = 0$, and there exist a pair of vectors w_1 and w_2, such that

$$\begin{bmatrix} -j\omega E & X - Y \\ X + Y & -j\omega E \end{bmatrix} \begin{bmatrix} w_1 \\ w_2 \end{bmatrix} = 0, \quad \begin{bmatrix} w_1 \\ w_2 \end{bmatrix} \neq 0. \tag{4.15}$$

Assuming $X - Y$ being invertible, we get $w_2 = j\omega(X - Y)^{-1} E w_1$ from the upper part of (4.15). Here w_1 is nonzero (otherwise w_2 is also zero). By virtue of this, (4.15) reduces to

$$\left[M_h - \omega^2 N_h\right] w_1 = 0. \tag{4.16}$$

Therefore, $\beta = \omega^2 \in \lambda(M_h, N_h)$ if $\gamma \in S(j\omega)$. Analogous to S-GHM, the converse can also be proved. Setting $\omega_2 = j\omega(X - Y)^{-1} E\omega_1$ we can reach (4.15) from (4.16). And then using $\lambda(M, N) = \lambda(M', N')$ we can return to Theorem 4.1.

□

Note that S-HGHM only requires the DS transfer matrix $S(j\omega)$ to be symmetric, and it does not pose any restrictions on the symmetry of the system matrices.

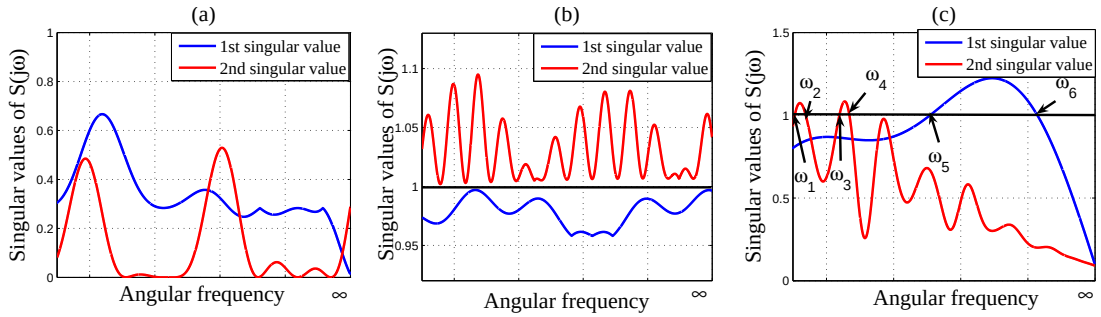

Figure 4.1: Illustrative examples for different kinds of DSs. (a) A globally strictly passive DS. This DS has no crossover points and its transfer matrix is always unit-bounded. (b) A consistently nonpassive DS. This DS does not have any crossover points, but it is nonpassive at any frequency point. (c) A DS with locally passive and nonpassive regions. This DS is nonpassive in intervals $l_2 = (\omega_1, \omega_2)$, $l_4 = (\omega_3, \omega_4)$ and $l_6 = (\omega_5, \omega_6)$.

4.4 Passivity Test of DSs

4.4.1 Passivity Test of S-Parameter DSs

In passivity test, we are interested in the special case of $\gamma = 1$, which represents the boundary of passivity violations of an S-parameter DS. By setting $\gamma = 1$, from S-GHM [in (4.5)] we get a passivity test matrix pencil $(M, N) = (M_0, N_0)$ for scattering DSs with

$$M_0 = \mathcal{M}, \qquad N_0 = N. \tag{4.17}$$

Here $\mathcal{M}$ is the Hamiltonian matrix defined in (4.3). Analogously, for symmetric cases, from S-HGHM [in (4.11)] one can get a half-size passivity test matrix pencil (M_{h0}, N_{h0}) defined as

$$M_{h0} = A - B(D - I)^{-1}C, \quad N_{h0} = E[(B(D + I)^{-1}C - A]^{-1}E. \tag{4.18}$$

If the matrix pencil (M_0, N_0) (or (M_{h0}, N_{h0}) for symmetric DSs) has any purely imaginary (or positive real) generalized eigenvalue $j\omega$ (or $\beta = \omega^2$), then ω is a crossover

frequency point where passivity violation happens.

Note that the scattering DS of interest may still be nonpassive even though no crossover points are computed via S-GHM or S-HGHM. To further identify the possible nonpassive regions, the following procedures could be used.

1. If no crossover points are found, check $S(j\omega_0)$ at an arbitrarily selected frequency point ω_0. If $||S(j\omega_0)|| < 1$, the DS is globally strictly passive [as illustrated in Fig. 4.1 (a)]. Otherwise, if $||S(j\omega_0)|| > 1$ the DS is nonpassive at any frequency point [as shown in Fig. 4.1 (b)].

2. If S-GHM/S-HGHM test produces p crossover points $\omega_1, \omega_2, ..., \omega_p$ which are increasingly ordered, one can select $p+1$ sampling points $\tilde{\omega}_k$ $(k = 1, 2, ..., p+1)$ such that $\tilde{\omega}_k \in \ell_k$ where $\ell_1 = (0, \omega_1)$, $\ell_i = (\omega_{i-1}, \omega_i)$ for $i = 2, ..., p$ and $\ell_{p+1} = (\omega_p, \infty)$. If $||S(j\tilde{\omega}_k)|| < 1$, the DS is passive in the interval ℓ_k; otherwise, it is nonpassive in ℓ_k. An illustrative example is given in Fig. 4.1 (c).

Note that if the DS (4.1) is a regular system (when E is invertible), it can be converted to a standard state-space model with $E = I$. Subsequently, for a regular system, the generalized eigenvalue solution in the test pencil (M_0, N_0) can be replaced by the standard eigenvalue computation of $M_0 = \mathcal{M}$. This is in fact the S-parameter Hamiltonian passivity verification (in (4.3) of Section II-A). For symmetric regular systems, substituting $E = I$ into the half-size test pencil in (4.18), the generalized eigenvalue problem reduces to the standard eigenvalue computation of $\mathcal{P}$ [defined in (4.4)]. Therefore, the S-parameter Hamiltonian method and the half-size singularity test in (4.3) and (4.4) are the subsets (or special cases) of S-GHM and S-HGHM, respectively.

4.4.2 Passivity Test of Hybrid DSs

Given a square admittance or impedance transfer matrix $H(s)$ with $\det(I+H(s)) \neq 0$ for all $\mathrm{Re}(s) > 0$, its Moebius-transformed function is defined as [77]

$$G(s) = (I - H(s))(I + H(s))^{-1}. \tag{4.19}$$

If $I + D$ is invertible, a realization of $G(s) = C_S(sE_S - A_S)^{-1}B_S + D_S$ is

$$\begin{aligned} &E_S = E,\ A_S = A - B(I+D)^{-1}C,\ B_S = -\sqrt{2}B(I+D)^{-1}, \\ &C_S = \sqrt{2}(I+D)^{-1}C,\ D_S = (I-D)(I+D)^{-1}. \end{aligned} \tag{4.20}$$

Conversely, $H(s)$ is also a Moebius-transformed function of $G(s)$. For Moebius transformation, the following properties hold [77].

1. Let $H(s) = C(sE - A)^{-1}B + D$ be a positive real DS transfer matrix with nonsingular $I + D$, then its Moebius-transformed function $G(s)$ is bounded real.

2. Given a bounded real DS transfer matrix $G(s) = C_S(sE_S - A_S)^{-1}B_S + D_S$ with $I + D_S$ being nonsingular and $\det(I + G(s)) \neq 0$ for all $\mathrm{Re}(s) > 0$, its Moebius-transformed function $H(s)$ is positive real.

Since D usually has a much lower dimension than E and A, the above transformation is very cheap. If we see $G(s)$ as a scattering system, then $H(s)$ is passive if and only if $G(s)$ is passive (i.e., bounded real). Therefore, we can test the passivity of $H(s)$ by checking the bounded realness of $G(s)$ using S-GHM. Further, we note that

$$G(s) = 2(I + H(s))^{-1} - I \tag{4.21}$$

Table 4.1: Applicability of different passivity tests

System model	S-GHM	S-HGHM	Hamiltonian method	Half-size singularity
singular system	yes	yes	no	no
regular system	yes	yes	yes	yes
asymmetric system	yes	no	yes	no
symmetric system	yes	yes	yes	yes

which implies that $G(s)$ is symmetric if and only if $H(s)$ is symmetric. Therefore, S-HGHM can also be used for symmetric hybrid cases after Moebius transformation.

4.4.3 Comparison with Traditional Approaches

Table 4.1 compares the applicability of different passivity tests. There are some distinctions among S-GHM/S-HGHM approach with traditional Hamiltonian method and half-size singularity test.

1. S-GHM/S-HGHM can be applied to both singular and regular LTI models, while S-parameter Hamiltonian method and half-size singularity test are only applicable to regular systems.

2. S-HGHM and half-size singularity test are exclusive to symmetric models, but their full-size counterparts can be used for general cases without symmetric restrictions.

3. S-GHM and S-HGHM search for the passivity violation points via generalized eigenvalue calculation, while traditional methods use standard eigenvalue computation.

4. Due to the half-size nature, S-HGHM and half-size singularity test are $8\times$ faster than S-GHM and Hamiltonian test, respectively.

5. As will be discussed in Section 4.4.4, S-GHM/S-HGHM can test the LTI models with $I - D^T D$ being singular, whereas the traditional approaches fail to work.

4.4.4 Numerical Issues

1. The requirement of $1 \notin \sigma(D)$ limits the applications of Hamiltonian method and half-size singularity test. For S-GHM and S-HGHM this restriction can be removed after a small modification called equivalent model conversion similar to the method in Chapter 2.4.3. The basic idea is to construct a new DS $S'(j\omega) = C'(j\omega E' - A')^{-1}B' + D'$, such that $S'(j\omega) = S(j\omega)$ and $1 \notin \sigma(D')$. $S'(j\omega)$ can be constructed in different ways. In this chapter, $S'(j\omega)$ is constructed, if necessary, as

$$\begin{aligned} E' &= \begin{bmatrix} E & \\ & 0 \end{bmatrix}, \quad A' = \begin{bmatrix} A & \\ & I \end{bmatrix}, \\ B' &= \begin{bmatrix} B \\ I \end{bmatrix}, \; C' = \begin{bmatrix} C & \alpha I - D \end{bmatrix}, \; D' = \alpha I \end{aligned} \tag{4.22}$$

   with $\alpha \in \mathbb{R}$ and $|\alpha| \neq 1$. Subsequently, the passivity of $S(j\omega)$ can be checked by performing S-GHM/S-HGHM on $S'(j\omega)$.

2. With the equivalent model conversion in (4.22), the restriction of $I + D$ being nonsingular in Moebius transformation can also be removed.

3. In S-HGHM passivity test, $A - B(D + I)^{-1}C$ is assumed to be nonsingular, which is equivalent to $1 \notin \lambda(S(0))$. A proof is given in Appendix 4.8.

4. The "purely" generalized eigenvalues of (M_0, N_0) may appear as conjugate pairs $\lambda_k = a_k \pm jb_k$ $(a_k, b_k \in \mathbb{R})$. Here a_k is the numerical noise induced by the finite machine precision, which is also observed in traditional Hamiltonian

method [14]. A small numerical tolerance $tol > 0$ can be used to eliminate the noise, and only those solutions with $|a_k| < tol$ are regarded as expected results.

The proposed passivity test is summarized in Algorithm 4.1.

4.5 Numerical Examples

This section presents some numerical examples to verify the validity and effectiveness of S-GHM/S-HGHM for S-parameter and hybrid DSs. All examples are tested in MATLAB R2006a on a 2.66 GHz 2G-RAM PC.

4.5.1 A Synthetic DS Model

To show the complete test flow, we consider the bounded realness of the following order-4 single-input single-output (SISO) DS:

$$E = \begin{bmatrix} 1 & & & \\ & 1 & & \\ & & 0 & 1 \\ & & & 0 \end{bmatrix}, \; A = \begin{bmatrix} -4 & & & \\ & -120 & & \\ & & 1 & \\ & & & 1 \end{bmatrix}, \; B = \begin{bmatrix} 1 \\ 1 \\ 0 \\ 10^{-5} \end{bmatrix}, \tag{4.23}$$
$$C = \begin{bmatrix} 10 & 200 & 10^{-5} & 0 \end{bmatrix}, \; D = -1.$$

The transfer function of this DS is

$$S(j\omega) = \frac{10}{j\omega + 4} + \frac{200}{j\omega + 120} - 1 + j\omega \times 10^{-10}. \tag{4.24}$$

Solving the equation

$$|S(j\omega)| = 1 \tag{4.25}$$

Algorithm 4.1: Passivity test by S-GHM/S-HGHM.

Input: An LTI model $\Sigma : (E, A, B, C, D)$, with $E, A \in \mathbb{R}^{n\times n}$, $B, C^T \in \mathbb{R}^{n\times m}$ and $D \in \mathbb{R}^{m\times m}$.

Output: The passive regions $U_{passive}$ and nonpassive regions $U_{nonpassive}$.

begin

1. Initialization: set $U_{passive} = U_{nonpassive} = \emptyset$

2. if $\Sigma : (E, A, B, C, D)$ *is a hybrid system* **then**

perform Moebius transform (4.20) and update Σ.

3. Compute crossover points.

if $1 \notin \sigma(D)$ *and* E *is nonsingular* **then**

if Σ *is symmetric* **then**

compute the crossover points by half-size singularity test (4.4);
$\Theta \leftarrow \{\omega_1, ..., \omega_p\}$, where the p crossover points ω_1, ..., ω_p are increasingly ordered.

else

compute the crossover points by traditional Hamiltonian method (4.3);
$\Theta \leftarrow \{\omega_1, ..., \omega_p\}$.

else

if $1 \in \sigma(D)$ **then**

perform equivalent model conversion (4.22), update Σ.

if Σ *is symmetric* **then**

compute the crossover points by S-GHM (4.17);
$\Theta \leftarrow \{\omega_1, ..., \omega_p\}$.

else

compute the crossover points by S-HGHM (4.18);
$\Theta \leftarrow \{\omega_1, ..., \omega_p\}$.

4. Locate the passive/nonpassive regions

if $\Theta = \emptyset$ **then**

compute $S(j\omega_0)$ (the transfer matrix of Σ) at ω_0

if $||S(j\omega_0)|| < 1$ **then**

$U_{passive} = [0, \infty)$;
system is strictly passive, return.

else

$U_{nonpassive} = [0, \infty)$;
system is consistently nonpassive, return.

else

$\ell_1 \leftarrow [0, \omega_1), \ell_2 \leftarrow (\omega_1, \omega_2), ..., \ell_p \leftarrow (\omega_{p-1}, \omega_p), \ell_{p+1} \leftarrow (\omega_p, \infty)$.

for $i = 1, ..., p + 1$ **do**

compute $S(j\dot{\omega}_i)$, with $\dot{\omega} \in \ell_i$;

if $||S(j\dot{\omega}_i)|| < 1$ **then**

$U_{passive} = U_{passive} \cup \ell_i$;

else

$U_{nonpassive} = U_{nonpassive} \cup \ell_i$.

we get two crossover frequency points: $\omega = 22.86\ rad/sec$ and $\omega = 304491.7\ rad/sec$. Then we use S-GHM/S-HGHM to compute the crossover points. Note that in this DS $D = -1$, so we need to use equivalent model conversion in advance, which produces an order-5 DS $S'(j\omega)$ with $D' = 0$. Since the transfer function is symmetric, S-HGHM can also be applied for passivity test. The computed results of S-GHM and S-HGHM are listed in Table 4.2. The results of S-GHM and S-HGHM coincide with the solutions to (4.25), which is illustrated in Fig. 4.2. Therefore, this scattering DS is bounded real in the angular frequency band of $(22.86, 304491.7)$, and it is nonpassive in the bands of $(0, 22.86)$ and $(304491.7, \infty)$.

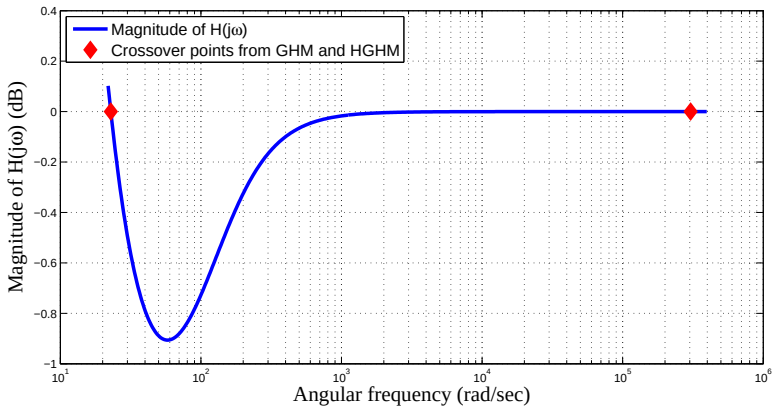

Figure 4.2: S-GHM and S-HGHM test results for the order-4 DS model.

Table 4.2: S-GHM/S-HGHM test results for the order-4 DS.

Imaginary results of$\lambda(M_0, N_0)$ $(j\omega)$	Positive results of $\lambda(M_{h0}, N_{h0})$ (β)	$\sqrt{\beta}$ (rad/sec)
5.5e-7 $\pm j304491.7$	92715196749	304491.7
2.05e-14 $\pm j22.86$	522.6	22.86

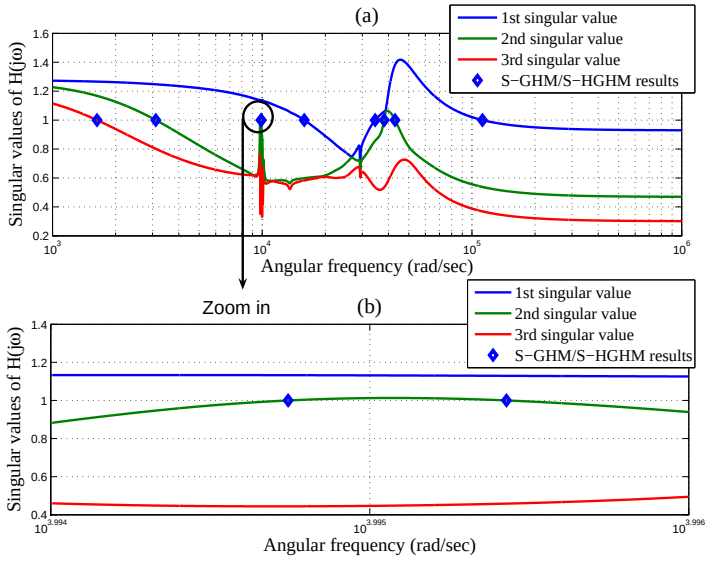

Figure 4.3: S-GHM and S-HGHM test results for the three-terminal filter.

4.5.2 A Symmetric S-Parameter Three-Terminal Filter

We use a three-terminal filter with symmetric port response to illustrate the application of S-GHM/S-HGHM and the connection to their standard state-space counterparts. The frequency-dependent scattering parameters are measured at 1601 sampling points ranging from 50 MHz to 6 GHz. Since it is impulse-free, the input-output response can be described by either a standard state space or a DS. To use the traditional Hamiltonian method and half-size singularity test, we first build an order-120 standard state-space model (A, B, C, D) by vector fitting [48] with 40 common poles. Both the traditional Hamiltonian method [10] and the half-size singularity test [13] show that this model has 9 crossover points. The imaginary eigenvalues of $\mathcal{M}$ and the positive real eigenvalues of $\mathcal{P}$ are illustrated in the first and second columns of Table 4.3, respectively. The obtained standard state-space model is then converted to a DS model $H_d(j\omega)$ described by $(E_d, A_d, B_d, C_d, D_d)$, via the following transformation

Table 4.3: Experimental results of various passivity tests for the three-terminal filter model.

Hamiltonian method: imaginary results of $\lambda(\mathcal{M})$	Half-size singularity test: positive real results of $\lambda(\mathcal{P})$/crossover points	S-GHM: imaginary results of $\lambda(M_0, N_0)$	S-HGHM: positive real results of $\lambda(M_{h0}, N_{h0})$/crossover points
6.9e-10 $\pm j$112253	12600780132/112253	2.17e-7 $\pm j$112253	12600780132/112253
2.6e-10 $\pm j$42988.4	18479990052/42988.4	2.58e-8 $\pm j$42988.4	18479990052/42988.4
1.3e-10 $\pm j$38173.7	14572294488/38173.7	1.06e-5 $\pm j$38173.7	14572294488/38173.7
2.2e-11 $\pm j$34551.3	1193794989.3/34551.3	2.93e-8 $\pm j$34551.3	1193794989.3/34551.3
4.0e-12 $\pm j$3109.22	9667288.145/3109.22	2.80e-6 $\pm j$3109.22	9667288.145/3109.22
2.1e-12 $\pm j$1631.07	2660378.573/1631.07	6.02e-7 $\pm j$1631.07	2660378.573/1631.07
3.0e-10 $\pm j$15871.8	251914404.4/15871.8	1.85e-8 $\pm j$15871.8	251914404.4/15871.8
8.7e-11 $\pm j$9879.71	97608669.57/9879.71	5.17e-7 $\pm j$9879.71	97608669.67/9879.71
8.5e-11 $\pm j$9895.29	97916796.34/9895.29	5.20e-7 $\pm j$9895.29	97916796.34/9895.29

$$E_d = \begin{bmatrix} I_{120} & \\ & 0 \end{bmatrix}, \quad A_d = \begin{bmatrix} A & \\ & I_3 \end{bmatrix}, \quad B_d = \begin{bmatrix} B \\ I_3 \end{bmatrix}, \tag{4.26}$$
$$C_d = \begin{bmatrix} C & -D \end{bmatrix}, \quad D_d = 0.$$

Then S-GHM and S-HGHM tests on $H_d(j\omega)$ also give 9 crossover points shown in the third and fourth columns of Table 4.3. Table 4.3 shows that the experimental results of all the four methods pinpoint the same boundary frequency points, which coincides with the singular value curves of the transfer matrix in Fig. 4.3.

4.5.3 A Symmetric Admittance PEEC Reduced Model

We use the PEEC example to show the validity of S-GHM and S-HGHM in the passivity test of admittance or impedance DS models. This example is also used in Chapter 2.5.2 to verify the validity of GHM/HGHM. The original SISO model is an order-480 DS describing a patch antenna structure with admittance parameter as its transfer function, which is obtained by partial element equivalent circuit (PEEC) method [63]. This PEEC model is nonpassive, which may be induced by poor meshing generation, inadequate numerical integration, matrix sparsification or inappropriate geometrical discretization [85]. After model order reduction via PRIMA [22], an order-53 reduced model is obtained, which is nonpassive in the low-frequency band.

Table 4.4: S-GHM and S-HGHM test results for the admittance reduced model (on the Moebius-transformed system).

$\lambda(M_0, N_0)\ (j\omega)$	$\lambda(M_{h0}, N_{h0})\ (\beta)$	$\sqrt{\beta}\ (rad/sec)$
1.309e-11 $\pm j0.505080$	0.255103	0.505080
1.307e-11 $\pm j0.505082$	0.255110	0.505082
1.127e-13 $\pm j1.234402$	1.523749	1.234402
3.650e-13 $\pm j2.465012$	6.076287	2.465012
3.169e-13 $\pm j2.560446$	6.555922	2.560446
7.587e-13 $\pm j4.074095$	16.59825	4.074095

Since this model is a hybrid system, S-GHM and S-HGHM can not be directly

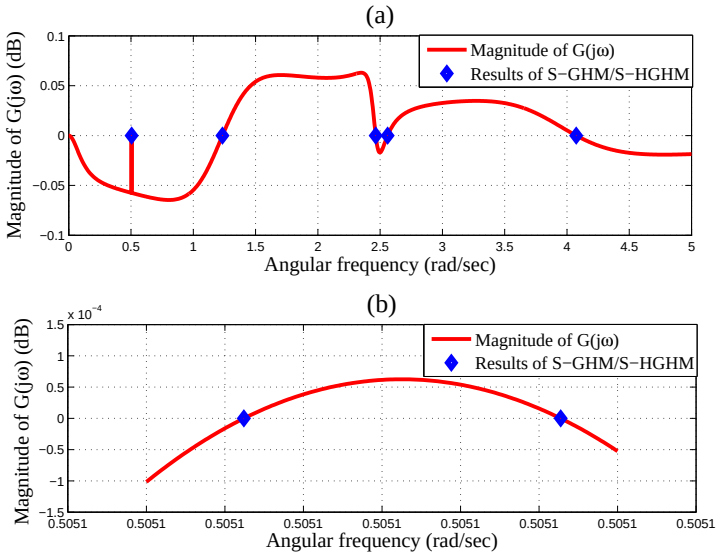

Figure 4.4: S-GHM and S-HGHM test results on the Moebius-transformed transfer function of the order-53 admittance reduced model.

used. The Moebius-transformed system is first constructed by (4.20), and then its transfer function $G(s)$ is tested by S-GHM and S-HGHM, respectively. The computed crossover points are listed in Table 4.4. Fig. 4.4 shows the magnitude of the Moebius-transformed transfer function equals unity at the computed crossover points. To show the validity, the real part of the original admittance transfer function $H(j\omega)$ is also

plotted in Fig. 4.5, which shows that the proposed S-GHM and S-HGHM methods have accurately found the passivity violation points of this hybrid DS.

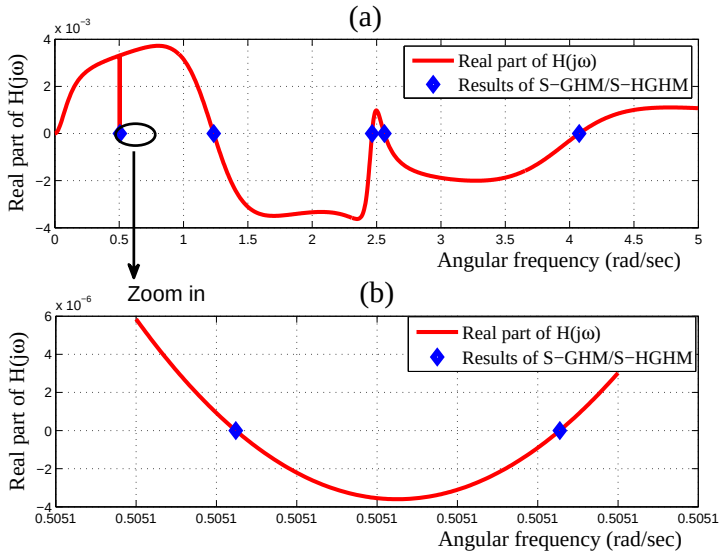

Figure 4.5: The real part of the transfer function of the original order-53 admittance DS model. The dots are the results from S-GHM and S-HGHM tests, which are accurately located at the boundaries of passivity violations.

4.5.4 A Multi-Port DS Model

Table 4.5: CPU time (sec) comparison of S-GHM and S-HGHM.

Model Size	Port Number	S-GHM	S-HGHM	Speedup
1080	60	241.2	30.45	7.92

This example is used to verify the validity of S-GHM and S-HGHM in general multi-port DS models, and to compare their numerical efficiency. The order-1080 symmetric DS model has 60 ports, and it is built from the measured S-parameter data of an electronic system, via the DS-format Loewner matrix fitting [49,50]. Using S-GHM and S-HGHM tests, 18 crossover points are obtained, which are plotted in

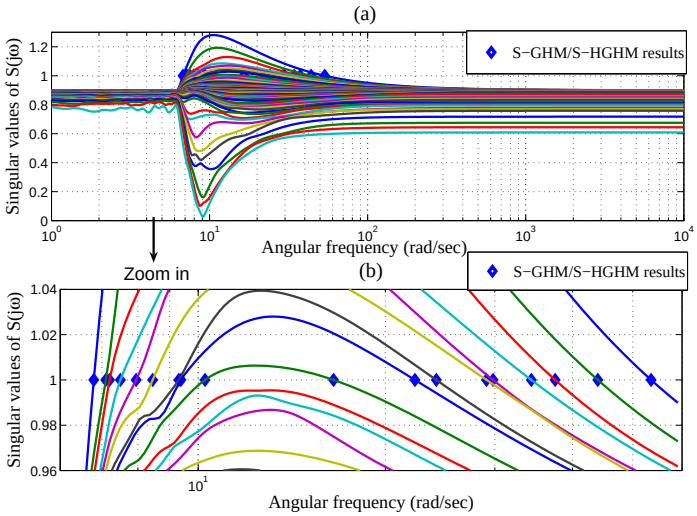

Figure 4.6: S-GHM/S-HGHM test results for the multi-port S-parameter DS model. The dots are the results from S-GHM and S-HGHM tests, which are accurately located at the boundaries of passivity violations.

Fig 4.6. Due to the large amount of crossover points, they are not listed by table. Clearly, Fig 4.6 (b) shows that the computed results are very accurate. We have listed the CPU times of S-GHM and S-HGHM tests in Table 4.5. It is clear that S-HGHM is about 8× faster over S-GHM, which is expected due to its half-size nature and the $O(n^3)$ complexity of generalized eigenvalue calculation.

4.6 Discussions

1. S-GHM and S-HGHM are purely algebraic passivity verification with similar accuracy to Hamiltonian method and half-size singularity test. Therefore, they are much more reliable and accurate than frequency sweeping methods, which has been verified by their hybrid counterparts (see Chapter 2). Compared with Hamiltonian method and half-size singularity test, S-GHM and S-HGHM are not restricted by the restriction on D matrix, as verified by the synthetic example.

2. As illustrated in Tables 4.2 to 4.4, the numerical results of S-GHM and Hamiltonian method contain some numerical noise in the real part, which can be eliminated by setting a tolerance. S-HGHM and half-size singularity tests do not suffer from this problem. From the numerical perspective, they are more accurate over the full-size S-GHM and Hamiltonian methods.

3. Due to the half-size nature and the $O(n^3)$ complexity of (generalized) eigenvalue computation, S-HGHM and half-size singularity test are $8\times$ faster than their full-size counterparts. This has been verified by the results in Chapter 2 and the CPU timings in Table 4.5. S-GHM and S-HGHM algorithms presented here are based on full-matrix eigensolver, so they are feasible to medium-size (e.g., order-1000) physical models. If we consider the Hamiltonian structure of M_0 and only compute the purely imaginary roots in S-GHM test, the proposed flow is expected to be faster and thus extensible to large and/or sparse DSs. This work has been discussed in Chapter 3.

4. In this chapter, the passivity at the interval of two adjacent crossover points is identified by the sampling scheme (as shown in Algorithm 4.1). An alternative approach is to compute the slope signs of the singular value curves at the calculated boundary points, according to the generalized eigenvalue perturbation theory of Hamiltonian matrix pencils. And furthermore, using the perturbation theory, our proposed S-GHM/S-HGHM approach also leads to a DS passivity enforcement scheme. These issues will be reported soon in the future document.

4.7 Summary

We have extended GHM and HGHM theories of Chapter 2 to S-parameter DSs, which reflect the relationship of the singular values of a DS transfer matrix with its

operating frequency. With the proposed methods, the passivity of S-parameter and hybrid DSs can be efficiently assessed, and the passive/nonpassive regions can be accurately located. For symmetric DSs, S-HGHM enjoys higher numerical accuracy and an 8× speedup over S-GHM.

4.8 Appendix

In S-HGHM passivity test, the assumption of $A - B(I + D)^{-1}C$ is equivalent to $\det[I - S(j\omega)] \neq 0$ at the DC point (i.e., $\omega = 0$). The proof is as follows.

Proof: Firstly, we assume that $A - B(I + D)^{-1}C$ is singular, then there exists a vector p such that

$$[A - B(I + D)^{-1}C]p = 0 \;\; p \neq 0. \tag{4.27}$$

Since A is nonsingular, the above equation is equivalent to

$$A^{-1}B(I + D)^{-1}Cp = p. \tag{4.28}$$

Denote $(I + D)^{-1}Cp$ by q, which should be a nonzero vector [otherwise, $p \neq 0$ in (4.28)]. Pre-multiplying both sides of (4.28) by C yields

$$CA^{-1}Bq = (I + D)q, \quad q \neq 0. \tag{4.29}$$

Because $S(0) = D - CA^{-1}B$, (4.29) can also be written as

$$[I - S(0)]q = 0, \quad q \neq 0 \tag{4.30}$$

which shows $I - S(0)$ is singular [i.e., $1 \in \lambda(S(0))$].

Next, we start with (4.29) to prove the converse. Since the right side of (4.29) is nonzero (because $1 \notin \sigma(D)$ and $q \neq 0$), we denote $p' = A^{-1}Bq$ which should also be

nonzero. Equation (4.29) is equivalent to

$$(I + D)^{-1}CA^{-1}Bq = q. \tag{4.31}$$

Pre-multiplying this equation by $A^{-1}B$ we get

$$A^{-1}B(I + D)^{-1}Cp' = p', \;\; p' \neq 0. \tag{4.32}$$

Hence, $A - B(I + D)^{-1}C$ is singular.

□

Chapter 5

Fast Positive-Real Balanced Truncation of Descriptor Systems

Modified nodal analysis (MNA) descriptions of linear VLSI circuits, such as RLC networks, normally yield index-1 or index-2 descriptor systems (DSs) which sometimes contain improper parts. This chapter presents an improper-part preserving passive model order reduction (MOR) procedure for RLC circuits, which consists of two steps: additive decomposition and passive MOR on the proper subsystem. In additive decomposition, spectral projectors are used to avoid unstable and prohibitively expensive Weierstrass decomposition. In the passive reduction of the proper part, we propose generalized quadratic alternating direction implicit (GQADI) iteration and its low-rank variant (LR-GQADI) to efficiently solve the generalized algebraic Riccati equations (GAREs). The effectiveness of the proposed algorithm is confirmed by some practical RLC benchmarks.

5.1 Motivation

The MNA description of a RLC networks yields the LTI DS

$$E_0\dot{x} = A_0x + B_0u, \;\; y = C_0x + D_0u, \tag{5.1}$$

where $E_0, A_0 \in \mathbb{R}^{n\times n}$, $B_0, C_0^T \in \mathbb{R}^{n\times m}$, $D_0 \in \mathbb{R}^{m\times m}$. The state vector x represents nodal voltages, and currents flowing through voltage sources and inductors; E_0 includes the capacitance and inductance terms, and A_0 denotes the conductance matrix. This DS model is widely used in interconnect [22] and power grid [24, 91] modeling.

Due to the huge size of the original DS model, linear model order reduction (MOR) [22, 24–27, 91] is normally used to reduce the circuit complexity. When the transfer matrix represent the admittance or impedance parameters (such as in interconnect modeling), it is desired to preserve system passivity to guarantee global stability. Typical passivity-preserving algorithms include MPVL [25] for symmetric RC circuits and PRIMA [22] for RLC models. These Krylov-subspace projection-based moment-matching schemes are applicable to DS models. However, they do not give numerical error bounds. Moreover, the possible impulsive response cannot be preserved [26]. Standard balanced truncation (BT, e.g. [28]) provides optimal approximations with global error bounds, and is generally much more accurate than Krylov-subspace projections. And the positive-real balanced truncation (PRBT, e.g., [26, 29, 30]) can further preserve such important system properties as passivity. However, for DS-form circuit models, a numerical transformation to the Weierstrass canonical form [26] is required before performing BT or PRBT. By Weierstrass canonical form, the possible improper part can be extracted, and the proper part is then constructed as a standard state-space model. Unfortunately, this procedure is prohibitively expensive and numerically unstable [17, 18, 20].

With spectral projectors in Chapter 3, the proper and improper parts can be

elegantly separated [20], and standard BT and PRBT can be extended to DS models with impulsive response [17, 18, 54]. The stability-preserving DS-BT requires solving the (projected) generalized algebraic Lyapunov equations (GALEs), which can be tackled by the generalized alternating direction implicit (GADI) iteration or its low-rank variant (LR-GADI) [55, 56]. To preserve passivity, DS-PRBT [17, 18] solves the (projected) generalized algebraic Riccati equations (GAREs), which utilizes Newton's iteration in recent literatures [17,59]. Inside each step of Newton's iteration, one needs to solve one (projected) GALE, so the complexity is comparable to solving tens of GALEs, which is still expensive.

Spectral projector construction is another bottleneck with DS-PRBT flow. Theoretically, spectral projectors can be obtained by the Weierstrass canonical form [17, 18, 54]. However, even for an order-1000 DS, computing its Weierstrass canonical form on a general machine can be prohibitively time consuming and numerically unstable. An alternative approach is to use the canonical projector technique [19, 20], which however requires expensive null space computation, matrix inversion and full matrix-matrix products. With the special topology of RLC circuits, [18] has proposed an explicit form for spectral projectors. In some cases where circuit topological information is unavailable (e.g., for those DS models obtained by EM field solver), the fast spectral projector construction in Chapter 3.5.1 can significantly reduce the computational load.

In this chapter, we propose a fast PRBT-based passive MOR algorithm for DSs. By exploiting the sparsity of circuit equations, the spectral projectors are constructed with a low cost as in Chapter 3.5.1. The proper and improper subsystems, say, of an RLC network, are then extracted by additive decomposition. Afterwards, the proper part is reduced by DS-PRBT, where generalized quadratic alternating direction implicit (GQADI) iteration and its low-rank version (LR-GQADI) (namely, extensions of the QADI and LR-QADI iterative schemes in [30]) are proposed to solve the GARE

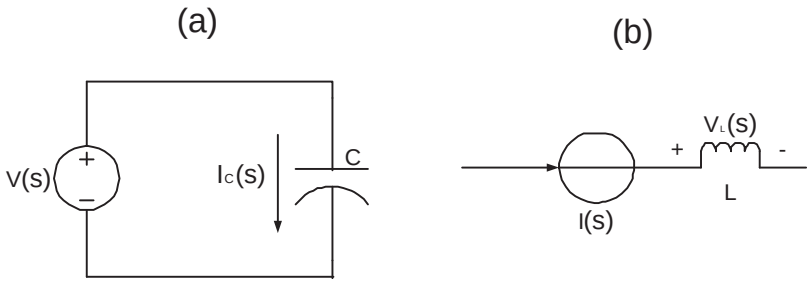

Figure 5.1: (a) A C-V loop. (b) An L-I cutset.

at approximately the cost of solving only one GALE. Both system passivity and the possible impulsive response are preserved by this DS-PRBT flow.

5.2 Preliminaries

5.2.1 Problems in DS MOR

Assume the matrix pencil (E_0, A_0) is regular (i.e., $\exists\ s_0 \in \mathbb{C}$, $\det(s_0E_0 - A_0) \neq 0$), then the DS transfer matrix reads

$$G(s) = \ D_0 + C_0(sE_0 - A_0)^{-1}B_0. \tag{5.2}$$

Assuming the DS is index-μ and recalling the results from Chapters 1, 2 & 4, we know that

$$G(s) = G_p(s) + G_{imp}(s) \tag{5.3}$$

where $G_p(s)$ and $G_{imp}(s)$ are the proper and improper parts, respectively. In the time domain, the improper part generates impulsive response. The DS in (5.1) is passive if and only if: i) $G_p(s)$ is positive-real; ii) $G_{imp}(s) = sM_1$ where $M_1 = -C_\infty N B_\infty \geq 0$.

The above DS circuit model can be reduced by either Krylov-subspace projection

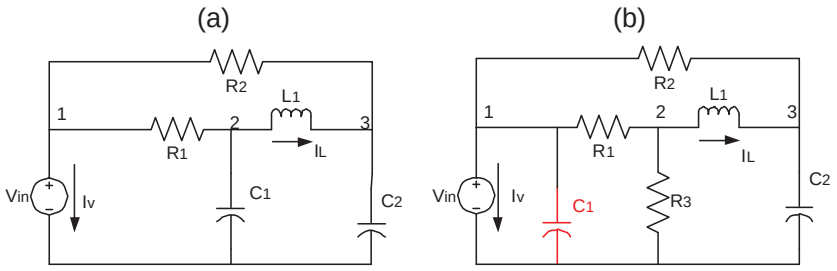

Figure 5.2: (a) An index-1 circuit without any L-V cutsets or C-V loops. (b) An index-2 circuit with a C-V loop formed by V_{in} and C_1.

or PRBT. For positive semidefinite (PSD) DS, PRIMA [22] can be used to preserve system passivity, but the improper part is normally lost. To preserve both the improper part and system passivity, [26] first decomposes the original system by Weierstrass decomposition and then uses PRBT to reduce the proper part. Unfortunately, Weierstrass decomposition is too expensive to implement and usually numerically unstable. Besides, the resulting proper part normally has dense and ill-conditioned matrices, which is not preferred for ARE solvers.

5.2.2 Projected GALEs and GAREs

The projected GALEs of the DS in (5.1) are given as

$$A_0^T \bar{X} E_0 + E_0^T \bar{X} A_0 + P_r^T C_0^T C_0 P_r = 0, \quad \bar{X} = P_l^T \bar{X} P_l, \tag{5.4a}$$

$$A_0 \bar{Y} E_0^T + E_0 \bar{Y} A_0^T + P_l B_0 B_0^T P_l^T = 0, \quad \bar{Y} = P_r \bar{Y} P_r^T. \tag{5.4b}$$

Here the left and right spectral projectors

$$P_l = W \begin{bmatrix} I_q & 0 \\ 0 & 0 \end{bmatrix} W^{-1}, \quad P_r = T^{-1} \begin{bmatrix} I_q & 0 \\ 0 & 0 \end{bmatrix} T, \tag{5.5}$$

project onto the left and right deflating subspaces of (E_0, A_0) corresponding to their finite eigenvalues, respectively. Some general assumptions are posed on the circuit topologies [18]: i) there exist no loops of voltage sources or cutsets of current sources; ii) the resistance, inductance and capacitance matrices are positive definite. Under the above assumptions, the DS index is at most 2 (i.e., $\mu \leq 2$). Specifically, if no loops consisting of capacitors and voltage sources (C-V loops) or cutsets connecting inductors and current sources (L-I cutsets) exist, the circuit is index-1; otherwise, the circuit is index-2 [5]. Illustrative examples are given in Figs. 5.1 & 5.2.

If (E_0, A_0) is stable, (5.4a) and (5.4b) have unique solutions $\bar{X}, \bar{Y} \geq 0$. Using the GALE (5.4b) as an example, it can be solved by the generalized ADI (GADI) [55]

$$(E_0 + s_i A_0)\bar{Y}_{i-\frac{1}{2}} A_0^T + A_0 \bar{Y}_{i-1}(E_0 - s_i A_0)^T = -P_l B_0 B_0^T P_l^T, \tag{5.6a}$$

$$(E_0 + \bar{s}_i A_0)\bar{Y}_i A_0^T + A_0 \bar{Y}_{i-\frac{1}{2}}(E_0 - \bar{s}_i A_0)^T = -P_l B_0 B_0^T P_l^T, \tag{5.6b}$$

with $s_1, ..., s_i \in \mathbb{C}^-$ where $\mathbb{C}^-$ denotes the open left-half plane. If we set $\bar{Y}_0 = 0$, $\bar{Y}_i$ can be obtained by

$$\begin{aligned} \bar{Y}_i = &-2\,\mathrm{Re}(s_i)(E_0 + s_i A_0)^{-1} P_l B_0 B_0^T P_l^T (E_0 + \bar{s}_i A_0)^{-T} + \\ &(E_0 + s_i A_0)^{-1}(E_0 - \bar{s}_i A_0)\bar{Y}_{i-1}(E_0 - s_i A_0)^T (E_0 + \bar{s}_i A_0)^{-T}. \end{aligned} \tag{5.7}$$

By exploiting the low-rank and positive semidefinite (PSD) properties of $\bar{Y}_i$, a low-rank variant of GADI is further developed in [56], which significantly speeds up the computation.

In DS-PRBT, one needs to get the positive-real gramians, i.e., the minimal solutions $X, Y (\in \mathbb{R}^{n\times n}) \geq 0$ to the dual projected GAREs

$$A^T XE + E^T XA + E^T XBB^T XE + P_r^T C^T CP_r = 0, \tag{5.8a}$$

$$AYE^T + EYA^T + EYC^T CYE^T + P_l BB^T P_l^T = 0, \tag{5.8b}$$

such that $X = P_l^T XP_l$, $Y = P_r YP_r^T$, $(E, A + BB^T XE)$ and $(E^T, A^T + C^T CYE^T)$ are stable [60]. Here $E = E_0$, $M_0 = D_0 - C_\infty B_\infty$, $B = B_0 D, C = D^T C_0, A = A_0 - P_l BCP_r$, D is defined by $DD^T = (M_0 + M_0^T)^{-1}$. A popular method of solving projected GARE (e.g., (5.8b)) is by Newton's iteration (as summarized by Algorithm 5.1) [18]. Inside each iteration, a (projected) GALE needs to be solved. One can solve this (projected) GALE by GADI or LR-GADI. Obviously, solving a (projected) GARE requires solving multiple (usually tens of) (projected) GALEs.

Algorithm 5.1: Newton's iteration for projected GARE (5.8b)

Input: $E, A \in \mathbb{R}^{n\times n}$, $B, C^T \in \mathbb{R}^{n\times m}$, P_l, P_r, an initial guess Y_0, and a numerical tolerance *tol*.

Output: The approximate solution Y_i to (5.8b).

begin

  for j = 1,2,... **do**

    Compute $K_j = EY_{j-1}A^T$ and $A_j = A + K_j A$.

    Solve the projected GALE: $EY_j A_j^T + A_j Y_j E^T = -P_l(BB^T - K_j K_j^T)P_l^T$, $Y_j = P_r Y_j P_r^T$.

    if $||Y_j - Y_{j-1}|| < tol$ **then**

      Return Y_j and exit;

    else

      Continue.

5.3 DS-MOR via DS-PRBT

The proposed DS-PRBT flow consists of two steps: i) additive decomposition that separates the proper and possible improper parts; ii) PRBT of the proper part.

5.3.1 Additive Decomposition

We first decompose the DS by using the right spectral projector P_r (either P_r or P_l is needed, and the procedures by using P_l are completely analogous). This chapter considers index-2 circuits (index-1 cases are trivial [18,20]). Directly computing P_r by Weierstrass decomposition is prohibitively expensive. From the circuit topology, P_r can be easily obtained by its closed form [18]. If the topology is unknown, canonical projector technique [19, 20] can be applied to compute P_r, by the sparse LU-based fast numerical implementation elaborated in Chapter 3.5.1.

With P_r, the proper and improper subsystems can be easily separated. First, we note

$$\begin{aligned}
\hat{G}(s) &= C_0(I - P_r)(sE_0 - A_0)^{-1}B_0 + D_0 \\
&= C_0 T^{-1} \begin{bmatrix} 0 & \\ & I \end{bmatrix} \begin{bmatrix} sI - J & \\ & sN - I \end{bmatrix}^{-1} W^{-1}B_0 + D_0 \\
&= C_\infty (sN - I)^{-1} B_\infty + D_0 = G_{imp}(s) + M_0.
\end{aligned} \tag{5.9}$$

Since the original linear RLC circuit is passive, we have $G_{imp}(s) = sM_1$, then M_0 and M_1 can be computed by

$$M_0 = \hat{G}(0), \quad M_1 = \frac{\hat{G}(s_1) - \hat{G}(s_2)}{s_1 - s_2} \tag{5.10}$$

where s_1 and s_2 are positive real scalars. Subsequently, an impulse-free DS $\mathcal{G}_p(s)$

realized by $(\mathcal{E}_0, \mathcal{A}_0, \mathcal{B}_0, \mathcal{C}_0, \mathcal{D}_0)$ is constructed as follows:

$$\begin{aligned} \mathcal{E}_0 &= E_0 P_r - A_0(I - P_r) = W \begin{bmatrix} I_q & \\ & -I_{n-q} \end{bmatrix} T \\ \mathcal{A}_0 &= A_0, \;\; \mathcal{C}_0 = C_0 P_r, \; \mathcal{B}_0 = B_0, \;\; \mathcal{D}_0 = M_0. \end{aligned} \tag{5.11}$$

It is straightforward to prove that $\mathcal{G}_p(s) = G_p(s)$, $\mathcal{E}_0$ is nonsingular, $(\mathcal{E}_0, \mathcal{A}_0)$ is stable. The flow of additive decomposition is summarized in Algorithm 5.2.

Algorithm 5.2: Additive Decomposition for RLC Circuits

Input: $E_0, A_0 \in \mathbb{R}^{n\times n}$, $B_0, C_0^T \in \mathbb{R}^{n\times m}$, $D_0 \in \mathbb{R}^{m\times m}$
Output: $\mathcal{E}_0, \mathcal{A}_0, \mathcal{B}_0, \mathcal{C}_0, M_0$ and M_1.
begin
1. Compute P_r via canonical projector technique;
2. Extract M_0 and M_1 by (5.10), construct $\mathcal{G}_p(s)$ by (5.11).

5.3.2 PRBT of the Proper Subsystem

To perform passive MOR on the proper subsystem $\mathcal{G}_p(s)$, one needs to solve the dual projected GAREs. Since $\mathcal{E}_0$ and $\mathcal{A}_0$ are nonsingular, the spectral projectors of $(\mathcal{E}_0, \mathcal{A}_0)$ are

$$\mathcal{P}_l = \mathcal{P}_r = I. \tag{5.12}$$

Consequently, the projected GAREs of $\mathcal{G}_p(s)$ reduce to

$$\mathcal{A}^T\mathcal{X}\mathcal{E} + \mathcal{E}^T\mathcal{X}\mathcal{A} + \mathcal{E}^T\mathcal{X}\mathcal{B}\mathcal{B}^T\mathcal{X}\mathcal{E} + \mathcal{C}^T\mathcal{C} = 0, \tag{5.13a}$$

$$\mathcal{A}\mathcal{Y}\mathcal{E}^T + \mathcal{E}\mathcal{Y}\mathcal{A}^T + \mathcal{E}\mathcal{Y}\mathcal{C}^T\mathcal{C}\mathcal{Y}\mathcal{E}^T + \mathcal{B}\mathcal{B}^T = 0, \tag{5.13b}$$

which are two GAREs. Here we define $\mathcal{D}$ by $\mathcal{D}\mathcal{D}^T = (\mathcal{D}_0 + \mathcal{D}_0^T)^{-1}$, $\mathcal{B} = \mathcal{B}_0\mathcal{D}$, $\mathcal{C} = \mathcal{D}^T\mathcal{C}_0$. $\mathcal{A} = \mathcal{A}_0 - \mathcal{B}\mathcal{C}$ and $\mathcal{E} = \mathcal{E}_0$. The unique PSD stabilizing solutions $\mathcal{X}$ and $\mathcal{Y}$

to (5.13a) and (5.13b) are the positive real observability and controllability gramians of $\mathcal{G}_p(s)$, respectively.

After getting the positive real gramian matrices, the proper subsystem $\mathcal{G}_p(s)$ can be balanced and reduced to a much smaller DS $\mathcal{G}_{pr} = \mathcal{C}_r(s\mathcal{E}_r - \mathcal{A}_r)^{-1}\mathcal{B}_r + M_0$. The complete DS-PRBT flow is listed in Algorithm 5.3.

Algorithm 5.3: DS-PRBT of The Proper Part

Input: A proper subsystem described by $(\mathcal{E}_0, \mathcal{A}_0, \mathcal{B}_0, \mathcal{C}_0, \mathcal{D}_0)$, reduced order r.
Output: The reduced model of $\mathcal{G}_p(s)$ described by $(\mathcal{E}_r, \mathcal{A}_r, \mathcal{B}_r, \mathcal{C}_r, \mathcal{D}_r)$.
begin

1. Solve the dual GAREs (5.13a) and (5.13b) to get the gramians $\mathcal{X}$ and $\mathcal{Y}$;
2. Compute the factors L and R such that $\mathcal{X} = LL^T$, $\mathcal{Y} = RR^T$;
3. Compute the skinny singular value decomposition

$$L^T\mathcal{E}_0R = \begin{bmatrix} U_1 & U_2 \end{bmatrix} \begin{bmatrix} \Sigma_1 & \\ & \Sigma_2 \end{bmatrix} \begin{bmatrix} V_1 & V_2 \end{bmatrix}^T, \text{ where } \Sigma_1 = \text{diag}(\sigma_1, ..., \sigma_r),$$

$\Sigma_2 = \text{diag}(\sigma_{r+1}, ..., \sigma_{\hat{n}})$ and $\sigma_1 \geq ... \geq \sigma_r \geq \sigma_{r+1} \geq ... \geq \sigma_{\hat{n}}$;
4. Compute the projection matrix: $T_L = \Sigma_1^{-\frac{1}{2}} U_1^T L^T, \quad T_R = RV_1\Sigma_1^{-\frac{1}{2}}$;
5. Compute the reduced model of the proper part
$(\mathcal{E}_r, \mathcal{A}_r, \mathcal{B}_r, \mathcal{C}_r, \mathcal{D}_r) = (T_L\mathcal{E}_0T_R, T_L\mathcal{A}_0T_R, T_L\mathcal{B}_0, \mathcal{C}_0T_R, M_0)$;

Finally, the transfer matrix of the reduced model of the original circuit is

$$G_r(s) = \underbrace{\mathcal{C}_r(s\mathcal{E}_r - \mathcal{A}_r)^{-1}\mathcal{B}_r + M_0}_{\mathcal{G}_{pr}(s)} + sM_1. \tag{5.14}$$

A DS realization of $G_r(s)$ by $(E_r, A_r, B_r, C_r, D_r)$ is

$$\begin{aligned} E_r &= \begin{bmatrix} \mathcal{E}_r & & \\ & 0 & I_m \\ & 0 & 0 \end{bmatrix}, \; A_r = \begin{bmatrix} \mathcal{A}_r & & \\ & I_m & \\ & & I_m \end{bmatrix}, \; B_r = \begin{bmatrix} \mathcal{B}_r \\ 0 \\ M_1 \end{bmatrix}, \\ C_r &= \begin{bmatrix} \mathcal{C}_r & -I_m & 0 \end{bmatrix}, \; D_r = M_0. \end{aligned} \tag{5.15}$$

The improper part sM_1 is preserved by additive decomposition without numerical

errors, the errors are only induced in the MOR of the proper part. Analogous to other BT methods [18], there exists an error bound for the proper subsystem:

$$\begin{aligned}\|\mathcal{G}_p - \mathcal{G}_{pr}\|_{H_\infty} \leq 2 \left\| \left(M_0 + M_0^T\right)^{-1} \right\| \left\|\mathcal{G}_p + M_0^T\right\|_{H_\infty} \\ \times \left\|\mathcal{G}_{pr} + M_0^T\right\|_{H_\infty} (\sigma_{r+1} + \cdots \sigma_{\hat{n}}),\end{aligned} \tag{5.16}$$

where $\|\mathcal{G}_p\|_{H_\infty} = \sup_{\omega\in\mathbb{R}} \|\mathcal{G}_p(j\omega)\|$.

The main computation in Algorithm 5.3 lies in solving the dual GAREs (5.13a) and (5.13b), which is tackled by GQADI or LR-GQADI described below.

5.4 GQADI and Low-Rank GQADI

This section presents the GQADI and LR-GQADI algorithms to solve the dual GAREs in (5.13a) and (5.13b). At the first glance, one may transform $\mathcal{G}_p(s)$ to a standard LTI by absorbing $\mathcal{E}_0$ into $\mathcal{A}_0$ and $\mathcal{B}_0$ and then perform PRBT via solving standard AREs [30]. However, computing $\mathcal{E}_0^{-1}\mathcal{A}_0$ consumes $O(n^3)$ operations and $O(n^2)$ physical memory. Furthermore, large numerical errors may be induced since $\mathcal{E}_0$ may be ill-conditioned. In [59], (5.13a) and (5.13b) are solved by Newton's iteration and LR-GADI, where the computation is about that of solving tens of GALEs.

5.4.1 GQADI

We use (5.13a) as an example to illustrate the proposed GQADI algorithm, which is a generalization of GADI [55, 56] and QADI [30]. GARE (5.13b) can be solved similarly. With an initial guess $\mathcal{X}_0 = 0$ and some shift parameters $s_1, s_2, ..., s_i \in \mathbb{C}^-$, the generalized QADI iteration for the GARE (5.13a) is given by:

$$(\mathcal{A}^T + \mathcal{E}^T\mathcal{X}_{i-1}^T\mathcal{B}\mathcal{B}^T + s_i\mathcal{E}^T)\mathcal{X}_{i-\frac{1}{2}}^T\mathcal{E} = -\mathcal{C}^T\mathcal{C} - \mathcal{E}^T\mathcal{X}_{i-1}^T(\mathcal{A} - s_i\mathcal{E}), \tag{5.17a}$$

$$(\mathcal{A}^T + \mathcal{E}^T\mathcal{X}_{i-\frac{1}{2}}\mathcal{B}\mathcal{B}^T + \bar{s_i}\mathcal{E}^T)\mathcal{X}_i\mathcal{E} = -\mathcal{C}^T\mathcal{C} - \mathcal{E}^T\mathcal{X}_{i-\frac{1}{2}}(\mathcal{A} - \bar{s_i}\mathcal{E}). \tag{5.17b}$$

Similar to [30], the solution $\mathcal{X}_i$ can be written as:

$$\mathcal{X}_i = \Pi_{11}^{(i)} + \Pi_{12}^{(i)}\mathcal{X}_{i-1}(I - \Pi_{22}^{(i)}\mathcal{X}_{i-1})^{-1}(\Pi_{12}^{(i)})^H \tag{5.18a}$$

$$\Pi_{11}^{(i)} = -2\,\mathrm{Re}(s_i)\mathcal{S}_i^H\mathcal{C}^H(I - \mathcal{C}\mathcal{S}_i\mathcal{B}\mathcal{B}^H\mathcal{S}_i^H\mathcal{C}^H)^{-1}\mathcal{C}\mathcal{S}_i, \tag{5.18b}$$

$$\Pi_{22}^{(i)} = -2\,\mathrm{Re}(s_i)\mathcal{E}\mathcal{S}_i\mathcal{B}(I - \mathcal{B}^H\mathcal{S}_i^H\mathcal{C}^H\mathcal{C}\mathcal{S}_i\mathcal{B})^{-1}\mathcal{B}^H\mathcal{S}_i^H\mathcal{E}^H \tag{5.18c}$$

$$\Pi_{12}^{(i)} = 2\,\mathrm{Re}(s_i)\mathcal{S}_i^H\mathcal{E}^H - I - \mathcal{S}_i^H\mathcal{C}^H\mathcal{C}\mathcal{E}^{-1}\Pi_{22}^i. \tag{5.18d}$$

Here $\mathcal{S}_i = (\mathcal{A}+\mathcal{E}s_i)^{-1}$, and the superscript ^{H} denotes conjugate transpose. We remark that we do not need to compute $\mathcal{E}^{-1}$ in (5.18d) since it is canceled with $\mathcal{E}$ in $\Pi_{22}^{(i)}$. The derivation of GQADI is detailed in Appendix 5.7.1.

5.4.2 Well Posedness

Analogous to [30], we demonstrate that the solution $\mathcal{X}_i$ is well defined and PSD. Since the existence of the PSD solution $\mathcal{X}$ to (5.13a) implies the strict bounded realness of the DS $\Sigma_1 : (\mathcal{E}, \mathcal{A}, \mathcal{B}, \mathcal{C}, 0)$, we have

$$\max\left(\sigma\big(\mathcal{C}(\mathcal{A} + s_i\mathcal{E})^{-1}\mathcal{B}\big)\right) = \max\left(\sigma(\mathcal{C}\mathcal{S}_i\mathcal{B})\right) < 1,\ \forall s_i \in \mathbb{C}^- \tag{5.19}$$

where $\sigma(o)$ denotes the set of singular values. Therefore, the matrix inversions in (5.18b)–(5.18d) are well defined.

Next, we prove the well posedness of (5.18a). The GARE (5.13a) can be rewritten as

$$(\mathcal{A} + \mathrm{Re}(s_i)\mathcal{E})^T\mathcal{X}\mathcal{E} + \mathcal{E}^T\mathcal{X}(\mathcal{A} + \mathrm{Re}(s_i)\mathcal{E}) + \mathcal{E}^T\mathcal{X}\mathcal{B}\mathcal{B}^T\mathcal{X}\mathcal{E} + \mathcal{C}^T\mathcal{C} - 2\,\mathrm{Re}(s_i)\mathcal{E}^T\mathcal{X}\mathcal{E} = 0 \tag{5.20}$$

which implies the LTI DS $\Sigma_2 : (\mathcal{E}_2, \mathcal{A}_2, \mathcal{B}_2, \mathcal{C}_2, 0)$ is also strictly bounded real where the corresponding system matrices are defined by

$$\begin{aligned} &\mathcal{E}_2 = \mathcal{E}, \quad \mathcal{A}_2 = \mathcal{A} + \mathrm{Re}(s_i)\mathcal{E}, \\ &\mathcal{B}_2 = \mathcal{B},\ \mathcal{C}_2 = \begin{bmatrix} \mathcal{C}^T & \sqrt{-2\,\mathrm{Re}(s_i)}\mathcal{E}^T\mathcal{Z} \end{bmatrix}^H, \end{aligned} \tag{5.21}$$

where $\mathcal{X} = \mathcal{Z}\mathcal{Z}^H$. Setting $\omega_i = -\mathrm{Im}(s_i)$ and $\mathcal{G}_2(j\omega_i) = \mathcal{C}_2(j\omega_i\mathcal{E}_2 - \mathcal{A}_2)^{-1}\mathcal{B}_2^T$, the bounded real lemma implies

$$\max(\sigma(\mathcal{G}_2^H(j\omega_i)\mathcal{G}_2(j\omega_i))) = \max(\sigma(\mathcal{B}^H\mathcal{S}_i^H(\mathcal{C}^H\mathcal{C} - 2\,\mathrm{Re}(s_i)\mathcal{E}^T\mathcal{X}\mathcal{E})\mathcal{S}_i\mathcal{B})) < 1. \tag{5.22}$$

Lemma 5.1: *If the GARE (5.13a) has a stabilizing solution $\mathcal{X} \geq 0$ and $\mathcal{X} \geq \mathcal{X}_{i-1}$, then we have $\mathcal{X} \geq \mathcal{X}_i$.*

Proof: Refer to Appendix 5.7.2.

□

Since $\mathcal{X}_0 = 0$, we have $\mathcal{X} \geq \mathcal{X}_0$. Then according to Lemma 1, $\mathcal{X} \geq \mathcal{X}_i$ follows for $i = 1, 2, \cdots$. Since $\mathcal{X} \geq \mathcal{X}_i$, (5.22) can be extended to

$$\max(\sigma(\mathcal{B}^H\mathcal{S}_i^H(\mathcal{C}^H\mathcal{C} - 2\,\mathrm{Re}(s_i)\mathcal{E}^T\mathcal{X}_i\mathcal{E})\mathcal{S}_i\mathcal{B})) < 1. \tag{5.23}$$

Using matrix inverse lemma [40], we get

$$\begin{aligned} &\mathcal{X}_{i-1}(I - \Pi_{22}^{(i)}\mathcal{X}_{i-1})^{-1} = \mathcal{X}_{i-1}[I + 2\,\mathrm{Re}(s_i)\mathcal{E}\mathcal{S}_i\mathcal{B}(I - \mathcal{B}^H\mathcal{S}_i^H\mathcal{C}^H\mathcal{C}\mathcal{S}_i\mathcal{B})^{-1}\mathcal{B}^H\mathcal{S}_i^H\mathcal{E}^H\mathcal{X}_{i-1}]^{-1} \\ &= \mathcal{X}_{i-1}\Big(I - \sqrt{-2\,\mathrm{Re}(s_i)}\mathcal{E}\mathcal{S}_i\mathcal{B}(I - \mathcal{B}^H\mathcal{S}_i^H\mathcal{C}^H\mathcal{C}\mathcal{S}_i\mathcal{B})^{-\frac{1}{2}}\sqrt{-2\,\mathrm{Re}(s_i)}(I - \mathcal{B}^H\mathcal{S}_i^H\mathcal{C}^H\mathcal{C}\mathcal{S}_i\mathcal{B})^{-\frac{1}{2}}\mathcal{B}^H\mathcal{S}_i^H\mathcal{E}^H\Big)^{-1} \\ &= \mathcal{X}_{i-1} - 2\,\mathrm{Re}(s_i)\mathcal{X}_{i-1}\mathcal{E}\mathcal{S}_i\mathcal{B}\big(I - \mathcal{B}^H\mathcal{S}_i^H(\mathcal{C}^H\mathcal{C} - 2\,\mathrm{Re}(s_i)\mathcal{E}^T\mathcal{X}_{i-1}\mathcal{E})\mathcal{S}_i\mathcal{B}\big)^{-1}\mathcal{B}^H\mathcal{S}_i^H\mathcal{E}^H\mathcal{X}_{i-1} \end{aligned} \tag{5.24}$$

From (5.23) and the last line of (5.24), we know that $\mathcal{X}_{i-1}(I - \Pi_{22}^{(i)}\mathcal{X}_{i-1})^{-1}$ is well defined and PSD, therefore $\mathcal{X}_i \geq 0$ is also well defined. The matrix inversion in the last line of (5.24) is numerically easy to compute due to the low dimension.

5.4.3 Convergence

Now we prove that $\mathcal{X}_i$ indeed converges to $\mathcal{X}$. Since $\mathcal{X}_0 = 0$, using equation (5.48) and the star product of linear fractional transform (LFT, [4]) (see (5.40) in Appendix 5.7.1 of this chapter), $\Delta_i = \mathcal{X} - \mathcal{X}_i$ can be formulated as a lower LFT of $\mathcal{X}$:

$$\Delta_i = F_l\left(\begin{bmatrix} 0 & \mathcal{M}_i \\ \mathcal{M}_i^H & \mathcal{N}_i \end{bmatrix},\ \mathcal{X}\right) = \mathcal{M}_i\mathcal{X}\left(I - \mathcal{N}_i\mathcal{X}\right)^{-1}\mathcal{M}_i^H, \tag{5.25a}$$

$$\mathcal{M}_i = \prod_{j=1}^{i} \hat{\mathcal{S}}_j^H \hat{\mathcal{T}}_j^H, \tag{5.25b}$$

$$\mathcal{N}_i = 2\,\mathrm{Re}\,(s_i)\sum_{j=1}^{i}\left(\prod_{k=1}^{j-1}\hat{\mathcal{S}}_k\hat{\mathcal{T}}_k\right)\hat{\mathcal{S}}_j\mathcal{B}\mathcal{B}^T\hat{\mathcal{S}}_j^H\left(\prod_{k=1}^{j-1}\hat{\mathcal{T}}_k^H\hat{\mathcal{S}}_k^H\right), \tag{5.25c}$$

where $\hat{\mathcal{S}}_j$ and $\hat{\mathcal{T}}_j$ are defined in Appendix 5.7.2. Since $s_i \in \mathbb{C}^-$, $-\mathcal{N}_i \geq 0$, assume $-\mathcal{N}_i = \mathcal{L}_i\mathcal{L}_i^H$ and $\mathcal{X} = \mathcal{Z}\mathcal{Z}^H$, then

$$\begin{aligned}
\mathcal{X}\left(I - \mathcal{N}_i\mathcal{X}\right)^{-1} &= \mathcal{Z}\mathcal{Z}^H\left(I + \mathcal{L}_i\mathcal{L}_i^H\mathcal{Z}\mathcal{Z}^H\right)^{-1} \\
&= \mathcal{Z}\mathcal{Z}^H\left(I - \mathcal{L}_i(I + \mathcal{L}_i^H\mathcal{Z}\mathcal{Z}^H\mathcal{L}_i)^{-1}\mathcal{L}_i\mathcal{Z}\mathcal{Z}^H\right) \\
&= \mathcal{X} - \mathcal{Z}\mathcal{Z}^H\mathcal{L}_i(I + \mathcal{L}_i^H\mathcal{Z}\mathcal{Z}^H\mathcal{L}_i)^{-1}\mathcal{L}_i\mathcal{Z}\mathcal{Z}^H.
\end{aligned} \tag{5.26}$$

The last line of (5.26) shows $\mathcal{X} \geq \mathcal{X}\left(I - \mathcal{N}_i\mathcal{X}\right)^{-1}$, hence

$$0 \leq \mathcal{X} - \mathcal{X}_i \leq \mathcal{M}_i\mathcal{X}\mathcal{M}_i^H. \tag{5.27}$$

Since the spectrum of $\hat{\mathcal{S}}_j\hat{\mathcal{T}}_j$ locates inside the unit circle on the complex plane, M_i approaches 0 as i increases. According to (5.27), $\mathcal{X}_i$ converges to $\mathcal{X}$ as $i \to \infty$. Analogous to [30,55,56], for k iterations of GQADI the shift parameters s_i $(i = 1, ..., k)$

can be selected by solving the minimax problem

$$\min_{s_1,\cdots,s_k\in\mathbb{C}^-}\left(\max_{\lambda_i\in spec(\mathcal{E},\hat{\mathcal{A}})}\left|\frac{(s_1-\lambda_i)\cdots(s_k-\lambda_i)}{(\bar{s}_1+\lambda_i)\cdots(\bar{s}_k+\lambda_i)}\right|\right). \tag{5.28}$$

Since $\hat{\mathcal{A}} = \mathcal{A}+\mathcal{B}\mathcal{B}^T\mathcal{X}\mathcal{E}$ (see Appendix B), directly computing $spec(\mathcal{E},\hat{\mathcal{A}})$ is not feasible.

Lemma 5.2: *Provided that $\mathcal{X}$ is a stabilizing solution to the GARE (5.13a), then we have $spec(\mathcal{E},\hat{\mathcal{A}})$=$spec(\mathcal{K},\mathcal{J})\cap\mathbb{C}^-$, where*

$$\mathcal{J}=\begin{bmatrix}\mathcal{A} & -\mathcal{B}\mathcal{B}^T\\ \mathcal{C}^T\mathcal{C} & -\mathcal{A}^T\end{bmatrix},\quad \mathcal{K}=\begin{bmatrix}\mathcal{E} & \\ & \mathcal{E}^T\end{bmatrix}. \tag{5.29}$$

Proof: Assume $\mathcal{X}$ is the stabilizing solution to (5.13a) and $\lambda\in spec(\mathcal{K},\mathcal{J})$ (i.e., $det(\mathcal{J}-\lambda\mathcal{K})=0$), we have

$$\begin{aligned}\det(\mathcal{J}-\lambda\mathcal{K}) &= \det\left(\begin{bmatrix} I & \\ \mathcal{E}^T\mathcal{X} & I\end{bmatrix}(\mathcal{J}-\lambda\mathcal{K})\begin{bmatrix} I & \\ -\mathcal{X}\mathcal{E} & I\end{bmatrix}\right)\\ &= \det\begin{bmatrix}\mathcal{A}+\mathcal{B}\mathcal{B}^T\mathcal{X}\mathcal{E}-\lambda\mathcal{E} & \mathcal{B}\mathcal{B}^T\\ 0 & -\mathcal{A}^T-\mathcal{E}^T\mathcal{X}\mathcal{B}\mathcal{B}^T-\lambda\mathcal{E}^T\end{bmatrix},\end{aligned} \tag{5.30}$$

which shows $spec(\mathcal{K},\mathcal{J}) = spec(\mathcal{E},\hat{\mathcal{A}})\cup spec(-\mathcal{E}^T,\hat{\mathcal{A}}^T)$. Since $\mathcal{X}$ is a stabilizing solution to (5.13a), we have $spec(\mathcal{E},\hat{\mathcal{A}})\in\mathbb{C}^-$ and $spec(-\mathcal{E}^T,\hat{\mathcal{A}}^T)\in\mathbb{C}^+$.

□

By Lemma 5.2, the spectral of $(\mathcal{E},\hat{\mathcal{A}})$ can be decided as $spec(\mathcal{K},\mathcal{J})\cap\mathbb{C}^-$.

5.4.4 Low-Rank GQADI (LR-GQADI)

Since $\mathcal{X}_i \geq 0$, we have $\mathcal{X}_i = \mathcal{Z}_i \mathcal{Z}_i^H$. The low-rank factor $\mathcal{Z}_i$ is defined as

$$Z_i = \left[\begin{array}{cc} \mathcal{H}_i & \Pi_{12}^{(i)} \mathcal{F}_i \end{array} \right]. \tag{5.31}$$

Here $\mathcal{H}_i$ and $\mathcal{F}_i$ are the low-rank factors of $\Pi_{11}^{(i)}$ and $\mathcal{X}_{i-1}(I - \Pi_{22}^{(i)} \mathcal{X}_{i-1})^{-1}$, respectively. Denote $\overline{\mathcal{SC}}_i := \mathcal{S}_i^H \mathcal{C}^H$, (5.18b) tells

$$\mathcal{H}_i = \sqrt{-2\,\mathrm{Re}(s_i)} \overline{\mathcal{SC}}_i (I - \overline{\mathcal{SC}}_i^H \mathcal{B}\mathcal{B}^H \overline{\mathcal{SC}}_i)^{-\frac{1}{2}}. \tag{5.32}$$

Since $\mathcal{X}_{i-1} = \mathcal{Z}_{i-1} \mathcal{Z}_{i-1}^H$, it is easy to prove that

$$\mathcal{X}_{i-1}(I - \Pi_{22}^{(i)} \mathcal{X}_{i-1})^{-1} = \mathcal{Z}_{i-1}(I - \mathcal{Z}_{i-1}^H \Pi_{22}^{(i)} \mathcal{Z}_{i-1})^{-1} \mathcal{Z}_{i-1}^H. \tag{5.33}$$

Then $\mathcal{F}_i$ is decided as

$$\mathcal{F}_i = \mathcal{Z}_{i-1}(I - \mathcal{Z}_{i-1}^T \Pi_{22}^{(i)} \mathcal{Z}_{i-1})^{-\frac{1}{2}}. \tag{5.34}$$

Denote $\overline{\mathcal{SB}}_i := \mathcal{S}_i \mathcal{B}$, the low-rank factor of $\Pi_{22}^{(i)}$ is expressed as

$$\mathcal{R}_i = \sqrt{-2\,\mathrm{Re}(s_i)} \mathcal{E} \overline{\mathcal{SB}}_i (I - \overline{\mathcal{SB}}_i^H \mathcal{C}^H \mathcal{C} \overline{\mathcal{SB}}_i)^{-\frac{1}{2}}. \tag{5.35}$$

Finally, the second column block of $\mathcal{Z}_i$ can be computed by

$$\begin{aligned} &\Pi_{12}^{(i)} \mathcal{F}_i = 2\,\mathrm{Re}(s_i) \mathcal{S}_i^H \mathcal{E}^H \mathcal{F}_i - \mathcal{F}_i \\ &- \sqrt{-2\,\mathrm{Re}(s_i)} \overline{\mathcal{SC}}_i \mathcal{C} \overline{\mathcal{SB}}_i (I - \overline{\mathcal{SB}}_i^H \mathcal{C}^H \mathcal{C} \overline{\mathcal{SB}}_i)^{-\frac{1}{2}} \mathcal{R}_i^H \mathcal{F}_i. \end{aligned} \tag{5.36}$$

The procedures of LR-GQADI are summarized in Algorithm 5.4, where all computations are based on low-rank operations.

Algorithm 5.4: LR-GQADI for the GARE (5.13a)

Input: $\mathcal{E}, \mathcal{A} \in \mathbb{R}^{n\times n}$, $\mathcal{B}, \mathcal{C}^T \in \mathbb{R}^{n\times m}$, and shift parameters $s_1, ..., s_i \in \mathbb{C}^-$.
Output: The approximate solution $\mathcal{X}_j = \mathcal{Z}_j\mathcal{Z}_j^H$ to (5.13a).
begin

$\mathcal{Z}_1 = \sqrt{-2\,\mathrm{Re}(s_1)}\overline{\mathcal{SC}}_1(I - \overline{\mathcal{SC}}_1^H\mathcal{B}\mathcal{B}^H\overline{\mathcal{SC}}_1)^{-\frac{1}{2}}$, where $\overline{\mathcal{SC}}_1 = \mathcal{S}_1^H\mathcal{C}^H$;
for i = 2,3,...,j **do**

1. Compute $\overline{\mathcal{SC}}_i := \mathcal{S}_i^H\mathcal{C}^H$ and $\overline{\mathcal{SB}}_i = \mathcal{S}_i\mathcal{B}$;
2. Compute $\mathcal{H}_i = \sqrt{-2\,\mathrm{Re}(s_i)}\overline{\mathcal{SC}}_i(I - \overline{\mathcal{SC}}_i^H\mathcal{B}\mathcal{B}^H\overline{\mathcal{SC}}_i)^{-\frac{1}{2}}$,
$\mathcal{R}_i = \sqrt{-2\,\mathrm{Re}(s_i)}\mathcal{E}\overline{\mathcal{SB}}_i(I - \overline{\mathcal{SB}}_i^H\mathcal{C}^H\mathcal{C}\overline{\mathcal{SB}}_i)^{-\frac{1}{2}}$,
and $\mathcal{F}_i = \mathcal{Z}_{i-1}(I - \mathcal{Z}_{i-1}^T\mathcal{R}_i\mathcal{R}_i^H\mathcal{Z}_{i-1})^{-\frac{1}{2}}$;
3. Compute $\Pi_{12}^{(i)}\mathcal{F}_i = 2\,\mathrm{Re}(s_i)\mathcal{S}_i^H\mathcal{E}^H\mathcal{F}_i - \mathcal{F}_i -$
$\sqrt{-2\,\mathrm{Re}(s_i)}\overline{\mathcal{SC}}_i\mathcal{C}\overline{\mathcal{SB}}_i(I - \overline{\mathcal{SB}}_i^H\mathcal{C}^H\mathcal{C}\overline{\mathcal{SB}}_i)^{-\frac{1}{2}}\mathcal{R}_i^H\mathcal{F}_i$;
4. Compute $Z_i = \left[\begin{array}{cc} \mathcal{H}_i & \Pi_{12}^{(i)}\mathcal{F}_i \end{array}\right]$.

5.4.5 Numerical Complexity

GQADI consumes approximately the cost of solving one projected GALE by GADI [see (5.7)]. Since Newton's iteration (Algorithm 5.1) needs to solve k (k is usually 10 to 30) GALEs for one projected GARE (and then perform GADI for each GALE), GQADI is about k times faster than the Newton's iteration method. If LR-GQADI is adopted, all full-size computations can be replaced by low-rank operations, which leads to a further speedup. In LR-GQADI, the main cost is dominated by computing $\overline{\mathcal{SC}}_i := \mathcal{S}_i^H\mathcal{C}^H$ and $\overline{\mathcal{SB}}_i = \mathcal{S}_i\mathcal{B}$, which can be tackled by direct or iterative linear solvers with $O(n^2)$ computation for sparse cases. Furthermore, by LR-GQADI, the low-rank factors of $\mathcal{X}$ and $\mathcal{Y}$ are readily available, so Step 2 of Algorithm 5.3 can be skipped and the SVD in Step 3 is very cheap due to the small size of $L^T\mathcal{E}_0R$.

5.5 Experimental Results

This section presents some RLC benchmarks to verify the proposed DS-MOR flow. Experiments are performed in Matlab R2009a on a 2.5GHz PC with 6G memory.

5.5.1 Subsystem Extraction

First, the proposed additive decomposition (Algorithm 5.2) is compared with Weierstrass decomposition used in [26]. Experiments are performed on four RLC circuits. In Weierstrass decomposition, the popular package GUPTRI [80] is used to compute the Weierstrass canonical form. As shown in Table 5.1, the proposed additive decomposition (Algorithm 5.2) is much faster than the method in [26] due to the efficient sparse LU-based spectral projector construction. As the system dimension increases, the speedup becomes more significant. In Weierstrass decomposition routines such

Table 5.1: CPU times (sec) of DS decompositions.

Circuit	Order	Weierstrass [26]	Algorithm 5.2	Speedup
ckt1	363	7.811	0.1813	43.10
ckt2	903	82.37	0.9984	82.50
ckt3	1505	392.5	2.8810	136.2
ckt4	10913	break down	129.47	N/A

Table 5.2: CPU times (sec) of solving one GARE (5.13a)

Circuit model	Newton's iteration with GADI	Newton's iteration with LR-GADI	GQADI	LR-GQADI
ckt1	43.60	9.425	3.328	0.724
ckt2	266.3	38.92	40.87	5.922
ckt3	2240	256.7	230.2	12.13
ckt4	break down	3965	break down	572.8

as GUPTRI [80], multiple SVD and QZ [40] factorizations are used. Due to the $O(n^2)$ physical memory requirement, they are not applicable to large sparse circuit

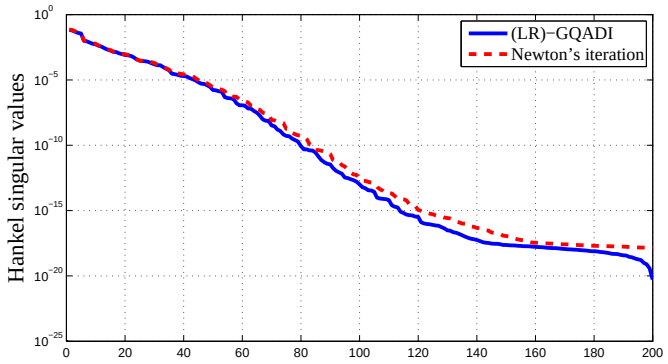

Figure 5.3: Approximate Hankel singular values of the proper subsystem of ckt3. Hankel singular values refer to the singular values of $L^T\mathcal{E}_0R$ (i.e., σ_1, σ_2, $\cdots$ in Step 3 of Algorithm 5.3).

systems. The proposed method is based on sparse operations with only $O(n)$ storage requirement, so it is applicable to large-scale RLC circuits (as shown by the results of ckt4).

5.5.2 Comparison of GARE Solvers

GQADI and LR-GQADI are then compared with the Newton's iteration based GARE solvers. We list the CPU times of solving one GARE [such as (5.13a)] in Table 5.2. To achieve similar accuracy, the relative error is set as 10^{-4} for all GARE solvers. Inside each Newton's iteration, the relative error of solving the GALE is set as 10^{-6}. We remark that inside each step of Newton's iteration, the amounts of (LR)-ADI iterations are quite different, depending on the convergence rates of the obtained GALEs. The CPU timing results show that GQADI and LR-GQADI enjoy significant speedup over GADI and LR-GADI, respectively. For our tested RLC circuits, the speedup of GQADI over LR-GADI based Newton's iteration is case-dependent (since the numbers of Newton's iterations vary from case to case). For example, GQADI is faster than LR-ADI based Newton's iteration for ckt1 and ckt3, but it is slightly

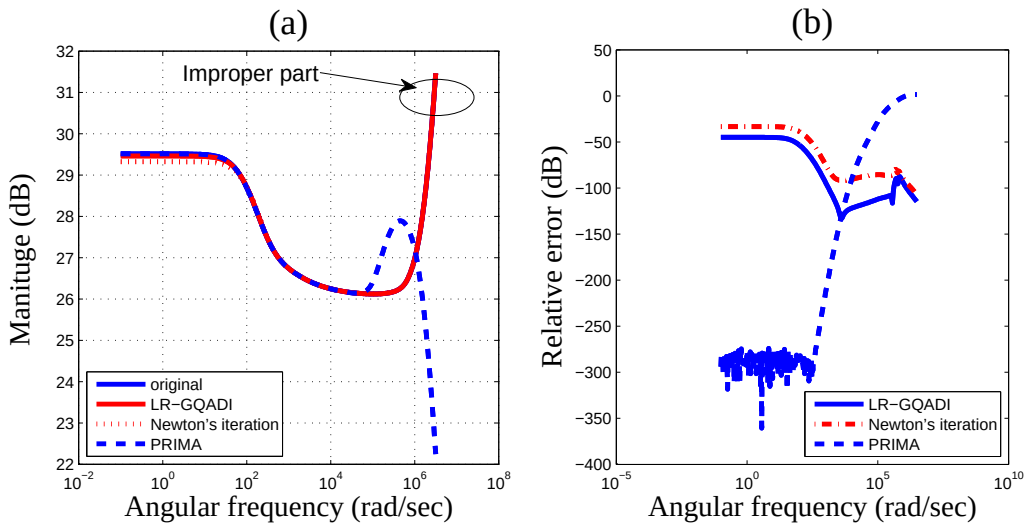

Figure 5.4: (a) Frequency response (port-1) of ckt3 and the reduced models (order=50) obtained by PRIMA and DS-PRBTs (solving the GAREs by LR-GQADI and Newton's iteration, respectively). (b) Relative errors.

slower over the latter for ckt2. Due to the low-rank property, LR-GQADI and LR-ADI based Newton's method can be applied to much larger systems (shown by the last row of Table 5.2), whereas the full-size algorithms break down due to the expensive physical memory requirement.

5.5.3 Model Reduction Results

We continue to reduce ckt3 (with 5 ports) by DS-PRBTs (proposed DS-PRBT and that based on Newton's iteration [18]) and PRIMA. We first perform additive decomposition, and then reduce the proper subsystem. Via LR-GQADI (Algorithm 5.4, after 40 iterations) and LR-GADI based Newton's iteration the 1505×200 low rank factors of $\mathcal{X}$ and $\mathcal{Y}$ (L and R in Algorithm 5.3) are obtained. Fig. 5.3 shows that the approximate Hankel singular values (i.e., the singular values of $L^T\mathcal{E}_0R$) decrease

dramatically. According to this property, the order of the reduced models is selected as 50. Fig. 5.4(a) shows the port-1 frequency response of ckt3 and the reduced models by various MOR methods. The results from DS-PRBT are indistinguishable from the original response. And more importantly, the improper part is preserved by additive decomposition. PRIMA is accurate in the low frequency band, but causes large errors in the high frequency band due to the inability of capturing the improper part. The relative error in Fig. 5.4(b) also shows the proposed DS-PRBT enjoys a higher numerical accuracy than that based on Newton's iteration.

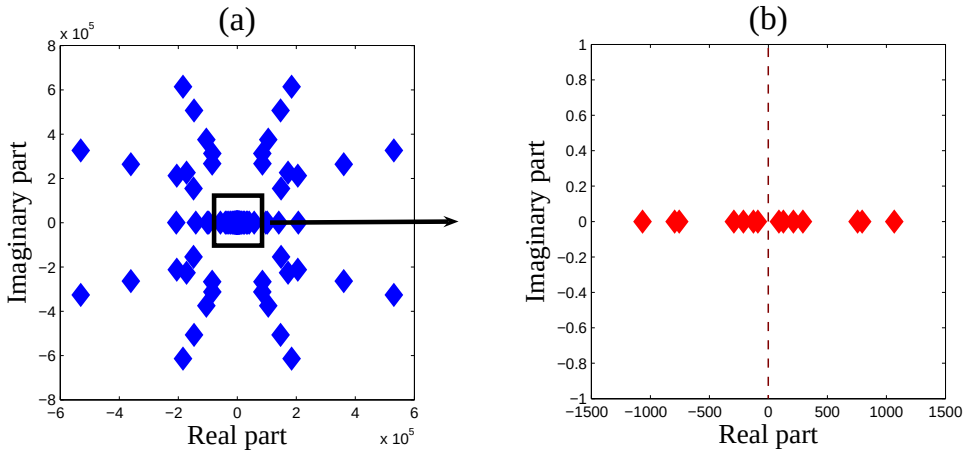

Figure 5.5: GHM passivity test results show that the reduced model is passive. (a) The eigenvalues of the generalized Hamiltonian matrix pencil. (b) Zoom in of the central part.

GHM method of Chapter 2 is used to verify the passivity of the reduced model. The eigenvalues of the generalized Hamiltonian matrix pencil are computed and plotted in Fig. 5.5. Since $M_0, M_1 > 0$ (which are preserved from the original system) and no eigenvalues of the passivity test matrix pencil are located on the imaginary axis, the reduced model is passive. We remark that, for symmetric DS, the passivity can also be checked by HGHM (half-size GHM) approach presented in Chapter 2.

We note that a passive DS MOR scheme is reported in [92], which is based on

the PSD structure of MNA equations and solves GALEs to get the projection matrix. However, the DS there is assumed to be regular, and practical examples show that the method fails when a finite improper part is involved. The recently proposed dominant spectral-zero (DSZ) interpolation [66] method reduces DS models by capturing those poles close to the imaginary axis, however it still misses the improper parts since the corresponding poles are located at infinity. These approaches are thereby not compared here.

5.6 Summary

This chapter has presented a fast improper-part preserving positive-real MOR for general DSs including RLC circuits. The proposed method first separates the proper and improper subsystems by additive decomposition at a negligible cost, and then reduces the proper part via solving GAREs by the newly proposed GQADI or LR-GQADI iterative methods. The proposed algorithms are much faster than existing DS-PRBT procedures and can capture the possible impulsive response which is normally missed by conventional Krylov-subspace projections.

5.7 Appendices

5.7.1 Derivation of GQADI

Similar to [30], we use linear fractional transform (LFT) [4] techniques to derive the formulation of GQADI. A lower LFT $F_l(P, \Delta)$ with

$$P = \begin{bmatrix} P_{11} & P_{12} \\ P_{21} & P_{22} \end{bmatrix} \tag{5.37}$$

is defined as

$$F_l(P, \Delta) = P_{11} + P_{12}\Delta(I - P_{22}\Delta)^{-1}P_{21}. \tag{5.38}$$

An upper LFT is defined as

$$F_u(Q, \Delta) = Q_{22} + Q_{21}\Delta(I - Q_{11}\Delta)^{-1}Q_{12}, \tag{5.39}$$

where Q is portioned similarly to P. An important result of LFT is the star product operation [4]:

$$F_l(P, F_l(Q, \Delta)) = F_l\left(W,\ \Delta\right) \tag{5.40}$$

with

$$W = \begin{bmatrix} F_l(P, Q_{11}) & P_{12}(I - Q_{11}P_{22})^{-1}Q_{12} \\ Q_{21}(I - P_{22}Q_{11})^{-1}P_{21} & F_u(Q, P_{11}) \end{bmatrix}. \tag{5.41}$$

From (5.17a) and (5.17b) we get

$$\mathcal{X}_{i-\frac{1}{2}} = F_l(\mathcal{P}_i,\ \mathcal{X}_{i-1}),\ \ \mathcal{X}_i = F_l(\mathcal{P}_i^H,\ \mathcal{X}_{i-\frac{1}{2}}). \tag{5.42}$$

Here $\mathcal{P}_i$ can be decided as

$$\mathcal{P}_i = \begin{bmatrix} -\tilde{\mathcal{C}}^H\tilde{\mathcal{C}}\tilde{\mathcal{S}}_i & \tilde{\mathcal{C}}^H\tilde{\mathcal{C}}\tilde{\mathcal{S}}_i\mathcal{B}\mathcal{B}^H - \tilde{\mathcal{T}}_i^H \\ \tilde{\mathcal{S}}_i & \tilde{\mathcal{S}}_i\mathcal{B}\mathcal{B}^H \end{bmatrix} \tag{5.43}$$

with $\tilde{\mathcal{C}} = \mathcal{C}\mathcal{E}^{-1}$, $\tilde{\mathcal{S}}_i = (\mathcal{A}\mathcal{E}^{-1} + s_i I)^{-1} = \mathcal{E}\mathcal{S}_i$ and $\tilde{\mathcal{T}}_i = \mathcal{A}\mathcal{E}^{-1} - \bar{s}_i I$. Setting $P = \mathcal{P}_i^H$, $Q = \mathcal{P}_i$ and $\Delta = \mathcal{X}_{i-1}$in (5.40), $\mathcal{X}_i$ can be expressed by $\mathcal{X}_{i-1}$ via the following LFT:

$$\mathcal{X}_i = F_l(\Pi^{(i)}, \mathcal{X}_{i-1}) = F_l\left(\begin{bmatrix} \Pi_{11}^{(i)} & \Pi_{12}^{(i)} \\ (\Pi_{12}^{(i)})^H & \Pi_{22}^{(i)} \end{bmatrix},\ X_{i-1}\right). \tag{5.44}$$

The sub-blocks of $\Pi^{(i)}$ are given in (5.18b)–(5.18d).

5.7.2 Proof of Lemma 5.1

Proof: Set $\hat{\mathcal{A}} = \mathcal{A} + \mathcal{B}\mathcal{B}^T\mathcal{X}\mathcal{E}$. Since $\mathcal{X}$ is a stabilizing solution of (5.13a), $(\hat{\mathcal{A}}, \mathcal{E})$ is stable, and $\hat{\mathcal{A}} + \bar{s}_i\mathcal{E}$ is nonsingular for any $s_i \in \mathbb{C}^-$. Denoting $\hat{\mathcal{S}}_i := \mathcal{E}(\hat{\mathcal{A}} + \bar{s}_i\mathcal{E})^{-1}$ and $\hat{\mathcal{T}}_i := (\hat{\mathcal{A}} - s_i\mathcal{E})\mathcal{E}^{-1}$, it is straightforward to prove that any multiplication among $\hat{\mathcal{S}}_m$, $\hat{\mathcal{T}}_n$ (m and n are any positive integers) and $\hat{\mathcal{A}}\mathcal{E}^{-1}$ is commutative.

According to (5.13a), (5.17a) can be rewritten as

$$\begin{aligned} &\mathcal{E}^T\left(\mathcal{X} - \mathcal{X}_{i-\frac{1}{2}}\right)\left(\hat{\mathcal{A}} + \bar{s}_i\mathcal{E} - \mathcal{B}\mathcal{B}^T(\mathcal{X} - \mathcal{X}_{i-1})\mathcal{E}\right) \\ &= \left(\hat{\mathcal{A}}^T - \bar{s}_i\mathcal{E}^T\right)(\mathcal{X} - \mathcal{X}_{i-1}), \end{aligned} \tag{5.45}$$

which implies

$$\mathcal{X} - \mathcal{X}_{i-\frac{1}{2}} = F_l\left(\hat{\mathcal{P}}_i,\ \mathcal{X} - \mathcal{X}_i\right). \tag{5.46}$$

Here $\hat{\mathcal{P}}_i = \begin{bmatrix} 0 & -\hat{\mathcal{T}}_i^H \\ \hat{\mathcal{S}}_i & \hat{\mathcal{S}}_i\mathcal{B}\mathcal{B}^T \end{bmatrix}$. Similarly, from (5.13a) and (5.17b) we get

$$\mathcal{X} - \mathcal{X}_i = F_l\left(\hat{\mathcal{P}}_i^H,\ \mathcal{X} - \mathcal{X}_{i-\frac{1}{2}}\right). \tag{5.47}$$

By the star product of LFT shown in (5.40), $\Delta_i = \mathcal{X} - \mathcal{X}_i$ can be expressed as the lower LFT with respect to $\Delta_{i-1} = \mathcal{X} - \mathcal{X}_{i-1}$:

$$\begin{aligned} \Delta_i &= F_l\left(\begin{bmatrix} 0 & \hat{\mathcal{S}}_i^H\hat{\mathcal{T}}_i^H \\ \hat{\mathcal{T}}_i\hat{\mathcal{S}}_i & 2\,\mathrm{Re}\,(s_i)\,\hat{\mathcal{S}}_i\mathcal{B}\mathcal{B}^T\hat{\mathcal{S}}_i^H \end{bmatrix},\ \Delta_i\right) \\ &= \hat{\mathcal{S}}_i^H\hat{\mathcal{T}}_i^H\Delta_{i-1}\left(I - 2\,\mathrm{Re}\,(s_i)\,\hat{\mathcal{S}}_i\mathcal{B}\mathcal{B}^T\hat{\mathcal{S}}_i^H\Delta_{i-1}\right)^{-1}\hat{\mathcal{T}}_i\hat{\mathcal{S}}_i. \end{aligned} \tag{5.48}$$

Denoting $\Delta_{i-1} = M_iM_i^T$ and $-2\,\mathrm{Re}\,(s_i)\,\hat{\mathcal{S}}_i\mathcal{B}\mathcal{B}^T\hat{\mathcal{S}}_i^H = N_iN_i^T$ (since both of them are

PSD), matrix inverse lemma [40] shows

$$\begin{aligned}
&\Delta_{i-1}\left(I-2\,\mathrm{Re}\,(s_i)\,\hat{\mathcal{S}}_i\mathcal{B}\mathcal{B}^T\hat{\mathcal{S}}_i^H\Delta_{i-1}\right)^{-1}\\
&=M_iM_i^T\left(I+N_iN_i^TM_iM_i^T\right)^{-1}\\
&=M_iM_i^T\left(I-N_i\left(I+N_i^TM_iM_i^TN_i\right)^{-1}N_i^TM_iM_i^T\right)\\
&=M_i(I+M_i^TN_iN_i^TM_i)^{-1}M_i^T\geq 0.
\end{aligned}\tag{5.49}$$

Therefore, it is obvious that $\Delta_i=\mathcal{X}-\mathcal{X}_i\geq 0$.

□

Chapter 6

Block-Diagonal Structured Model Reduction for Power Grid Analysis

This chapter proposes a block-diagonal structured model order reduction (BDSM) scheme for multi-port LTI models, with power grid as a typical example in VLSI design. Compared with existing power grid model order reductions (MORs), BDSM has several advantages. First, unlike many power grid reductions that are based on terminal reduction and thus error-prone, BDSM utilizes an exact column-by-column (or row-by-row) moment matching scheme to provide higher numerical accuracy. Second, with similar accuracy and macromodel size, BDSM generates very sparse block-diagonal reduced-order models (ROMs) for massive-port systems at lower cost, whereas traditional frameworks such as PRIMA produce full dense models rendering inefficient simulation. Third, different from those MORs based on extended Krylov subspace (EKS) technique, BDSM is input-signal independent, so the resulting ROM is reusable under different excitations. Finally, due to its special structure, the obtained ROM can be simulated flexibly: it can be solved either in a parallel fashion or in a serial flow; and in the column-by-column moment-matching BDSM framework, the problem size can be scaled with the active port number. The accuracy and

efficiency of BDSM are then verified by industrial power grid benchmarks.

6.1 Introduction

Power grid analysis has been a major topic in modern VLSI design. The challenges for power grid analysis mainly stem from the large problem size and massive port number. A typical power grid model usually has millions of nodes and up to thousands of input sources, rendering it extremely difficult to simulate. During the past decade, numerous efforts have been made to speed up the analysis and/or simulation of power grid networks, such as domain decomposition technique [93], preconditioned Krylov-subspace iterative method [94], random walk algorithm [95], simulations based on grid locality [96], and multi-grid reduction technique [97, 98]. One issue of these methods is that the computation on the large model needs to be repeated for different inputs or time steps.

A viable solution is to approximate the many-port original network by MOR, and then use the much smaller model in subsequent simulation. Krylov-subspace projections [22, 25] and balanced truncations [28] have been highly successful in interconnect MOR. With some modifications, these standard techniques have been adapted to reduce more sophisticated models in circuit simulation [33, 34]. Krylov-subspace projections such as PRIMA [22] have superior efficiency over balanced truncations. Therefore, they have been modified to reduce power grid models [24, 91, 100]. However, the efficiency significantly degrades as the port number increases. First, the MOR cost increases linearly with the port number, making the computation inefficient. Second, the ROM size increases linearly with the port number, resulting in a quadratic increase on storage cost. Consequently, the normally large and dense ROMs make the simulation very inefficient.

To address the problems induced by the large port number, extended Krylov subspace (EKS [100]) and extended truncated balance realization (ETBR [101]) treat the product of input vector and input matrix as a new frequency-dependent "single-input matrix", and then reduce a "single-input multi-output" systems. Based on a similar idea, triangularization based structure preserving MOR (TBS [91]) generates structured ROMs to further speed up power grid simulation. However, these methods are highly dependent on the input signals, and the obtained ROMs can not be reused for different input patterns. Since there exist some correlations between the input-output pairs, singular value decomposition (SVD) can be used to compress the terminals before MOR [102]. Similarly, [103] uses frequency-dependent packing to improve the numerical accuracy; B. Yan *et al.* has proposed decentralized MOR (DeMOR [104]) for multi-port system reduction. However, the terminal reduction process is error-prone, because the *true* transfer matrix moments can not be matched.

In this chapter, we present a novel method, called block-diagonal structured MOR (BDSM), for power grid reduction subject to the following criteria:

1. The ROMs should be cheap to simulate, which means that the obtained ROM should be compact enough or has a special structure that permits fast computation;

2. The ROMs should be reusable, which means that the ROM is accurate no matter what kind of signal waveforms are posed on the input ports;

3. The MOR accuracy should be comparable to that of PRIMA, which means that a certain number of moments are *accurately* matched in a predefined frequency band.

By BDSM, we get ROMs having the same sizes and similar accuracy as those from PRIMA. Even more, the models from BDSM are sparse and block-diagonal, thereby

facilitating fast simulation. Since BDSM does not involve terminal reduction, it is more accurate over terminal-reduction based MOR. On the other hand, BDSM is input-independent, so the ROMs can be reused for different input patterns. Due to their block-diagonal structure, the ROMs can be efficiently simulated and allows for parallel calculations. Furthermore, if we consider the active/dead inputs, the problem size can be largely reduced, which provides further simulation speedup for power grids with consideration of clock gating [108].

6.2 Review of Power Grid MOR

6.2.1 Power Grid Model

We consider the modified nodal analysis (MNA) equation of a power grid network

$$C\frac{dx(t)}{dt} = Gx(t) + Bu(t), \quad y(t) = Lx(t) \tag{6.1}$$

where $C, G \in \mathbb{R}^{n\times n}$, $B \in \mathbb{R}^{n\times m}$, $L \in \mathbb{R}^{p\times n}$. The input vector $u(t)$ normally represents time-varying current sources from transistor-level circuit blocks; the output vector $y(t)$ contains the voltage or current variables of interest; the state vector $x(t)$ represents nodal voltages and the branch currents across inductive components. The system matrix C includes the capacitance and inductance terms; G denotes the conductance matrix; B and L are the input and output matrices, respectively. In this chapter, we focus on the cases with multiple sources, which is very common in power/ground network models. Sometimes (e.g., in transient simulation) we may need to solve $x(t)$ for a given $u(t)$. In such a case, L is set to I_n (a dimension-n identity matrix), so $y(t) = x(t)$.

Provided the matrix pencil (C, G) being regular (i.e., $\exists s \in \mathbb{C}$ such that $(sC - G)$

is nonsingular), in Laplace domain, the $p \times m$ transfer matrix can be written as

$$H(s) = L(sC - G)^{-1}B. \tag{6.2}$$

Due to the grounded capacitors at the input nodes, the DS models from power grid networks are normally impulse-free. In power grid MOR, we attempt to find the left and right projection matrices $W, V \in \mathbb{R}^{n\times q}$ with $q \ll n$, to construct a small size-q linear system $\Sigma_r : (C_r, G_r, B_r, L_r)$

$$C_r \frac{dz(t)}{dt} = G_r z(t) + B_r u(t), \quad y_r(t) = L_r z(t) \tag{6.3}$$

with $C_r = W^T CV$, $G_r = W^T GV$, $B_r = W^T B$ and $L_r = LV$, such that $H_r(s) = L_r(sC_r - G_r)^{-1}B_r \approx H(s)$ or $y_r(s) = H_r(s)u(s) \approx y(s)$, subject to some accuracy requirements.

If $W = V$, the projection is a congruence transform. For simplicity, we use congruence transform in chapter. The projection matrices can be constructed by (rational) Krylov subspace moment matching [22, 25, 106] or balanced truncations (BT) [28]. Although BT approaches may provide *a priori* error estimation, they become inefficient for such large-scale systems as power grid networks whose problem sizes may be in the millions. Therefore, Krylov-subspace projections are discussed in this chapter.

6.2.2 Problems with Standard Krylov-Subspace Projection

Given a matrix M and (block) vector R with compatible sizes, an l-th order (block) Krylov subspace $\mathcal{K}_l(M, R)$ is the space spanning the range of a set of (block) vectors, i.e.,

$$\mathcal{K}_l(M, R) = \{R, MR, M^2R, \cdots, M^{l-1}R\}.$$

By (block) Arnoldi algorithm [22], the projection matrices for a congruence transform can be constructed as

$$W = V = \mathcal{K}_l\{(s_0C - G)^{-1}C, (s_0C - G)^{-1}B\} \tag{6.4}$$

with s_0 being a specific expansion point. Then a size-q ROM with $q = ml$ can be constructed, such that $H_r(s)$ matches the first l moments of $H(s)$ around the expansion point s_0, i.e.,

$$H(s) = H_r(s) + O\left((s - s_0)^l\right). \tag{6.5}$$

If the input signals are distributed in a wide frequency band, multi-point Krylov-subspace projection may be used to improve the numerical accuracy [106]. For example, to match the first l moments of $H(s)$ at k expansion points s_0, s_1, $\cdots$, s_{k-1}, the projection matrices are constructed by the union of the Krylov subspace at each expansion point. We proceed with single-point projection, and the multi-point scheme readily follows.

The standard projections have some problems when applied to power grid networks. First, the obtained ROMs are not efficient for computer-aided simulation. Since the ROM size q increases linearly with the port number m, it is clear that the ROM size can be very large. Since the ROM's matrices from standard projections are normally dense, storing the ROMs becomes challenging for a general PC, let alone simulating the ROM. Second, the cost of projection matrix construction is high for large many-port systems. To construct the projection matrix in (6.4), we need to perform $\frac{ml(ml-1)}{2}$ steps of long-vector orthonormalization, whose cost quadratically increases with m. Therefore, standard moment-matching based projection would be inefficient for power grid reduction.

Some modifications have been made for MOR of power grid networks. These

approaches are mainly based on terminal reduction [102–104] or the ideas similar to extended Krylov-subspace projection [91, 100, 101]. The former capture the moments of a low-rank approximated transfer matrix [102–104], rather than the original one. Therefore, essentially the model compactness is obtained at the cost of model accuracy. EKS, ETBR and TBS generate compact ROMs via moment matching of the output response under a predefined input excitation [91, 100, 101]. However, due to their strong dependency on input signal waveforms, the ROMs need to be rebuilt every time as the excitation vector changes. Since the cost in MOR is much more expensive over simulating a ROM, this kind of approaches may be inefficient for power grid analysis if we need to simulate the response under different excitations.

6.3 BDSM Scheme

This section presents the proposed BDSM algorithm to generate block-diagonal structured ROMs for power grid networks. We first decompose the original MIMO (multi-input multi-output) system into m MIMO subsystems (each with a $p \times m$ transfer matrix), via input matrix splitting. Then, we show that the Krylov-subspace projection matrix of each MIMO subsystem is in fact identical to that of a SIMO (single-input multi-output) subsystem. To match l moments, the proposed method generates an $ml \times ml$ ROM as by PRIMA. However, the resulting ROM's system matrices only contain m blocks in the diagonal, with each one being a small $l \times l$ matrix. As will be discussed in Section 6.4, this structure makes the subsequent simulation highly efficient. For simplicity, we only discuss the projection at a single point, and the multi-point projection follows analogously.

6.3.1 Input Matrix Splitting

Denoting the i-th column of $B \in \mathbb{R}^{n\times m}$ by b_i, the input matrix can be splitted to m rank-1 matrices, i.e.,

$$B = \sum_{i=1}^{m} B_i, \quad \text{with } B_i \in \mathbb{R}^{n\times m},\ B_i(:,j) = \begin{cases} b_i, \text{ if } i = j \\ 0, \text{ if } i \neq j \end{cases} \tag{6.6}$$

for $i, j = 1,\ 2,\ \cdots, m$. Here $B_i(:,j)$ denotes the j-th column vector of B_i. The linear time-invariant (LTI) system (C, G, B_i, L) is called a *splitted system*, denoted by Σ_i. Σ_i's transfer matrix is written as $H_i(s) = L(sC - G)B_i$. Clearly, the original transfer matrix $H(s)$ can be rewritten as

$$H(s) = \sum_{i=1}^{m} H_i(s). \tag{6.7}$$

Subsequently, the original network can be reformulated as the *parallel connection* of $\Sigma_i's$, and then realized by a size-mn model $(\mathcal{C},\ \mathcal{G},\ \mathcal{B},\ \mathcal{L})$:

$$\begin{aligned} \mathcal{C} &= \begin{bmatrix} C & & \\ & \ddots & \\ & & C \end{bmatrix}, \quad \mathcal{G} = \begin{bmatrix} G & & \\ & \ddots & \\ & & G \end{bmatrix} \\ \mathcal{B} &= \begin{bmatrix} B_1^T & \cdots & B_m^T \end{bmatrix}^T, \quad \mathcal{L} = \begin{bmatrix} L & \cdots & L \end{bmatrix}. \end{aligned} \tag{6.8}$$

This larger-size block-diagonal system is an equivalent model of the original power grid network. Note that $H_i(s)$ is a $p \times m$ matrix with only one column vector (the i-th column) being non-zero, which is identical to the i-th column of $H(s)$.

Generally, if we attempt to match the first l moments of a general m-port size-mn model via standard Krylov subspace projection such as PRIMA [22] at a single expansion point, a size-ml ROM would be generated. During the projection, the

block-diagonal structure would be destroyed and a dense ROM would be produced, which makes the ROM-based simulation very inefficient. Additionally, reducing a size-mn linear system is normally much more expensive over reducing a size-n system, since more calculations are needed in the LU decomposition, linear system solution and Gram-Schmidt orthonormalization. In BDSM, we aim to keep the block-diagonal structure of (6.8) such that the storage and calculations could be much cheaper in the subsequent simulation steps. We also expect the MOR cost to be cheaper than traditional projection frameworks on (6.1). More importantly, the resulting ROM is expected to be *reusable* for repeated simulation under varying input patterns.

To proceed, we consider the i-th splitted system Σ_i. Excited by the input vector $u(s)$, the output vector is $y_i(s) = H_i(s)u(s)$, and it can be rewritten as

$$y_i(s) = L(sC - G)^{-1}B_i u(s) = L(sC - G)^{-1}b_i u_i(s) \tag{6.9}$$

since B_i has only one nonzero vector in the i-th column. Here, $u_i(s)$ denotes the i-th input scalar. This reformulation shows that $y_i(s)$ is only dependent on the input u_i, and B_i shields the effects induced by other input signals, although the splitted system Σ_i has m input ports. Since $y(s)$ is the sum of $y_i(s)$ for $i = 1, \cdots, m$, the above input matrix splitting is physically equivalent to decomposing the output response into m independent components, with each excited by a single input signal. This property in fact allows for a block-diagonal structure-preserving reduction for model (6.8), at a lower computational cost over PRIMA.

6.3.2 Block-Diagonal Structured Projection

Unlike traditional projection reduction methods that directly match the moments of $H(s)$, BDSM uses an *indirect* moment matching method. Specifically, the ROM of each splitted model Σ_i, denoted by Σ_{ir}, is built such that its transfer matrix $H_{ir}(s)$

matches the first l moments of $H_i(s)$, and then all reduced models are parallely connected to approximate the original linear network (6.1).

Let us consider the splitted model $\Sigma_i : (L, C, G, B_i)$. At a single expansion point s_0, a projection matrix spanning the l-th order block Krylov subspace can be constructed:

$$V^{(i)} = \mathcal{K}_l\{(s_0C - G)^{-1}C,\ (s_0C - G)^{-1}B_i\}. \tag{6.10}$$

Then the ROM of Σ_i, denoted by $\Sigma_{ir} : (C_{ir}, G_{ir}, B_{ir}, L_{ir})$, can be constructed by the congruence transform

$$\begin{aligned} &C_{ir} = (V^{(i)})^T C V^{(i)} \ \ G_{ir} = (V^{(i)})^T G V^{(i)} \\ &B_{ir} = (V^{(i)})^T B_i \ \text{ and } L_{ir} = L V^{(i)}. \end{aligned} \tag{6.11}$$

It can be proved that the ROM's transfer matrix H_{ir} matches the first l moments of $H_i(s)$, i.e.,

$$H_{ir}(s) = L_{ir}(s_iC_{ir} - G_{ir})^{-1}B_{ir} = H_i(s) - O\left((s - s_0)^l\right) \tag{6.12}$$

Since $B_i \in \mathbb{R}^{n\times m}$, it seems that $V^{(i)}$ is a $n \times ml$ matrix and the size of the ROM Σ_{ir} would be ml. By noting that B_i has only one nonzero vector b_i as its i-th column, it is straightforward to prove

$$V^{(i)} = \mathcal{K}_l\left\{(s_0C - G)^{-1}C,\ (s_0C - G)^{-1}b_i\right\} \in \mathbb{R}^{n\times l} \tag{6.13}$$

provided that no vectors are deflated in the orthonormalization steps. Therefore, $V^{(i)}$ is in fact a $n \times l$ projection matrix, and Σ_{ir} is a very small size-l ROM, although Σ_i is an MIMO.

After computing the projection matrix for each splitted system Σ_i, a projection matrix can be constructed for model (6.8). Using the congruence transform $C_r =$

$\mathcal{V}^T\mathcal{C}\mathcal{V}$, $G_r = \mathcal{V}^T\mathcal{G}\mathcal{V}$, $B_r = \mathcal{V}^T\mathcal{B}$ and $L_r = \mathcal{L}\mathcal{V}$, the system matrices of the final ROM of (6.8) [denoted by Σ_r, which is also the final ROM of (6.1)], can be decided as

$$\begin{aligned} &C_r = \text{blkdiag}\left(C_{1r}, \cdots, C_{mr}\right), \quad G_r = \text{blkdiag}\left(G_{1r}, \cdots, G_{mr}\right) \\ &B_r = \begin{bmatrix} B_{1r} \\ \vdots \\ B_{mr} \end{bmatrix} = \text{blkdiag}\left((V^{(1)})^T b_1, \cdots, (V^{(m)})^T b_m\right) \\ &\text{and } L_r = \mathcal{L}\mathcal{V}, \quad \text{with } \mathcal{V} = \text{blkdiag}\left(V^{(1)}, \cdots, V^{(m)}\right). \end{aligned} \tag{6.14}$$

Here "blkdiag" denotes the Matlab function that constructs a block-diagonal matrix from the input arguments. It is clearly shown that the final size-ml ROM is block-diagonal structured. All diagonal blocks of C_r and G_r (i.e., C_{ir} and G_{ir} for $i = 1, \cdots, m$) are small $l \times l$ matrices. The i-th block of B_r (i.e., B_{ir}) contains only one nonzero vector as its i-th column.

From (6.14) and (6.12), the transfer matrix of Σ_r can be written as

$$H_r(s) = \sum_{i=1}^{m} H_{ir}(s) = H(s) - O\left((s - s_0)^l\right). \tag{6.15}$$

Therefore, $H_r(s)$ matches the first l moments of $H(s)$, and BDSM has similar accuracy to PRIMA [22]. In PRIMA, the first l moments of $H(s)$ are matched in a matrix format. However, in BDSM, each $p \times m$ transfer matrix $H_{ir}(s)$ captures the first l moments of $H(s)$'s i-th column. Consequently, their sum, $H_r(s)$, captures $H(s)$'s first l moment matrices in a *column-by-column* style, as illustrated in the BDSM flow of Fig 6.1.

6.3.3 Numerical Complexity

The detailed implementation is presented in Algorithm 6.1. Assume that no vectors

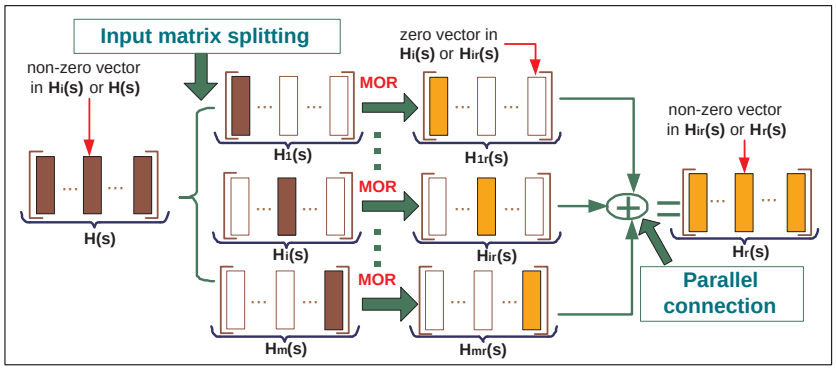

Figure 6.1: The BDSM model reduction scheme for a linear network with m input ports, which is based on column-by-column moment matching. After input matrix splitting, the original model is decomposed into m MIMO subsystems. Then using the projection process, $H_{ir}(s)$ captures the first l moments of $H(s)$'s i-th column. Finally, the parallel connection of all ROMs guarantees the preservation of $H(s)$'s first l moments.

are deflated in the Krylov subspace projection. To match l moments for a system with m inputs, BDSM and PRIMA both need one sparse LU factorization, $l-1$ multiplications of sparse matrices and block vectors, and l steps of backward plus forward substitutions. The cost difference comes from the orthonormalization process (cf. Step 3 of Algorithm 6.1). In PRIMA, all nl column vectors need to be orthonormalized, which costs $\frac{ml(ml-1)}{2}O(n)$ complexity. While in BDSM algorithm, the vectors are clustered into m groups, and then each group of vectors are orthonormalized separately. Consequently, BDSM has a total complexity of $\frac{ml(l-1)}{2}O(n)$ in the orthonormalization step, which brings in remarkable computational savings in many-terminal system reduction. An explanation of the cluster-and-orthonormalization flow is given in Fig 6.2.

Next, we contrast the resulting ROMs. PRIMA generate dense ROMs with $O(m^2l^2)$ nonzeros, while only ml^2 nonzero entries need to be stored in a BDSM ROM. When m becomes large, the ROMs by BDSM would be very sparse (with $\frac{1}{m}$

Algorithm 6.1: Block-diagonal structured MOR (BDSM)

Input: $C, G \in \mathbb{R}^{n\times n}$, $B \in \mathbb{R}^{n\times m}$,$L \in \mathbb{R}^{p\times n}$, and l.
Output: Matrices of the reduced model C_r, G_r, L_r and B_r.
begin
1. Perform LU factorization: $LU = (s_0C - G)$, calculate $X = U^{-1}(L^{-1}B)$, and normalize each column of X;
2. Set $V^{(i)} = X(:, i)$ for $i = 1, \cdots, m$;
3. **for** $j = 1, \cdots, l-1$ **do**
  calculate $X_{\text{temp}} = CX$;
  calculate $X = U^{-1}(L^{-1}X_{\text{temp}})$;
  for $j = 1, \cdots, l-1$ **do**
    orthonormalize $X(:, i)$ to all columns of $V^{(i)}$ to obtain $\bar{x}_i$;
    update $V^{(i)}$: $V^{(i)} = \left[V^{(i)}, \bar{x}_i\right]$;
4. Construct the reduced model for Σ_i as in (6.11) for $i = 1, \cdots, m$, and then form the reduced model of (6.1) by (6.14).

sparsity). The resulting sparse and block-diagonal structured ROMs would significantly facilitate numerical simulation, as will be demonstrated in Section 6.4 and Section 6.6.

6.4 Fast Power Grid Simulation

6.4.1 BDSM-Based Simulation

This section discusses the BDSM-based transient simulation for power grid networks. Using backward Euler discretization, the time-domain circuit equation can be written as

$$(\frac{C}{h} - G)x(t) = C\frac{x(t-h)}{h} + Bu(t), \quad y(t) = Lx(t) \tag{6.16}$$

which is a large-size linear system solution problem and extremely expensive to solve. Here the small constant h is a predefined time step. After performing BDSM MOR, we replace the original model with the much smaller block-diagonal structured ROM,

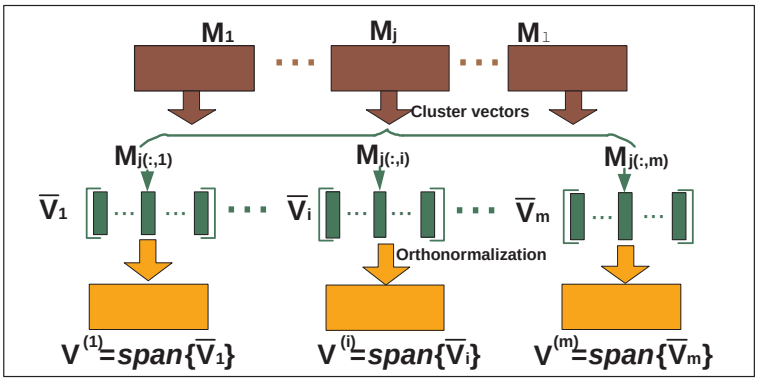

Figure 6.2: Projection matrix construction in the proposed BDSM scheme. Here, $M_j = ((s_0C - G)^{-1}C)^{j-1}(s_0C - G)^{-1}B$, $j = 1, \cdots, l$. The i-th columns of M_j's are grouped to form $\bar{V}_i$ $(i = 1, \cdots, m)$. And then V_i is computed such that $V_i = \bar{V}_i$, for $i = 1, \cdots, m$. Note that in PRIMA the projection matrix for (6.1) is constructed without clustering, such that $V = \text{span}\{M_1, \cdots, M_l\}$ with more computational cost.

i.e.,

$$\underbrace{(\frac{C_r}{h} - G_r)}_{A_r} z(t) = \underbrace{C_r \frac{z(t-h)}{h} + B_r u(t)}_{b_r(t)}, \quad y_r(t) = L_r z(t). \tag{6.17}$$

If we attempt to solve all elements of $x(t)$, the output matrix could be set as $L = I_n$, thus $L_r = \mathcal{I}\mathcal{V}$ with $\mathcal{I} = [I_n, \cdots, I_n] \in \mathbb{R}^{n \times mn}$, and then $x(t) \approx \left[V^{(1)}, \cdots, V^{(m)}\right] z(t)$. Due to the special structure of A_r, $z(t)$ can be directly solved as

$$z(t) = A_r^{-1} b_r(t). \tag{6.18}$$

The dimension of A_r is ml, which could be up to tens of thousands in power grid problems. However, due to the block-diagonal structure, the matrix inversion can be finished at a low cost of $O(ml^3)$. Since l is very small (at most several tens), the matrix inversion is trivial to compute. After that, $z(t)$ can be computed by matrix-vector production at a cost of $O(ml^2)$. Therefore, using the BDSM ROM, the total

cost of power grid simulation is

$$\text{Cost}_{total} = O(ml^3) + N_t O(ml^2) \tag{6.19}$$

where N_t is the number of time points used in simulation.

We assume that the state vector of Σ_{ir} is $z_i(t)$, denote $A_{ir} = \frac{C_{ir}}{h} - G_{ir}$ and $b_{ir}(t) = C_{ir}\frac{z_i(t-h)}{h} + B_{ir}u(t)$, $y(t) \approx L_r z(t)$ can be represented as

$$y(t) \approx \sum_{i=1}^{m} \overbrace{L_{ir} \underbrace{A_{ir}^{-1} b_{ir}(t)}_{z_i(t)}}^{y_{ir}(t)}. \tag{6.20}$$

Then we propose two methods that can be used to further speed up the above calculation.

6.4.2 Problem Size Scaling

Assume that the power grid network is initially zero-conditioned, then $z_i(t) = 0$ if the i-th input excitation $u_i(t)$ is zero during the simulation period, because all entries of B_{ir} are zero except for its i-th column. This assumption is reasonable in power grid simulation, especially when power gating technique is adopted in low-power design. Under power gating, many circuit blocks are disabled and thus the excitations from these "dead" transistor networks can be regarded as zero [108].

If $u_i(t) = 0$ in the simulation, Σ_{ir} can be skipped in the simulation. To simplify the discussion, we define a vector $\xi \in \mathbb{R}^{m\times 1}$:

$$\xi_j = \begin{cases} 1, \text{ if the } j\text{-th input is active} \\ 0, \text{ if the } j\text{-th input is zero.} \end{cases} \tag{6.21}$$

Provided that ξ has m_e nonzero elements, which means that there are m_e active

inputs, then a scaled ROM $\Sigma_{re} : (C_{re}, G_{re}, B_{re}, L_{re})$ can be used to replace Σ_r in the simulation. Here Σ_{re} is a LTI obtained by the parallel connection of all Σ_{jr}'s with $u_j(t)$ being *active* (or nonzero), and C_{re}, G_{re}, B_{re}, L_{re} are obtained by deleting the blocks inside C_r, G_r, B_r, L_r corresponding to zero inputs, respectively. Denote the state vector of Σ_{re} by $z_e(t)$, then the power grid model can be solved by

$$\begin{aligned} &\underbrace{(\frac{C_{re}}{h} - G_{re})}_{A_{re}} z_e(t) = \underbrace{C_{re}\frac{z_e(t-h)}{h} + B_{re}u(t)}_{b_{re}(t)} \\ &y(t) \approx y_r(t) = L_{re} z_e(t). \end{aligned} \tag{6.22}$$

Clearly, the problem size has been reduced to $q_e = m_e l$, and the computational cost after size scaling would be reduced to

$$\text{Cost}_{scale} = \frac{m_e}{m}\text{Cost}_{total}. \tag{6.23}$$

To distinguish the ROMs before and after size scaling, we call the scaled ROM Σ_{re} as effective reduced-order model (**EROM**) and its size q_e as *effective size*. The problem size scaling procedure is summarized in Algorithm 6.2.

Algorithm 6.2: Problem Size Scaling

Input: $C_r, G_r \in \mathbb{R}^{q\times q}$, $B_r \in \mathbb{R}^{q\times m}$, $L_r \in \mathbb{R}^{p\times q}$, $\xi \in \mathbb{R}^{m\times 1}$.
Output: Matrices of the EROM: C_{re}, G_{re}, L_{re} and B_{re}.
begin
  1. Initialize the EROM: $C_{re} = G_{re} = L_{re} = B_{re} = [\,]$;
  2. **for** $i = 1, \cdots, m$ **do**
    if $\xi_i \neq 0$ **then**
      $C_{re} = \text{blkdiag}(C_{re}, C_{ir})$, $G_{re} = \text{blkdiag}(G_{re}, G_{ir})$, $B_{re} = \begin{bmatrix} B_{re} \\ B_{ir} \end{bmatrix}$,
      $L_{re} = \begin{bmatrix} L_{re} & L_{ir} \end{bmatrix}$.

6.4.3 Parallel Computation

Equation (6.20) shows that $y_{ir}(t)$ only depends on L_{ir}, A_{ir} and $b_{ir}(t)$. On a multi-core platform, ROMs of the splitted systems can be clustered into several groups, and then each group can be simulated simultaneously. Provided the m splitted ROMs are clustered into N groups ($N \leq m$), the simulation cost would be reduced to

$$\begin{aligned} &\text{Cost}_{parallel} = N_b \left(O(l^3) + N_t \times O(l^2) \right) \\ &\text{with } N_b = \begin{cases} \dfrac{m}{N}, \text{ if } \dfrac{m}{N} = \left[\dfrac{m}{N} \right] \\ \left(\left[\dfrac{m}{N} \right] + 1 \right), \text{ otherwise.} \end{cases} \end{aligned} \tag{6.24}$$

Here, N_b is the maximum block number in each group, and $[o]$ represents the integral part of o. In the extremal case, an $m\times$ speedup can be achieved if each Σ_{ir} is regarded as an individual group (when $N = m$).

Simulation of Σ_{re} (the EROM) can be tackled in a similar way. Keeping N unchanged and replacing m with m_e in (6.24), a new maximum block number N_{be} will be obtained which is normally smaller than N_{be}. Therefore, the two acceleration schemes can be used together to achieve the fastest computation if the active port number is very large.

6.5 Discussions of BDSM

6.5.1 Comparison with Existing Power Grid MORs

Table 6.1 has compared BDSM with some typical massive-port MOR schemes: EKS [100], PRIMA [22], and SVDMOR [102] (a typical MOR based on terminal reduction). In PRIMA and BDSM, we assume that l moments of the transfer matrix are matched; in SVDMOR, we assume that the port compression ratio is α (i.e., the ratio of port

MOR method	ROM size	ROM pattern	Matched moments	ROM reusable?	ROM scalable?
BDSM	ml	block-diagonal	l	yes	yes
PRIMA	ml	full dense	l	yes	no
SVDMOR	αml	full dense	N/A	yes	no
EKS	l	full dense	N/A	no	no

Table 6.1: Comparison of various multi-port MOR schemes. In SVDMOR, α represents the port compression ratio.

number after terminal reduction *w.r.t* the original port number), and then l moments of the "thin" transfer matrix is matched; in EKS, it is assumed that the first l moments of the response under a *predefined* excitation are captured. In SVDMOR and EKS, the "true" moments of $H(s)$ are not captured, so they are *not* exact moment matching schemes. Among these approaches, PRIMA and SVDMOR generate full dense matrices, which are expensive for subsequent frequency/time-domain simulation. Although SVDMOR could compress the port size to some extent (at the cost of accuracy sacrifice), the obtained dense-matrix ROMs are still memory- and time-consuming for many-terminal systems. And when the input-output correlation is not strong, large errors may be induced by the terminal reduction process. EKS is capable of generating very small (size-l) macromodels, but the resulting ROMs are *not* reusable. These problems lead to remarkable efficiency degradation in ROM-based simulation. Compared with these existing MORs, BDSM does not have these limitations, thereby allowing for more efficient simulation of massive-port networks.

We remark that EKS ROM is very inaccurate under varying input patterns, due to its strong dependency on the predefined input waveforms. To increase its accuracy, more moments of the response should be captured. However, as will be shown in Section 6.6, EKS is not comparable with PRIMA and BDSM in terms of accuracy, even if the ROM size is increased to ml, at a cost similar to that of PRIMA which would be inefficient for power grid networks.

6.5.2 A Variant: Row-by-Row BDSM Scheme

If the input port number is larger than the output port number (i.e., $p < m$), a variant of BDSM based on row-by-row moment matching could be developed to generate a smaller ROM. First, the output position matrix L could be splitted as

$$L = \sum_{i=1}^{p} L_i, \text{ with } L_i \in \mathbb{R}^{p\times n},\ L_i(j,:) = \begin{cases} l_i, \text{ if } i = j \\ 0, \text{ if } i \neq j \end{cases} \tag{6.25}$$

for $i, j = 1,\ 2,\ \cdots, p$. Here l_i denotes the i-th row of L. Then the splitted LTI system Σ_i can be realized by (C, G, B, L_i), and the transfer matrix is written as $\tilde{H}_i(s) = L_i(sC - G)B$, and the original transfer matrix can be expressed as

$$H(s) = \sum_{i=1}^{p} \tilde{H}_i(s). \tag{6.26}$$

For Σ_i, a projection matrix can be constructed by

$$V^{(i)} = \mathcal{K}_l\{(s_0C - G)^{-T}C^T,\ (s_0C - G)^{-T}L_i^T\} \tag{6.27}$$

which is an $n \times l$ matrix since L_i only contains one nonzero row vector. After that, Σ_{ir} can be generated by the approach in (6.11). And finally, by parallel connection of all Σ_{ir}'s, a size $pl \times pl$ block-diagonal structured ROM could be constructed for the original power grid model. This model contains p diagonal blocks with each block being size-l.

It can be proved that Σ_{ir}'s transfer matrix captures the i-th rows of $H(s)$'s first l moment matrices. Therefore, this MOR is in fact a row-by-row moment matching. Due to the special matrix structure, the resulting ROM can also be simulated in a parallel style. However, using row-by-row moment matching, the problem size can not be scaled with the active input number, because the input matrix have multiple

nonzero columns in each block.

6.5.3 System Passivity

A passive system is one that does not generate energy internally. System passivity is expected to be preserved when the transfer matrix is square (i.e., $p = m$) and represents the admittance/impedance parameters. In such a case $u(t)^T y(t)$ is a power metric, and the resulting ROM should be positive real. The proposed BDSM can not automatically guarantee system passivity, thus passivity enforcement/compensation [10] procedures are needed if nonpassive models are produced. The main bottleneck of passivity enforcement on Σ_r lies in passivity verification. To ensure that all possible nonpassive regions are detected, Hamiltonian method [10] or generalized Hamiltonian method (GHM, c.f. Chapters 2 & 3) should be used which, however, consume $O(q^3)$ complexity (q is the size of Σ_r). Since q might be up to thousands for multi-port models, the passivity verification and enforcement can be prohibitively expensive.

Fortunately, the block-diagonal structure of Σ_r can significantly facilitate the calculations. For simplicity, we assume that Σ_r is obtained by single-point projection thus the size of Σ_{ir} is l. We further assume that C_{ir} is nonsingular after projection (otherwise, the Weierstrass decomposition [with $O(l^3)$ complexity] or canonical projector technique [20] could be used to convert Σ_{ir} to a nonsingular system), then Σ_{ir} can be transformed to a standard state-space model Σ_{ir}^s: (I, G_{ir}^s, B_{ir}^s, L_{ir}), with $G_{ir}^s = C_{ir}^{-1} G_{ir}$ and $B_{ir}^s = C_{ir}^{-1} B_{ir}$. An eigenvalue decomposition can be performed on G_{ir}^s at a cost of $O(l^3)$

$$G_{ir}^s = X_i \Lambda_i X_i^{-1} \tag{6.28}$$

where Λ_i is a diagonal matrix whose diagonal elements contain the eigenvalues of G_{ir}^s. Then Σ_{ir} can be realized by (I, Λ_i, $X_i^{-1} B_{ir}^s$, $L_{ir} X_i$), and similar to B_i, $X_i^{-1} B_{ir}^s$ also has only one nonzero vector at the i-th column. To this end, Σ_r can be realized as a

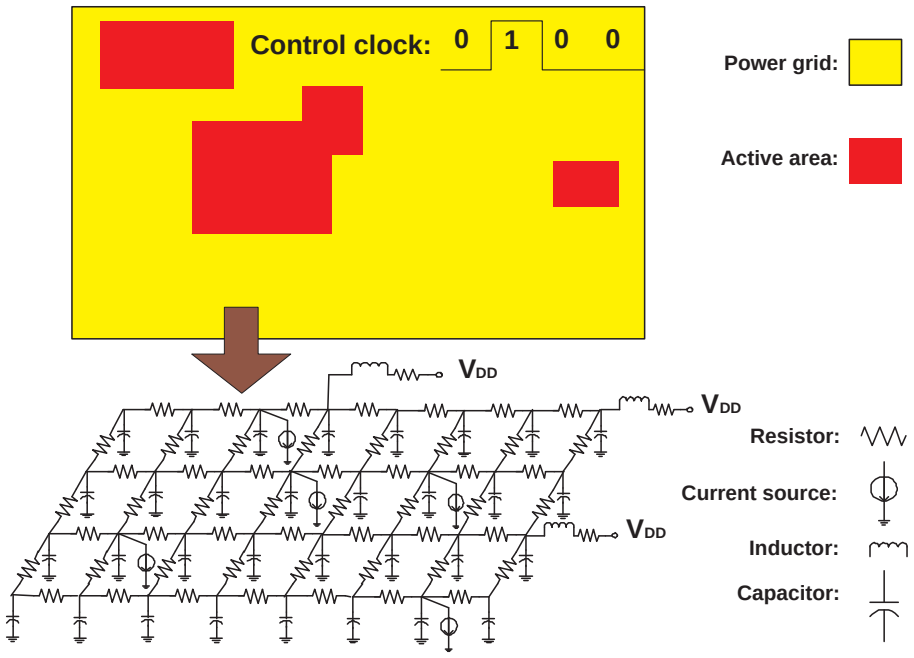

Figure 6.3: The upper part represents a power grid with consideration of clock gating; the bottom part is the RLC model.

diagonal-structured LTI via parallel connection of all Σ_i's. And finally, the passivity test and enforcement can be largely simplified via Laguerre's method at the cost of only $O(q^2)$ [109].

However, we remark that, unlike interconnect macromodeling, in may cases, system passivity is not necessarily required to be preserved in power grid reduction. First, the input and output numbers might not be identical (e.g., in some cases $y(t) = x(t)$ and $p \gg m$), thus $H(s)$ is not a square matrix. Second, even though $m = p$, the output variables may not be the nodal voltage (or branch current) variables corresponding to the input current (or voltage) excitations, which means that physically $H(s)$ does not represent the admittance/impedance parameters.

6.6 Numerical Results

We use several multi-domain clock gating power grid benchmarks to verify the proposed scheme. As shown in Fig. 6.3, the yellow rectangular represents a power grid system, which is modeled as a large-scale linear circuit including resistance, capacitance and packaging inductance (cf. the bottom part of Fig. 6.3). Time-varying current sources are used to describe the behavior of active circuit blocks. If clock gating technique is adopted in low power design to control the behavior of transistor circuit blocks, only part of the transistor networks are active (as marked by the red areas in Fig. 6.3), whereas other blocks are disabled. The current sources from these "dead" blocks can be regarded as zero in transient simulation [108]. The MNA LTI models are extracted from some industrial Spice netlists. All experiments are performed on a 2.6GHz 4-GB RAM Linux workstation.

6.6.1 MOR Efficiency and Accuracy

We begin by timing different MOR schemes using single-point moment matching on 5 RLC power grid benchmarks (ckt1-ckt5 in Table 6.2). The port numbers range from several tens to over $1k$; and the node numbers are from $6k$ to $1.7M$. For simplicity, all ports are first assumed to be active and excited by unit-impulse signals in EKS [91]; in SVDMOR, α is set around 0.6 for all examples. Specifically, $H(s)$ is first approximated by $U_l^T \mathcal{H}(s) U_r$ with $\mathcal{H}(s) \in \mathbb{C}^{\hat{p}\times\hat{m}}$, $\hat{p} = [\alpha p]$ and $\hat{m} = [\alpha m]$ [102], and then the "thiner" LTI $\mathcal{H}(s)$ is reduced by PRIMA. Since sparse LU may still introduce large amounts of nonzero elements for some cases, this factorization is skipped in ckts3-5 to save memory, at the cost of more simulation time.

The CPU times and resulting ROM sizes are listed in Table 6.2. With the same number of moments matched, BDSM and PRIMA generate ROMs with the same size. Since much fewer long-vector orthonormalizations are needed, BDSM is faster than

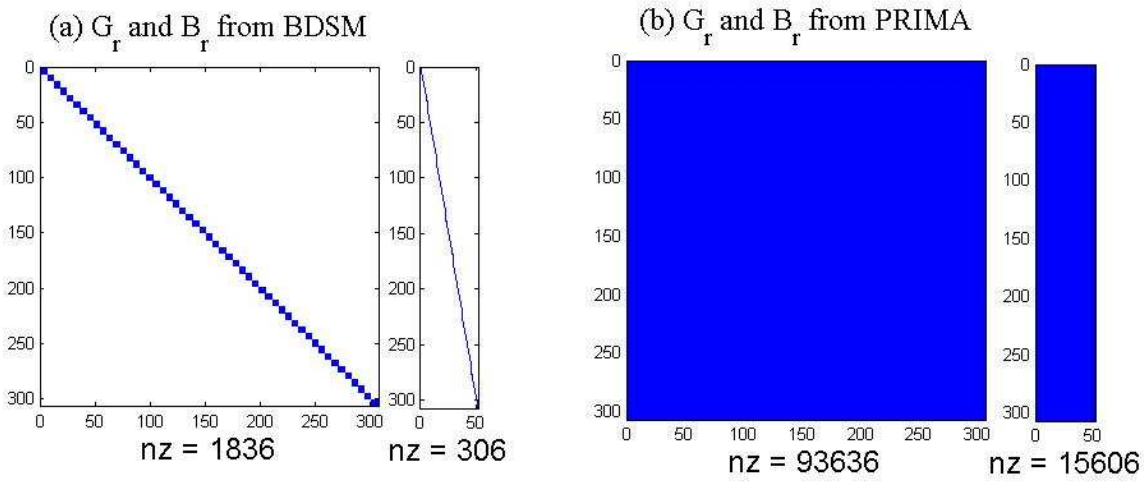

Figure 6.4: The matrix structures of ckt1's ROMs, obtained from BDSM and PRIMA, respectively.

PRIMA, and this speedup becomes more remarkable as the problem size and port number increase. In SVDMOR, although the terminals can be reduced to some extent, it still needs more orthonormalization steps and thus is slower than BDSM in many-terminal cases (cf. ckts3-4). Even more, PRIMA and SVDMOR may fail in very-large-size many-port cases (cf. ckts4-5). This is because: 1) the resulting full-dense ROMs of PRIMA and SVDMOR can be memory-consuming in many-port cases; 2) the "fat" projection matrix V ($\in \mathbb{R}^{n\times ml}$ or $\mathbb{R}^{n\times \alpha ml}$) is also dense and even more CPU-consuming. While in BDSM the projection matrix $V^{(i)}$ for each splitted system is very thin, and the final sparse block-diagonal ROM is cheap to store. To illustrate this, Fig. 6.4 has compared the ROM matrix structures of ckt1, from BDSM and PRIMA, respectively. Due to the special structure of G_r, C_r and B_r, much smaller EROMs can be extracted from BDSM ROMs if only a small portion of ports are active (cf. column 4 of Table 6.2) under clock gating, which can be very efficient in subsequent simulation. EKS is the fastest one among these schemes. However, the EKS ROM need to be rebuilt each time when the input pattern changes, making the simulation

ckt	node	port number		PRIMA [22]		SVDMOR [102]		EKS [100]		BDSM			No. of matched moments
		total	active	Time	Size	Time	Size	Time	Size	Time	Size		
											ROM	EROM	
ckt1	6k	51	6	29.37	306	35.60	180	0.30	6	8.18	306	36	6
ckt2	20k	108	19	5.0×10^3	1080	1.4×10^3	640	15.4	10	3.7×10^3	1080	190	10
ckt3	80k	204	21	1.2×10^4	2040	1.0×10^4	1220	17.7	10	7.1×10^3	2040	210	10
ckt4	123k	315	46	break down	N/A	break down	N/A	39.8	8	2.6×10^4	2520	368	8
ckt5	1.7M	1429	103	break down	N/A	break down	N/A	610	10	5.9×10^4	14290	1030	10

Table 6.2: CPU times (sec) of various MOR schemes. In SVDMOR, we match the moments of the approximated low-rank transfer matrix after terminal reduction. In EKS, the moments of the response under unit impulse excitations are captured, but the transfer matrix's moments can not be captured, therefore, the EKS ROM is *not* reusable.

very inefficient in practice. Furthermore, it is also difficult to *exactly* predict the input signals of a power grid network, whereas inexactly modeled inputs may make the EKS ROM unreliable. Therefore, a *reusable* ROM is preferred for repeated circuit simulation. As shown by Table 6.2, BDSM provides the best numerical efficiency among those reusable power grid MOR schemes.

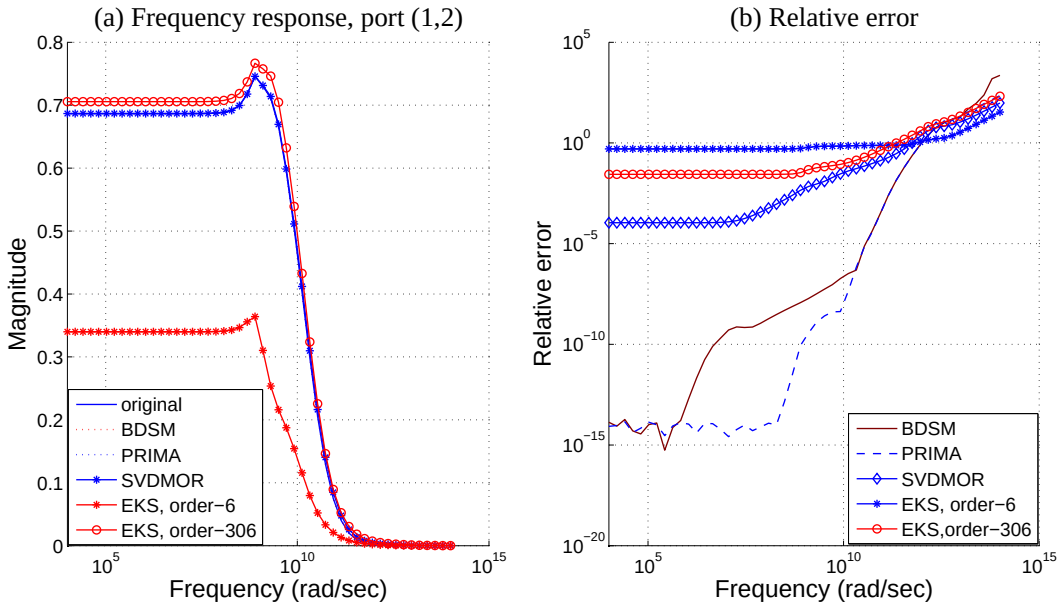

Figure 6.5: Comparison of MOR accuracy for ckt1.

Fig. 6.5 plots the transfer function of port(1,2) for ckt1. In EKS, all inputs are set

ckt	stime without MORs	PRIMA [22]		SVDMOR [102]		EKS [100]		BDSM				No. of expansion points	No. of matched moments
		stime	size	stime	size	stime	size	without scaling		with scaling			
								stime	size	stime	size		
ckt1	320	266	1020	44.3	600	0.20	20	12.1	1020	1.31	120	5	20
ckt2	529	2.3×10^3	3240	331	1920	0.50	30	43.2	3240	6.20	570	6	30
ckt3	2.5×10^3	1.8×10^3	3060	259	1830	0.05	15	23.7	3060	2.44	315	5	15
ckt4	5.1×10^3	N/A	N/A	N/A	N/A	0.20	15	61.9	4725	8.84	690	5	15
ckt5	5.9×10^4	N/A	N/A	N/A	N/A	0.21	18	291	25722	21.7	1854	6	18

Table 6.3: CPU times (sec) of 1000-point backward Euler time-domain simulation via ROMs obtained by multi-point projection.

as unit impulse signals. For fairness, 6 moments are matched in all MOR schemes. EKS's size-6 ROM has very low accuracy. Then we construct a larger EKS ROM by matching 306 moments of the response, which costs $36sec$ for ckt1. However, the size-306 EKS ROM is still very inaccurate. This is not surprising, because the EKS ROM under a specific excitation is not reusable for new input patterns. Fig. 6.5 plots the relative errors of these MOR schemes. PRIMA and BDSM has very high accuracy (relative error $< 10^{-6}$ for $\omega < 10^{10} rad/sec$), due to their *exact* moment matching properties. The error of SVDMOR ROM is several orders larger over those of BDSM and PRIMA, due to the error-prone terminal reduction.

6.6.2 Time-Domain Performance

We continue to compare the behaviors of different ROMs in time-domain transient simulation. Since practical signals are usually distributed in wide frequency bands, rational Krylov-subspace [106] projection is employed to improve numerical accuracy. In all MORs, l moments are matched at each expansion point, so totally $l_{\text{tot}} = lk$ moments would be matched if k points are used. For simplicity, pulse waveforms are added to all *active* ports as excitations. The CPU times of 1000-step transient simulation (denoted by "stime") are listed in Table 6.3. Because PRIMA and SVDMOR generate large dense matrices, the numerical efficiency of their ROMs degrades remarkably in large multi-port systems, and solving the dense ROMs can

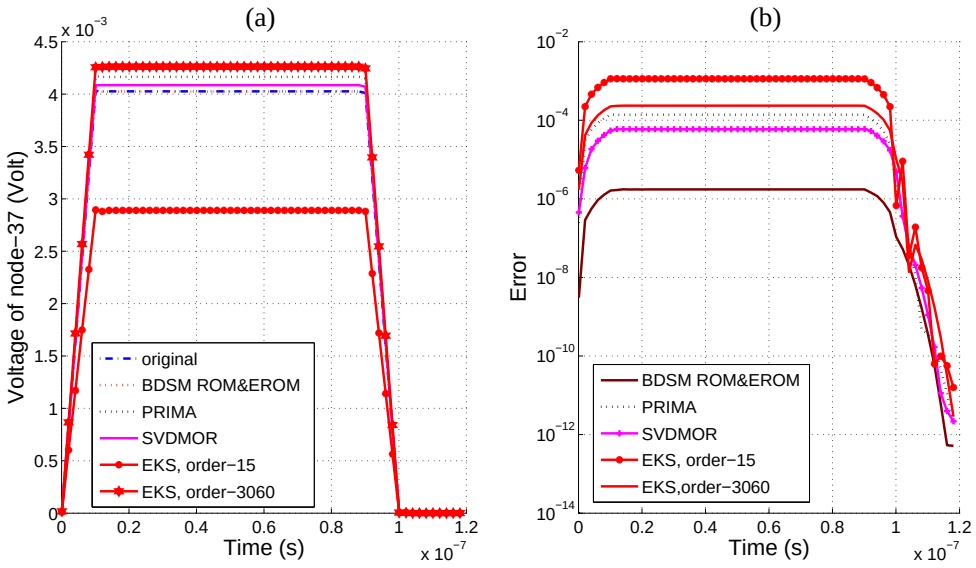

Figure 6.6: The voltage waveforms of node-37 in ckt3.

be even more expensive than simulating the original networks (as shown by ckt2). Thanks to the sparse block-diagonal structure, BDSM ROMs can be simulated very fast even when the ROM size reaches above $20k$ for many-terminal models (cf. ckt5). Furthermore, with consideration of clock gating, EROM could further speedup the time-domain simulation (which is around $10\times$ in our tested cases). Although EKS is very fast in the subsequent simulation, EKS ROMs need to be rebuilt for repeated simulation. On the other hand, EKS is not comparable to other MOR schemes in terms of accuracy. To show this, Fig. 6.6 plots the voltage waveforms at 37th node of ckt3, where 5 expansion points are utilized in all projection schemes. Clearly, EKS ROM's waveform could not capture the behavior of ckt3 with acceptable accuracy (even when the ROM size is increased to 3060, whose simulation cost is about 2×10^3sec). The waveforms from ROMs of BDSM, PRIMA and SVDMOR are close to the original one. Among them, the result from BDSM can not be distinguished from the original one, and the error is below 10^{-5}. The parallel acceleration is not implemented here, as its speedup factor has been analytically derived.

6.7 Summary

This chapter has proposed a novel model reduction scheme, BDSM, for multi-port systems such as power grid networks. BDSM has similar accuracy to PRIMA due to the same number of matched moments; it is faster and more memory-efficient over PRIMA (and SVDMOR in many-terminal cases) in model generation, since lots of long-vector orthonormalizations are skipped; unlike EKS and TBS, because BDSM is input-independent, the obtained ROMs are reusable for time/frequency-domain analysis under varying input patterns; more importantly, BDSM ROMs have block-diagonal structures which in turn allow for very fast subsequent simulation. Some acceleration techniques in the subsequent simulation, including problem size scaling and parallel computation, have also been presented. Additional issues such as row-by-row moment matching and passivity issue are discussed. The efficiency and accuracy of BDSM in both model extraction as well as subsequent time-domain simulation have been verified by industrial benchmarks.

Chapter 7

Thesis Conclusion

This thesis is centered on some theoretical and numerical problems on linear time-invariant descriptor systems (LTI DSs), with emphasis on their passivity assessment and model order reduction (MOR). We focus on the LTI cases, rather than linear time-variant (LTV) or nonlinear cases, because: 1) there exist many open questions for LTI DSs; 2) as the fundamentals of LTV and nonlinear cases, the advancements on LTI DS studies would be applied to analyze more complex circuit systems.

7.1 Part 1: DS Passivity Assessments

Specifically, in the first part (Chapters 2 to 4), we focus on the passivity assessments of LTI DSs, including both admittance/impedance systems and scattering systems. Works in this part include:

1. A generalized Hamiltonian method (GHM) and its half-size version (HGHM) have been developed, including theoretical derivation and numerical realization. The most significant advantage of GHM/HGHM passivity test is that they are purely algebraic routines, and therefore the test results are very accurate. Not only they can tell a LTI DS is passive or not, but they also accurately locate

the possible nonpassive regions, and thereby provide a versatile tool for DS passivity enforcement (if necessary).

2. Based on the work of Chapter 2, we have further presented a projector-based passivity test for large-size LTI DS models which can not be tackled by GHM. It is the first time that we use spectral projectors, based on a novel fast construction, to efficiently decompose a large DS model to its proper and improper subsystems. After the projector-based system decomposition, the proper part is tested by GHM based on a fast numerical implementation. The fast GHM implementation only computes a small part of the generalized eigenvalues that are close to the imaginary axis, using a multi-shift Arnoldi algorithms. Since this method is based on Krylov iteration, the algorithm is CPU-friendly and is applicable to very large circuit models.

3. We notice that in high-frequency applications, S-parameters are more frequently used. Motivated by this, Chapter 4 has developed the S-parameter generalized Hamiltonian method (S-GHM) and its half-size algorithm (S-HGHM). Similar to GHM and HGHM, S-GHM and S-HGHM can locate all possible nonpassive regions with high numerical accuracy. Furthermore, we have also proposed a passivity test flow for admittance/impedance DSs, based on S-GHM and S-HGHM. It is realized by two steps. First, the admittance/impedance model is converted to a "scattering" DS via Moebious transform. After that, the Moebious-transformed system is tested by S-GHM or S-HGHM to find the possible nonpassive frequency intervals.

An interesting observation about the (S-parameter) generalized Hamiltonian methods is that, they are the superset of standard Hamiltonian methods and therefore

applicable to either DS or standard state-space models. Besides that, based on equivalent model conversion, they can be applied to more general DSs or standard state-space LTI models, without restrictions on system matrices as required by traditional approaches.

7.2 Part 2: DS Model-Order Reduction

The second part of this thesis aims to solve two issues about DS MOR:

1. Passivity and improper part preserving MOR;
2. Efficient MOR for multi-port LTI DSs that allows for fast subsequent circuit simulation.

Chapter 5 focuses on the first issue. The improper part of a DS is preserved by additive system decomposition based on fast spectral projector technique. After additive decomposition, the improper part remains unchanged, and the proper part is reduced via DS-format positive-real balanced truncation (DS-PRBT). Since the main bottleneck of DS-PRBT is in solving the dual generalized algebraic Riccati equations (GAREs), we have developed a generalized quadratic alternate implicit (GQADI) algorithm to efficiently compute the positive-real Gramians. The proposed GARE solver is faster than the most advanced solver (e.g., Newton's iteration based on LR-ADI). Detailed algorithmic description, including convergence and well posedness have been presented. To further speed up the matrix solver, a low-rank version (LR-GQADI) has also been devised, which reduces the complexity from $O(n^3)$ to $O(n^2)$.

Finally, we aimed to construct "good" macromodels for multi-port LTI DS, such as power grid models. Due to the large number of ports, existing MOR techniques are not efficient for power grids. Some fast algorithms have been developed at the expense of model accuracy. To overcome this problem, we have developed a MOR

routine based on input matrix splitting, called BDSM. The BDSM ROM is as accurate as standard Krylov-subspace based moment-matching MORs; its resulting ROMs are block-diagonal structured, and thereby are cheap to solve and easy to compute in a parallel fashion; a very interesting result about BDSM is that, when used in power grid simulation, the ROM size can be further significantly scaled down if power gating is considered; finally and most importantly, the resulting ROM is reusable, so it could be used under various input wave patterns.

Bibliography

[1] E. L. Yip and R. F. Sincovec, "Solvability, controllability and observability of continuous descriptor systems," *IEEE Trans. Automat. Control*, vol. AC-26, no. 3, pp. 702–707, 1981.

[2] L. Dai, *Singular Control Systems*, ser. Lecture Notes in Control and Information Sciences 118. Berlin/Heidelberg: Springer-Verlag, 1989.

[3] A. Varga, "A descriptor systems toolbox for MATLAB," in *Proc. IEEE Intl. Symp. Computer-Aided Control System Design*, 2000, pp. 150–155.

[4] K. Zhou, J. C. Doyle, and K. Golver, *Robust and Optimal Control*. Upper Sadder River, NJ: Prentice-Hall, 1996.

[5] D. E. Schwarz and C. Tischendorf, "Structural analysis of electric circuits and consequences for MNA," *Intl. J. Circuit Theory Appl.*, vol. 28, pp. 131–162, 2000.

[6] D. Ioan and G. Ciuprina, "Reduced order models of on-chip passive components and interconnects, workbench and test structures," in *Model Order Reduction: Theory, Research Aspects and Applications*. Springer, Berlin Heidelberg, Aug 2008, pp. 447–467.

[7] B. Bond and L. Daniel, "Stable Reduced Models of Nonlinear Descriptor Systems through Piecewise Linear Approximation and Projection," *IEEE Trans. CAD of Integrated Circuits and Systems*, vol. 28, no. 10, pp. 1467–1480, 2009.

[8] S. Grivet-Talocia, "An adaptive sampling technique for passivity characterization and enforcement of large interconnect macromodels," *IEEE Trans. Advanced Packaging*, vol. 31, no. 4, pp. 673–683, Nov 2008.

[9] D. Saraswat, R. Achar, and M. Nakhla, "Fast passivity verification and enforcement via reciprocal systems for interconnects with large order macromodels," *IEEE Trans. VLSI Syst.*, vol. 15, no. 1, pp. 48–59, Jan 2007.

[10] S. Grivet-Talocia, "Passivity enforcement via perturbation of Hamiltonian matrices," *IEEE Trans. Circuits Syst. I*, vol. 51, no. 9, pp. 1755–1769, Sept 2004.

[11] S. Grivet-Talocia and A. Ubolli, "A comparative study of passivity enforcement schemes for linear lumped macomodels," *IEEE Trans. Advanced Packaging*, vol. 31, no. 4, pp. 673–683, Nov 2008.

[12] D. Saraswat, R. Achar, and M. Nakhla, "Global passivity enforcement algorithms for macromodels of interconnect subnetworks characterized by tabulated data," *IEEE Trans. VLSI Syst.*, vol. 13, no. 7, pp. 819–831, Jul 2005.

[13] B. Gustavsen and A. Semlyen, "Fast passivity assessment for S-parameter rational models via half-size test matrix," *IEEE Trans. Microwave Theory and Technology*, vol. 56, no. 12, pp. 2701–2708, Dec 2008.

[14] A. Semlyen and B. Gustavsen, "A half-size singularity test matrix for fast and reliable passivity assessment of rational models," *IEEE Trans. Power Delivery*, vol. 24, no. 1, pp. 345–351, Jan 2009.

[15] E. Griepentrog and R. März, "Basic properties of some differential-algebraic equations," *Zeitschrift für Analysis und ihre Anwendungen*, vol. 8, no. 1, pp. 25–40, 1989.

[16] T. Reis and T. Stykel, "Positive real and bounded real balancing for model reduction of descriptor systems," Institut für Mathematik, Technische Universität Berlin, Tech. Rep. 2008/25, 2008. [Online]. Available: http://www.math.tu-berlin.de/∼stykel/Publications/pr_08_25.pdf

[17] T. Reis and T. Stykel, "Passivity-preserving model reduction of differential-algebraic equations in circuit simulation," in *Proc. Appl. Math. Mechanics*. Zurich, Switzerland, Jul 2007, pp. 1 021 601–1 021 602.

[18] T. Stykel, "Balancing-related model reduction of circuit equations using their toplogical structure," May 2009, available at http://www.math.tu-berlin.de/∼stykel/.

[19] R. März, "Canonical projectors for linear differential algebraic equations," *Computers Math. Applications*, vol. 31, no. 4, pp. 121–135, Feb. 1995.

[20] N. Wong, "An efficient passivity test for descriptor systems via canonical projector techniques," in *Proc. Design Automation Conference*. San Fransisco, CA, Jul 2009.

[21] B. Brogliato, R. Lozano, B. Maschke and O. Egeland, *Dissipative Systems Analysis and Control: Theory and Applications*, 2nd ed., Springer, 2007.

[22] A. Odabasioglu, M. Celik, and L. Pileggi, "PRIMA: passive and reduced-order interconnect macromodeling algorithm," *IEEE Trans. CAD of Integrated Circuits and Systems*, vol. 17, no. 8, pp. 645–654, Aug 1998.

[23] Y. Hao, Y. Shi, and L. He, "Fast analysis of structured power grid by triangularization based structure preserving model oder reduction," in *Proc. Design Automation Conf.*, July 2006, pp. 205–210.

[24] Y. M. Lee, Y. Cao, T.-H. Chen, J. Wang, and C. C. Chen, "HiPRIME: hierarchical and passivity preserved interconnect macromodeling engine for RLKC power delivery," *IEEE Trans. CAD of Integrated Circuits and Systems*, vol. 24, no. 6, pp. 797 – 806, Jun. 2005.

[25] P. Feldmann and R. W. Freund, "Reduced-order modeling of large linear subcircuits via a block Lanczos algorithms," in *Proc. Design Automation Conf.*, 1995, pp. 474–479.

[26] J. R. Phillips, L. Daniel, and L. M. Silveira, "Guaranteed passive balancing transformations for model order reduction," *IEEE Trans. CAD of Integrated Circuits and Systems*, vol. 22, no. 8, pp. 1–15, Aug 2003.

[27] L. M. Silveira and J. R. Phillips, "Resampling plans for sample point selection in multipoint model-order reduction," *IEEE Trans. CAD of Integrated Circuits and Systems*, vol. 25, no. 12, pp. 2775 – 2783, Dec 2006.

[28] J. R. Phillips and L. M. Silveira, "Poor man's TBR: a simple model reduction scheme," *IEEE Trans. CAD of Integrated Circuits and Systems*, vol. 24, no. 1, pp. 43 – 55, Jan 2005.

[29] G. Muscato, G. Nunnari, and L. Fortuna, "Singular perturbation approximation of bounded real and of positive real transfer matrices," in *American Control Conf.*, June-1 July 1994, pp. 3416–3420.

[30] N. Wong and V. Balakrishnan, "Fast positive-real balanced truncation via quadratic alternating direction implicit iteration," *IEEE Trans. CAD of Integrated Circuits and Systems*, vol. 26, no. 9, pp. 1725–1731, Sept 2007.

[31] B. N. Bond and L. Daniel, "A piecewise-linear moment-matching approach to parameterized model-order reduction for highly nonlinear systems," *IEEE Trans. CAD of Integrated Circuits and Systems*, vol. 26, no. 12, pp. 2116 – 2129, Dec 2007.

[32] P. Li and L. Pileggi, "Compact reduced-order modeling of weakly nonlinear analog and RF circuits," *IEEE Trans. CAD of Integrated Circuits and Systems*, vol. 24, no. 2, pp. 184–203, Feb 2005.

[33] N. Dong and J. Roychowdhury, "General-purpose nonlinear model order reduction based on piecewise polynomial representations," *IEEE Trans. CAD of Integrated Circuits and Systems*, vol. 27, no. 2, pp. 249–261, Feb 2008.

[34] L. Daniel, C. S. Ong, S. C. Low, K. H. Lee, and J. White, "A multiparameter moment matching model reduction approach for generating geometrically parameterized interconnect performance models," *IEEE Trans. CAD of Integrated Circuits and Systems*, vol. 23, no. 5, pp. 678–693, May 2004.

[35] N. Mi, S. X.-D. Tan, Y. Cai, and X. Hong, "Fast variational analysis of on-chip power grids by stochastic extended Krylov subspace method," *IEEE Trans. CAD of Integrated Circuits and Systems*, vol. 27, no. 11, pp. 1996–2006,

[36] Y. Liu, L. Pileggi and A. J. Strojwas, "Model order-reduction of RC(L) interconnect including variational analysis," in *Proc. Design Automation Conference*, vol. 27, no. 11, pp. 1996–2006, June 1999

[37] M. Pedram and S. Nazarian, "Thermal modeling, analysis and management in VLSI circuits: principles and methods," *Proc. of IEEE, Special Issue on Thermal Analysis of ULSI*, Vol. 94, No. 8, pp. 1487–1501, Aug. 2006.

[38] A. H. Ajami, K. Banerjee, and M. Pedram, "Modeling and analysis of non-uniform substrate temperature effects in high performance VLSI," *IEEE Trans. CAD of Integrated Circuits and Systems*, Vol. 24, No. 6, pp. 849-861, Jun. 2005.

[39] R. W. Freund, "An extension of positive real lemma to descriptor systems," *Optimization Methods and Software*, vol. 19, no. 1, pp. 69–87, Feb 2004.

[40] G. H. Golub and C. F. V. Loan, *Matrix Computations*, 3rd ed. Johns Hopkins University Press, Baltimore, MD, 1996.

[41] Y. Liu and N. Wong, "Fast sweeping methods for checking passivity of descriptor systems," in *Proc. IEEE Asia Pacific Conf. on Circuits and Systems*, Dec. 2008, pp. 1794–1797.

[42] D. Chu and R. C. E. Tan, "Algebraic characterizations for positive realness of descriptor systems," *SIAM J. Matrix Anal. Appl.*, vol. 30, no. 1, pp. 197–222, 2008.

[43] C. Yang, Q. Zhang, Y. Lin, and L. Zhou, "Positive realness and absolute stability problem of descriptor systems," *IEEE Trans. Circuits Syst. I*, vol. 54, no. 5, pp. 1142–1149, May 2007.

[44] L. Zhang, J. Lam, and S. Xu, "On positive realness of descriptor systems," *IEEE Trans. Circuits and Syst. I*, vol. 49, no. 3, pp. 401–407, Mar. 2002.

[45] H. S. Wang, C. F. Yung, and F. R. Chang, "Bounded real lemma and H_∞ control for descriptor systems," *IEE Proc. Control Theory Appl.*, vol. 145, no. 3, pp. 316–322, 1998.

[46] N. Wong and C. Chu, "A fast passivity test for stable descriptor systems via skew-Hamiltonian/ Hamiltonian matrix pencil transformations," *IEEE Trans. Circuits and Syst. I*, vol. 55, no. 2, pp. 635–643, Mar 2008.

[47] P. Benner and D. Chu, "A new test for passivity of descriptor systems," Oberwolfach reports, Mathematisches Forschungsinstitut Oberwolfach, Tech. Rep. 11/2005, Feb. 2005.

[48] B. Gustavsen and A. Semlyen, "Rational approximation of frequency domain responses by vector fitting," *IEEE Trans. Power Delivery*, vol. 14, no. 3, pp. 1052–1061, July 1999.

[49] A. Mayo and A. Antoulas, "A framework for the solution of the generalized realization problem," *Linear Algebra Appl.*, vol. 425, no. 2–3, pp. 634–662, Sep. 2007.

[50] S. Lefteriu and A. C. Antoulas, "Modeling multi-port systems from frequency response data via tangential interpolation," in *Proc. IEEE Workshop on Signal Propagation on Interconnects*, May 2009, pp. 1–4.

[51] A. C. Antoulas, D. C. Sorensen and S. Gugercin, "A survey of model reduction methods for large-scale systems," *Contemporary Mathematics*, vol. 280, pp. 193–219, 2001.

[52] L. T. Pillage and R. A. Rohrer, "Asymptotic Waveform Evaluation for Timing Analysis," *IEEE Trans. CAD of Integrated Circuits and Systems*, pp. 352-366, April 1990.

[53] K. J. Kerns , I. L. Wemple and A. T. Yang, "Stable and efficient reduction of substrate model networks using congruence transforms," in *Proc. Intl. Conf. Computer-Aided Design*, pp. 207–214, Nov. 1995, San Jose, CA

[54] T. Stykel, "Gramian based model reduction for descriptor systems," *Mathematics of Control, Signals, and Systems*, vol. 16, no. 4, pp. 297–319, Mar 2004.

[55] ——, "Generalized alternating direction implicit method for projected generalized algebraic Lyapunov equations," in *Proc. Appl. Math. Mechanics*, 2004, pp. 686–687.

[56] ——, "Low-rank iterative methods for projected generalized Lyapunov equations," *Electron. Trans. Numer. Anal.*, vol. 30, pp. 187–202, 2008.

[57] J. Li and J. White, "Reduction of large circuit models via low rank approximate gramians", *International Journal of Applied Mathematics and Computer Science*, vol. 11, no. 5, pp. 101–121, 2001.

[58] J. Li and J. White, "Low rank solution of Lyapunov equations", *SIAM J. Matrix Anal. Appl.*, vol. 24, no. 1, pp. 260–280, 2004

[59] J. M. Badia, P. Benner, R. Mayo, and E. Quintana-Orti, *Parallel solution of large-scale and sparse generalized algebraic Riccati equations.* Springer Berlin, 2006.

[60] R. Byers and P. Benner, "A structure-preserving method for generalized algebraic Riccati equations based on pencil arithmetic," in *Proc. Euro. Control Conf.* Cambridge, UK, Sep 2003.

[61] H. Banks, R. del Rosario, and H. Tran, "Proper orthogonal decomposition-based control of transverse beem vibrations: experimental implementations," *IEEE Trans. Control Syst. Techonl.*, vol 10, no. 5, pp. 717–726, Sep. 2000.

[62] M. Rathinam and L. R. Petzold, " A new look at proper orthogonal decomposition," *SIAM J. Numer. Anal.*, vol 41, no. 5, pp. 1893–1925, 2003.

[63] H. Heeb and A. Ruehli, "Three-dimensional interconnect analysis using partial element equivalent circuits," *IEEE Trans. Circuits Syst. I*, vol. 39, no. 11, pp. 974–982, Nov 1993.

[64] Z. Bai and R. Freund, "Eigenvalue-based characterization and test for positive realness of scalar transfer functions," *IEEE Trans. Autom. Contr.*, vol. 45, no. 12, pp. 2396–2402, Dec 2000.

[65] Z. Zhang, C. U. Lei, and N. Wong, "GHM: a generalized Hamiltonian method for passivity test of impedance/admittance descriptor systems," in *Proc. Intl. Conf. Computer Aided Design*. San Jose, CA, Nov 2009.

[66] R. Ionutiu, J. Rommes, and A. Antoulas, "Passivity-preserving model reduction using dominant spectral-zero interpolation," *IEEE Trans. CAD of Integrated Circuits and Systems*, vol. 27, no. 12, pp. 2250–2263, Dec 2008.

[67] K. E. Brenan, S. L. Campbell, and L. Petzold, *Numerical Solution of Initial-Value Problems in Differential Algebraic Equations*, 2nd ed., ser. Classics in Applied Mathematics. Philadelphia, PA: SIAM, 1996, vol. 14.

[68] E. Eich-Soellner and C. Führer, *Numerical Methods in Multibody Dynamics*. Stuttgart, Germany: B. G. Teubner, Jul. 1998.

[69] M. Günther and U. Feldmann, "CAD-based electric-circuit modeling in industry I: Mathematical structure and index of network equations. II Impact of circuit configurations and parameters." *Surveys Math. Indust.*, vol. 8, no. 2, pp. 97–129, 131–157, 1999.

[70] I. Balk, "On a passivity of the Arnoldi based model order reduction for full-wave electromagnetic modeling," *IEEE Trans. Adv. Packag.*, vol. 24, no. 3, pp. 304–308, Aug. 2001.

[71] B. Yan, S.-D. Tan, and B. McGaughy, "Second-order balanced truncation for passive-order reduction of RLCK circuits," *IEEE Trans. Circuits Syst. II*, vol. 55, no. 9, pp. 942–946, Sep. 2008.

[72] R.-C. Li, "Test positive realness of a general transfer function matrix," Department of Mathematics, University of Kentucky, Tech. Rep. 2000-20, 2004. [Online]. Available: http://www.ms.uky.edu/∼math/MAreport/00-20.ps

[73] E. Griepentrog and R. März, "Basic properties of some differential-algebraic equations," *Zeitschrift für Analysis und ihre Anwendungen*, vol. 8, no. 1, pp. 25–40, 1989.

[74] R. März, "Projectors for matrix pencils," Humboldt-Universität zu Berlin, Tech. Rep. 04-24, 2004. [Online]. Available: http://www.mathematik.hu-berlin.de/publ/pre/2004/P-04-24.ps

[75] W. Cauer, *Synthesis of Linear Communication Networks*. New York: McGraw-Hill, 1958.

[76] Z. Zhang and N. Wong, "Passivity test of immitance descriptor systems based on generalized Hamiltonian methods," *IEEE Trans. Circuits Syst. II*, vol. 57, no. 1, pp. 61–65, Jan. 2010.

[77] T. Reis and T. Stykel, "Passivity-preserving balanced truncation for electrical circuits," Institut für Mathematik, Technische Universität Berlin, Tech. Rep. 2008/32, 2008. [Online]. Available: http://www.math.tu-berlin.de/∼stykel/Publications/pr_08_32.pdf

[78] S. Grivet-Talocia and A. Ubolli, "On the generation of large passive macromodels for complex interconnect structures," *IEEE Trans. Advanced Packaging*, vol. 29, no. 1, pp. 39–54, Feb. 2006.

[79] P. Kowal. (2006, May) Null space of a sparse matrix. Matlab Central. [Online]. Available: http://www.mathworks.co.uk/matlabcentral/fileexchange/11120

[80] J. Demmel and B. Kågström, "The generalized Schur decomposition of an arbitrary pencil A-λB: robust software with error bounds and applications. Part I: theory and algorithms," *ACM Trans. Math. Softw.*, vol. 19, no. 2, pp. 160–174, Jun. 1993.

[81] M. Gerdin, "Computation of a canonical form for linear differential-algebraic equations," Department of Electrical Engineering, Link?ping University, SE-581 83 Linköping, Sweden, Tech. Rep. LiTH-ISY-R-2602, Apr. 2004.

[82] B. Kagström and P. V. Dooren, "A generalized state space approach for the additive decomposition of a transfer matrix," *Intl. J. Numer. Lin. Alg. Appl.*, vol. 1, no. 2, pp. 165–181, 1992.

[83] P. Benner, *Scientific Computing in Electrical Engineering SCEE 2008*, ser. Mathematics in Industry, J. Roos and L. R. J. Costa, Eds. Berlin/Heidelberg: Springer-Verlag, 2009, vol. 14. [Online]. Available: http://www-user.tu-chemnitz.de/∼benner/pub/Benner_SCEE2008_revised.pdf

[84] Y. Chahlaoni and P. V. Dooren, "A collection of benchmark examples for model reduction of linear time invariant dynamical systems," Feb. 2002, SLICOT Working Note. [Online]. Available: http://www.icm.tu-bs.de/NICONET/benchmodred.html

[85] J. Ekman, G. Antonini, A. Orlandi, and A. E. Ruehli, "Stability of PEEC models with respect to partial element accuracy," in *Intl Symp. Electromagnetic Compatibility*, Aug. 2004, pp. 271–276.

[86] P. Benner, V. Mehrmann, V. Sima, S. Van-Huffel, and A. Varga, "SLICOT-a subroutine library in systems and control theory," *Appl. and Comput. Control, Signals, and Circuits*, vol. 1, pp. 499–539, 1999.

[87] H. Wu and A. C. Cangellaris, "Model-order reduction of finite-element approximations of passive electromagnetic devices including lumped electrical-circuit models," *IEEE Trans. Microwave Theory and Tech.*, vol. 52, no. 9, pp. 2305 – 2313, Sep 2004.

[88] N. Marques, M. Kamon, L. Silveira, and J. White, "Generating compact, guaranteed passive reduced-order models of 3-D RLC interconnects," *IEEE Trans. Advanced Packaging*, vol. 27, no. 4, pp. 569–580, Nov 2004.

[89] Z. Zhang and N. Wong, "An extension of the generalized Hamiltonian method to S-parameter descriptor systems," in *Proc. Asia South Pacific Design Autom. Conf.* Taipei, Jan 2010, pp. 43–47.

[90] Z. Zhang and N. Wong, "An efficient projector-based passivity test for descriptor systems," *IEEE Trans. CAD of Integrated Circuits and Systems, accepted.*

[91] Y. Hao, Y. Shi, and L. He, "Fast analysis of structured power grid by triangularization based structure preserving model oder reduction," in *Proc. Design Automation Conf.*, July 2006, pp. 205–210.

[92] Y. Yan, S. Tan, P. Liu and B. McGaughy, "Passive interconnect macromodeling via balanced truncation of linear systems in descriptor form," in *Proc. Asia South Pacific Design Automation Conf.*, Jan 2007, pp. 355–360

[93] Q. Zhou, K. Sun, K. Mohanram, and D. C. Sorensen, "Large power grid analysis using domain decomposition," in *Proc. European Design and Test Conf.* Munich, Germany, J 2006, pp. 27–22.

[94] T. Chen and C. C. Chen, "Efficient large-scale power grid analysis based on preconditioned Krylov -subspace iterative method," in *Proc. Design Autom. Conf.*, Jun 2001, pp. 559–562.

[95] H. F. Qian, S. R. Nassif, and S. S. Sapatnekar, "Random walks in a supply network," in *Proc. Design Autom. Conf.*, Jun 2003, pp. 93–98.

[96] E. Chiprout, "Fast flip-chip power grid analysis via locality and grid shells," in *Proc. IEEE Intl. Conf. Computer Aided Design*, Nov 2004, pp. 485–488.

[97] J. N. Kozhaya, S. R. Nassif, and F. N. Najm, "A multi-grid like technique for power grid analysis," *IEEE Trans. CAD of Integrated Circuits and Systems*, vol. 21, no. 10, pp. 1148–1160, Oct 2002.

[98] Z. Feng and P. Li, "Multigrid on GPU: tackling power grid analysis on parallel SIMT platforms," in *Proc. IEEE Intl. Conf. Computer Aided Design.* San Jose, CA, Nov 2008, pp. 647–654.

[99] J. Li, F. Wang, and J. White, "An efficient Lyapunov equation-based approach for generating reduced-order models of interconnect," in *Proc. Design Automation Conf.*, Aug 1999, pp. 1–6.

[100] J. M. Wang and T. V. Nguyen, "Extended Krylov subspace method for reduced order analysis of linear circuits with multiport sources," in *Proc. Design Automation Conf.*, 2000, pp. 247–252.

[101] D. Li, S. X.-D. Tan, and B. McGaughy, "ETBR: Extended truncated balanced realization method for on-chip power grid network analysis," in *Proc. European Design and Test Conf.*, 2008, pp. 432–437.

[102] P. Feldman and F. Liu, "Sparse and efficient reduced order modeling of linear subcircuits with large number of terminals," in *Proc. Intl. Conf. on Computer Aided Design*, 2004, pp. 88–92.

[103] P. Li and W. Shi, "Model order reduction of linear networks with massive ports via frequency-dependent port packing," in *Proc. Design Automation Conf.*, 2006, pp. 267–272.

[104] B. Yan, L. Zhou, S. X.-D. Tan, J. Chen, and B. McGaughy, "DeMOR: decentralized model order reduction of linear networks with passive ports," in *Proc. Design Automation Conf.*, 2008, pp. 409–414.

[105] S. Huda, M. Mallick, and J. H. Anderson, "Clock gating architectures for FPGA power reduction," in *Proc. Intl. Conf. Field Programmable Logic and Appl.*, 2009, pp. 112–118.

[106] I. M. Elfadel and D. L. Ling, "A block rational Arnoldi algorithm for multipoint passive model order reduction of multiport RLC networks," in *Proc. Intl. Conf. Computer Aided Design*. San Jose, CA, Nov 1997, pp. 66–71.

[107] T. V. Nguyen and J. Li, "Multipoint Pade approximation using a rational block Lanczos algorithm," in *Proc. Intl. Conf. Computer Aided Design*. San Jose, CA, Nov 1997, pp. 72–75.

[108] W. Zhang, W. Yu, X. Hu, L. Zhang, R. Shi, H. Peng, Z. Zhu, L. Chua-Eoan, R. Murgai, T. Shibuya, N. Ito, and C.-K. Cheng, "Efficient power network analysis considering multidomain clock gating," *IEEE Trans. CAD of Integrated Circuits and Systems*, vol. 28, no. 9, pp. 1348–1358, Sept 2009.

[109] Z. Ye, L. M. Silveira, and J. R. Phillips, "Fast and reliable passivity assessment and enforcement with extended Hamiltonian pencil," in *Proc. Intl. Conf. Comput.-Aided Design*. San Jose, CA, Nov 2009, pp. 774–769.

Publications during M.Phil Study

Journal Articles

1. Y. Wang, **Z. Zhang**, C.-K. Koh, G. K.-H. Pang and N. Wong, "Passivity enforcement for descriptor systems via Hamiltonian matrix pencil perturbation," *IEEE Transactions on Computer-Aided Design of Integrated Circuits and Systems*, under review.

2. **Z. Zhang** and N. Wong, "An efficient projector-based passivity test for descriptor systems," *IEEE Transactions on Computer-Aided Design of Integrated Circuits and Systems*, vol. 29, no. 8, pp. 1203-1214, Aug. 2010.

3. **Z. Zhang** and N. Wong, "Passivity check of S-parameter descriptor systems via S-parameter generalized Hamiltonian methods," *IEEE Transactions on Advanced Packaging*, vol., no., pp., 2010, accepted and in press.

4. N. Wong and **Z. Zhang**, "Discussion of "A half-size singularity test matrix for fast and reliable passivity assessment of rational models," *IEEE Transactions on Power Delivery*, vol. 25, no. 2, pp. 1212-1213, Apr. 2010.

5. **Z. Zhang** and N. Wong, "Passivity test of immittance descriptor systems based on generalized Hamiltonian methods," *IEEE Transactions on Circuits and Systems II*, vol. 57, no. 1, pp. 61-65, Jan. 2010.

Conference Papers

1. **Zheng Zhang**, Xiang Hu, Chung-Kuan Cheng and Ngai Wong, "A block-diagonal structured model reduction scheme for power grid networks," in *Proc. Design, Automation and Test in Europe (DATE)*, submitted.

2. C. Y. Lin, **Z. Zhang**, N. Wong and H. K.-H. So, "Design space exploration for sparse matrix-matrix multiplication on FPGAs," in *Proc. Intl. Conf. on Field-Programmable Technology (FPT)*, Dec. 2010, to appear

3. Y. Wang, **Z. Zhang**, C.-K. Koh, G. K.-H. Pang and N. Wong, "PEDS: passivity enforcement for descriptor systems via Hamiltonian-Symplectic matrix pencil perturbation," in *Proc. Intl. Conf. Computer Aided Design (ICCAD)*, pp. , Nov. 2010, to appear

4. C. Y. Lin, **Z. Zhang**, N. Wong and H. K.-H. So, "Power-delay and energy-delay tradeoffs in sparse matrix-matrix multiplication on FPGAs," in *Proc. Intl. Workshop on Highly Efficient Accelerators and Reconfigurable Technologies (HEART)*, Jun. 2010, to appear

5. **Z. Zhang** and N. Wong, "An extension of the generalized Hamiltonian method to S-parameter descriptor systems," in *Proc. Asia and South Pacific Design Automation Conference (ASP-DAC)*, pp. 43-47, Jan. 2010.

6. **Z. Zhang**, C.-U. Lei and N. Wong, "GHM: a generalized Hamiltonian method for passivity test of impedance/admittance descriptor systems," in *Proc. Intl. Conf. Computer Aided Design (ICCAD)*, pp. 767-773, Nov. 2009.